Faculty of bioscience engineering

Hydrogeophysical characterization and monitoring of a peatland in the Hautes Fagnes

Author: BULLIARD Florentin
Supervisors: Prof. LAMBOT Sébastien (SST/ELI/ELIE)
PhD student HENRION Maud (SST/ELI/ELIE/ELIC)
Readers: Prof. BIELDERS Charles (SST/ELI/ELIE)
Prof. JAVAUX Mathieu (SST/ELI/ELIE)

Academic year: 2022 - 2023

Master's thesis presented in order to obtain the diploma of Bioengineer: environmental sciences and technologies.

Acknowledgement

This master's thesis could not have been completed without the help of several people. I would like to express my gratitude to these people in the following few lines.

First of all, I would like to greatly thank my supervisors: Prof. Sébastien LAMBOT for giving me the opportunity to work on this fascinating project and for helping me during the writing. PhD student Maud HENRION for helping me throughout the project, on the field, for the processing of the data and for the writing. Their guidance, their support and their advice during this master's thesis was very helpful and improved significantly the quality of this work. Thanks to PhD student Yanfei LI for the drone-data acquisition on the site.

Secondly, I would like to thank the ELIE technical team, especially Sébastien FRANCOIS for his help on the field and Olivier LEBBE for his help in the laboratory.

I would like to express my gratitude to Prof. Charles BIELDERS and Prof. Mathieu JAVAUX for accepting to be part of my jury and to read my master's thesis.

More personally, I would like to thank my family, my friends and especially my girlfriend for their interest in my master's thesis. Their support, not only during this master's thesis but also throughout my years of study, was very important and made it possible for me to complete this work.

Contents

List of Figures

List of Tables

List of acronyms

TDR Time Domain Reflectometry

SWRC Soil Water Retention Curve

VWC Volumetric Water Content

CZ Critical Zone

GHG GreenHouse Gases

vGM van Genuchten – Mualem

1 Introduction

Peatlands have high-water storage capacity, which allows them to function as water reservoirs. Water is by definition an indispensable element for peatlands, as for all wetlands. Its quantity, quality, acidity, mineralisation, nutrient richness, etc., as well as their variations in time and space, influence the creation, evolution and eventual disappearance of these peatlands [1]. Any change in the quality or quantity of water feeding the peatland can damage it in a more or less reversible way. Because of their high organic content, peatlands are important carbon stores. Although they represent only 3% of the land surface, peatlands contain almost 30% of the world's soil carbon stock [2]. The water properties of peatlands therefore play a key role in maintaining conditions favourable to carbon accumulation. These properties can be variable within the same site and between different sites according to spatial and temporal variability. Knowledge of these hydraulic properties is therefore important in order to be able to protect or, in the event of an identified malfunction, to intervene in the sectors at stake, including on the scale of the peatland catchment area.

These hydraulic and hydrogeophysical properties can be studied and monitored using several methods. This is what this master’s thesis will focus on, as the study area is located in the Belgian Hautes Fagnes.

An in-situ method was used, namely the TDR (Time Domain Reflectometry) sensors which allow to study the VWC (Volumetric Water Content) of the soil and its evolution over time and at various depths. The pressure cell apparatus, a laboratory method, is used to determine some hydraulic parameters in the laboratory by taking samples in the field. By combining these parameters with the vGM (van Genuchten – Mualem) model, SWRC (Soil Water Retention Curves) can be determined. To combine all these results, direct modelling can be used.

This document will start with giving a brief overview of the climate in Belgium, especially in the Hautes Fagnes. This will be followed by an overview of the CZ (Critical Zone) and the role of water and soil in this zone. It will then focus on peat soils and peatlands climatic issues. As the main objective is the characterization of the hydrology of a peatland soil, a description of methods used to achieve this objective will be presented. As this thesis is a part of a larger project, the LandSense project, its objectives will also be explained. The study site will be reported. The methodology will then be described before presenting the results of TDR sensors, SWRC and direct hydraulic modelling.

1.1 Context

1.1.1 Critical zone

The CZ is defined as the heterogeneous near-surface environment in which complex interactions between rock, soil, water, air and living organisms regulate the natural habitat and determine the availability of vital resources (Figure 1) [3] [4]. It is the place for interactions between the atmosphere, the hydrosphere, the pedosphere, rocks and ecosystems [5].

This area is complex, made up of various entities, and its study is shared between many: geology, geochemistry, biogeochemistry, geophysics, pedology, hydrology, hydrogeology, ecology, climatology, mineralogy, agronomy, etc. This specialisation is an obstacle to a global scientific approach to the Earth's surface and the processes that drive it [6].

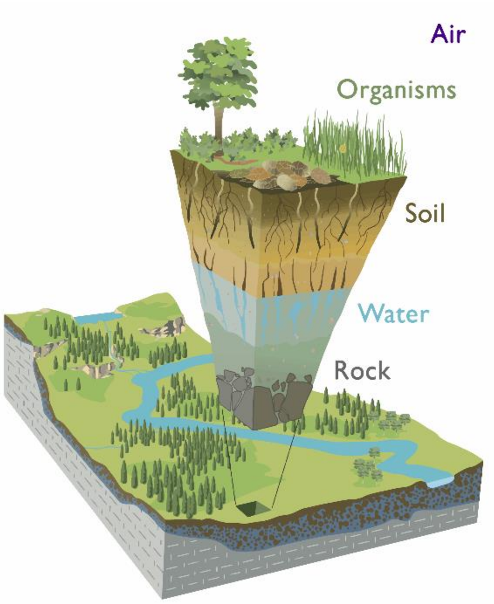

Figure 1: Critical zone extend [3]

CZ is a reactive zone for the planet and plays a key role in its global regulation. As a support for life, this thin layer is strongly impacted by humans who shape the landscape, extract its resources and store its waste. Anthropogenic actions modify the major biogeochemical cycles and profoundly affect the resources on which humans depend (water and soil) from both a quantitative and qualitative point of view [5].

The CZ has an integral role in the dynamics of the Earth System and its major biogeochemical cycles, water, carbon and nitrogen cycles. The same applies to its feedbacks on the climate through these major cycles. Thus, the understanding of processes, their parameterisation and the quantification of exchanges of matter, water, contaminants and energy must be integrated into global models of the Earth System, where the water cycle is an essential prerequisite [5] [7].

The concept of CZ questions the hydrological sciences because of its interactions on spatial scales, its interactions on temporal scales, and the interactions between biogeochemical processes. CZ poses new challenges for the study of its functioning, whether for the study of transfers at different scales of water, matter (dissolved and suspended) and contaminants, or for the study and characterisation of processes for the preservation and/or degradation of the structure and quality of the environments [5] [8].

1.1.2 Soil and water

Soil water represents only 0.064% of the total fresh water. However, it plays an essential role as it is the water used by plant roots [9]. Water is a constituent element of the plant where the plant matter contains 60 to 95% water. It provides the plant with essential mineral elements for its nourishment. Water is therefore, through the soil solution, the essential basis of plant nutrition [10].

It is through the soil that water circulates between underground reserves and the atmosphere, mainly through plant transpiration [11]. Soil and vegetation control the distribution of rainfall between runoff and groundwater flow and between evaporation and infiltration [12]. Soils play an important role in the water cycle because it filters, absorbs and retains water [5]. Soil filters water and buffers the surface water regime and groundwater recharge [11].

Soils also provides water for living organisms and plays a major role in the storage, mobility and transformation of biogenic elements (C, N, P) and inorganic, organic and microbiological contaminants [5]. Water in the soil plays a major role in many environmental processes through the dissolution, deposition, transformation, degradation and transport of various substances. Water is a fundamental factor in the pedogenesis and in soil evolution [10]. Many chemical reactions take place at the interface between the solution and the solid phase or soil organisms. It should be noted that GHG (GreenHouseGases) emissions and carbon storage in soils are strongly determined by water conditions [11].

The total amount of water that the soil can hold, as well as the amount of useful water, varies according to two main intrinsic criteria: grain size and the depth of the soil. Water content is a function of soil porosity so the volume of water in soils depends mainly on the grain size of the soil [9]. The smaller the pores, the more water is retained. Well-connected pores will facilitate the circulation of water [11]. The deeper the soil, the greater its water reserve: near the surface, the soil is not saturated, the voids contain water and air. From a certain depth the soil is saturated. This area forms a water table [9]. Note that some rocks, such as chalk, can also act as a water reserve and replenish the soil as it dries out [11].

In a soil, the pore size distribution determines the share of gravity water, useful reserve water and bound water, respectively located in smaller and smaller pores. The limits between these three types of water correspond to the notions of "field capacity" and "wilting point". The effective porosity is the amount of water that can be freely extracted from a soil under the action of gravity alone, this water being located in the largest pores. It is expressed in relation to the total volume of the medium considered. It corresponds to the volume of water between saturation and field capacity [13].

The porosity of a soil is also influenced by organic matter, fauna and flora, and human activity.

1.1.3 Peat soils general information

Peat is defined as the product of the fossilisation of plant debris by micro-organisms in wetland, oxygen-poor environments (known as peatlands) over a period of time ranging from 1.000 to 7.000 years. Peat forms the major part of peatland soils [14].

For peat initiation and accumulation, there are requirements: waterlogging, low pH, low nutrient availability, low oxygen supply and reduced decomposition rate. And these requirements are similar in every geographical location. However, the physical and chemical characteristics differ according to specific site characteristics of landscape area and topography, climate, water depth and flow, nutrient availability and biogeographical availability of plant species [14]. The rate at which organic matter accumulates to form ‘peat’ depends on the productivity of the aquatic vegetation that in turn is determined by the nutrient content of the water and, initially, the mineral substrate [15].

In temperate, boreal and sub-arctic regions, where low temperatures reduce the rate of decomposition, peat is formed mainly from bryophytes (mosses), herbs, shrubs and small trees. In the lowland humid tropics, peat is derived mostly from rain forest trees (leaves, branches, trunks and roots) under near constant annual high temperatures. In other geographical regions peat can be formed from other species of plants that are able to grow in water-saturated conditions [16].

From a pedological point of view, peat is usually classified into two categories: calcium peat which forms on a calcareous substrate. Its pH is neutral and the C/N ratio is less than 30. Acidic peat which forms in areas where the water is poor in calcium. The pH is acidic (between 4 and 5) and the C/N ratio is around 40 [17]. These two categories are called differently: fens and bogs. Fens rely on runoff and groundwater for their moisture, which are often mineral-rich and result in fens being primarily alkaline and nutrient-rich in nature. By contrast, bogs have little to no groundwater and instead rely on precipitation that collects atop their thick, plush peat soils and sphagnum mosses. As a result, bogs are acidic, low in nutrients, and contain very little oxygen in their water [18].

Peat consists mainly of water (70-80% by weight) and poorly decomposed organic matter (20-30% by weight). The carbon content can be up to 50% by weight. But, depending on the country, there is disagreement on the minimum thickness of the soil surface organic layer and the minimum percentage of organic matter [15]. In Belgium, a soil is defined as peat when there is more than 30 % of organic matter in the soil.

The organic matter in peat is mainly cellulose and lignin. These two constituents are generally considered to be inert to adsorption reactions. But the organic matter also contains humic substances that have a high absorption capacity. The high accumulation of organic matter in the soil results in a significant decrease in mineral content. Thus the plants in the bog must be adapted to this mineral shortage [15].

Peat has long been used in agriculture, notably as a substrate for in situ agriculture, but also extracted for ex situ use as organic fertiliser. It is also commonly used as fuel. In the past, it has long been used as a building material in regions where wood is in short supply [16]. Dried, it gives a brown to blackish fuel that heats less than wood and coal. Because of its burial, peat is subject to special conditions of pressure and temperature, and after a period of about one million years it turns into coal. Peat can thus be considered as an intermediate stage in the formation of coal [17].

1.1.4 Peat hydro-physical properties

The organic nature of peatlands induces certain particularities, notably a great spatial and temporal variability of their properties, making them sometimes difficult to predict. Spatial variability is explained by the diversity of vegetation, as well as by local topographical and climatic conditions. Temporal variability is due in particular to the compressibility of the peat, which influences the pore volume by affecting the related properties [19]. This swelling character is also reflected in seasonal fluctuations of the topographic surface, estimated at a few centimetres in annual amplitude [20] [21].

Sphagnum bogs have a particular stratification. On the surface, the living vegetation consists of mats of Sphagnum mosses, within which other specialised species settle. Sphagnum mosses grow continuously upwards, while the lower part of the moss dies, gradually being buried by newer vegetation. The dead organic matter undergoes a process of humification, accompanied by a loss of material and some mineralization, which remains very low. This transformation is limited in time; beyond a certain depth, the acid and anoxic conditions of the environment prevent the transformation from continuing. Thus, organic matter, more or less humified, accumulates over thicknesses that can reach several metres in a few thousand years. As shown in Figure 2, the 10-level qualitative scale of von Post are graduated from H1 (living vegetation) to H10 (very humified peat). The degree of humification of a peat can be defined as the proportion of products of humification in relation to the total matter [22]. As humification proceeds, the plant structures become less distinct, the bulk density increases, and less and less water is extracted by manual pressure. On the other hand, the organic matter content always remains close to 100% of the dry weight, due to the very low mineralisation. The degree of humification naturally tends to increase from top to bottom, but this growth is not necessarily regular [23].

The total porosity is the total volume of voids in relation to the total volume of the medium considered. In various peat bogs, total porosity is around 90% [23] [24]. It varies little with the degree of humification. The total porosity expresses the quantity of water that an aquifer can contain. The total porosity of peat soils is clearly higher than that of other types of loose formations (around 50% for clays, 40% for sands) [25].

In peatlands, as the living vegetation transforms into more humified peat, the initial coarse porosity evolves into a predominantly finer porosity. The effective porosity therefore tends to decrease with increasing humification, which is reflected in the profiles by values that decrease with depth (Figure 2) [23] [26] [19]. Effective porosity expresses the amount of water an aquifer can supply. For comparison, effective porosity is about 30% in sands, whereas it is only about 5-10% in clays.

The hydraulic conductivity at saturation expresses the capacity of an aquifer to transmit water. From this point of view, surface vegetation or peat with low humification behave like a good aquifer: the values are close to those of unconsolidated sands or gravels. On the other hand, highly humified peat can be considered impermeable, as its behaviour is similar to that of clay.

Bogs comprise two main strata [23], described as acrotelme and catotelme [26]. This subdivision is based on the humification, porosity and permeability profiles described above (Figure 2). The acrotelme is the upper stratum, formed by living vegetation and dead, but only slightly decomposed, sphagnum moss. This layer is a few tens of centimetres thick. It corresponds to the zone of periodic aeration, as it is in this zone that the hydrostatic level fluctuates. It contains aerobic bacteria that contribute to the formation of peat. The effective porosity and hydraulic conductivity parameters are very high at the surface and decrease towards the base of the acrotelme. The lower stratum, or catotelme, is the most important mass of the bog and can be several metres thick. It is characterised by low effective porosity and hydraulic conductivity, permanent water saturation and therefore the absence of aerobic microbial activity [23].

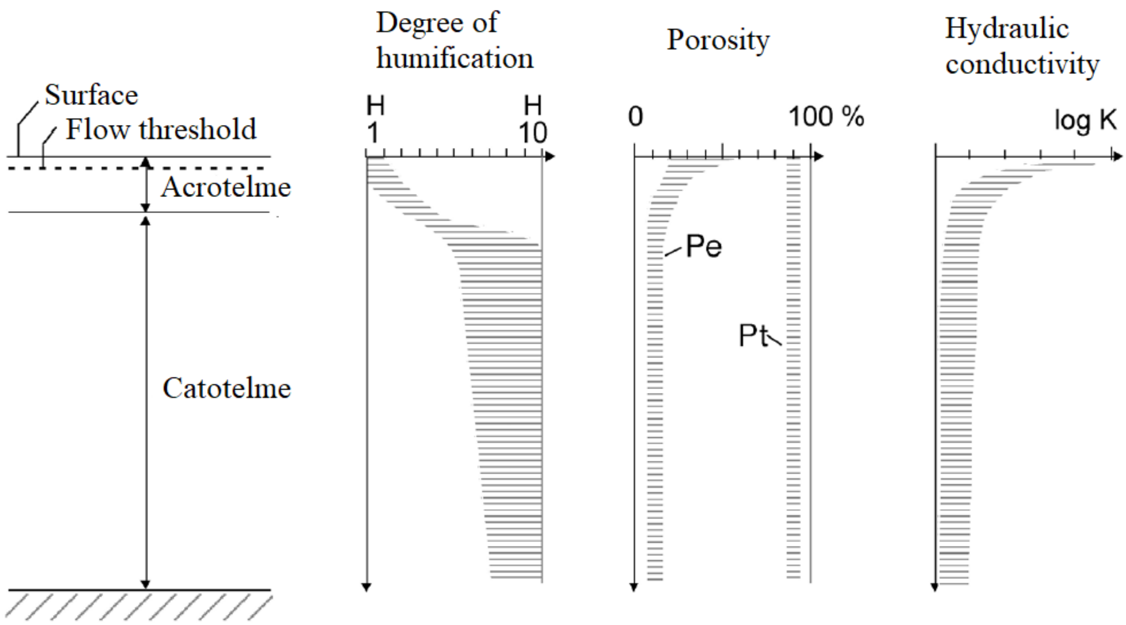

Figure 2: Schematic profile of a bog and some hydro-physical parameters.

H: degree of humification. K: hydraulic conductivity at saturation. Pt: total porosity. Pe: effective porosity [13]

1.1.5 Peatlands distribution

Peatlands are terrestrial wetland ecosystems in which waterlogged conditions prevent plant material from fully decomposing. Consequently, the production of organic matter exceeds its decomposition, which results in a net accumulation of peat. In cool climates, peatland vegetation is mostly made up of Sphagnum mosses, sedges and shrubs and are the primary builder of peat, whereas in warmer climates graminoids and woody vegetation provide most of the organic matter [27].

Peatlands occur in every climatic zone and continent and cover 4.23 million km^2, which corresponds to 2.84% of the Earth's terrestrial surface. About 84% of the world's peatlands are considered to be in natural, or near-natural state. Drained peatlands make up about 16% of the world's peatlands, or 0.5% of the Earth's terrestrial surface [28].

The majority of the world's peatlands occur in boreal and temperate parts of the Northern Hemisphere, especially, Europe, North America and Russia where they have formed under high precipitation-low temperature climatic regimes as shown in Figure 3 [29].

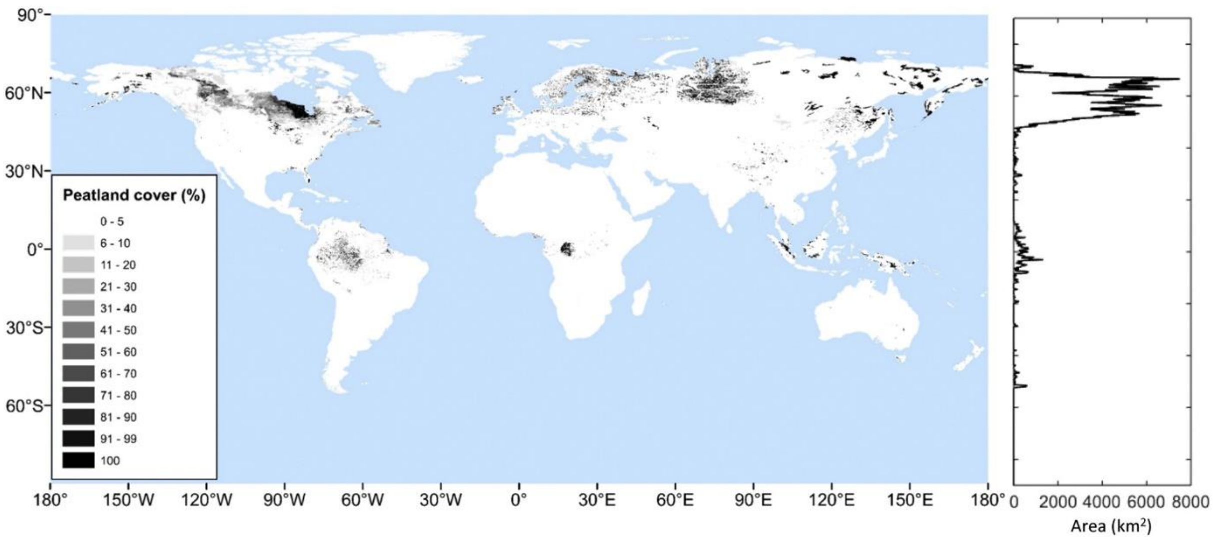

Figure 3: A global estimate of peatland and its distribution along the latitude [30]

Peatlands are found in Belgium at the highest altitudes, i.e. on the Ardennes plateaux: Hautes Fagnes, Tailles, Saint Hubert, Recogne and Croix-Scaille. Other peatlands, on the plains, in very humid areas with an Atlantic climate, have almost entirely disappeared. At present, there are about 13,000 ha of peaty areas in Belgium. However, most of these are severely degraded. There are barely 300 ha considered as sub-intact, mainly in the Hautes Fagnes and the Plateau des Tailles. Since 1957, about 25% of the peatland has disappeared or been severely degraded in the Hautes Fagnes [29].

1.1.6 Peatlands climatic issues

At the level of individual peatland sites, the diversity of organisms can be exceptional. The drivers of peatland biodiversity loss are: the loss of habitat, invasive species, over-exploitation for agriculture, forestry and peat extraction, nutrient pollution and climate change. The mixture of plant and animal species living on and in peatlands are essential for the process of peat formation, thus protecting and/or restoring the peat-forming plant species, and the animals that help those plants to regenerate, is essential [16] [17].

Peatlands have a regulatory function. It regulates the climate at global, regional and local scale, the catchment hydrology, the GHG emissions and other climatic processes (precipitation, air temperatures, etc). It has a role in water regulation: water storage, groundwater recharge and discharge. Peatlands are important for water purification and waste treatment (regulation of catchment hydrochemistry): retention, recovery and removal of excess nutrients and pollutants. It has also a role in erosion protection by regulating soil conditions: peat blanket protecting the underlying soils from erosion [16].

Peatlands interact with climate through the uptake and release of GHG. Since peatlands store large amounts of organic matter in their soils by the process of peat accumulation, they are carbon rich ecosystems that store and sequester more carbon than any other type of terrestrial ecosystem. Peatlands exceeds thereby the global above-ground carbon stock of forest ecosystems [16]. This carbon has been taken out of the atmosphere as carbon dioxide (CO_2) by peatland plants in the process of photosynthesis. Once deposited in the soils, this carbon accumulates due to the slow rate of decay in the water-saturated soils. Some CO_2 is released by plant respiration and the slow litter decomposition (also called microbial respiration), but without disturbance, peatlands have a net uptake of CO_2. This removal of CO_2 from the atmosphere has a cooling effect [31].

Water-saturated soils lead to slow decay because there is little oxygen available for the microbes that breakdown organic materials. In these low oxygen conditions, one of the products of decay is methane (CH_4), a potent GHG. Because peatlands have wet soils, they represent a globally significant source of CH_4, accounting for about 10% of all global emissions. This emission of CH_4 has a warming effect on the atmosphere, but the lifetime of CH_4 in the atmosphere is much shorter than for CO_2. Therefore, over short time periods, many peatlands may have a net warming effect on the atmosphere when both the uptake CO_2 and release of CH_4 are considered. But, over longer time periods, the effect of CH_4 emissions reaches an equilibrium, and the uptake of CO_2 becomes more important, most peatlands are then net coolers of the atmosphere over long time scales [32].

Peatlands can also act as a source of nitrous oxide (N_2O), also a potent GHG. In an undisturbed state, losses of N_2O from most peatlands are small. However, drainage and fertilization of peatlands can greatly increase N_2O emissions, making an important contribution to the peatland GHG balance [33].

Ongoing climate change may affect the ability of peatlands to take up and store carbon and GHG. Warmer soils increase the rate of organic material decay and this may result in the release of the carbon stored in peatland soils. Changes in hydrologic conditions will also affect how quickly organic material decays and the types of plants that grow on the peatland surface. When peatlands are drained, the carbon from organic matter contained in peat dries and oxidizes gradually to CO_2, and is permanently lost from the system. Over time, this process also results in soil compaction and subsidence, making it difficult to restore proper hydrology without water table management [17]. Drained peatlands are also more susceptible to wildfire, with the potential for massive GHG emissions [34].

The balance between these changing conditions will ultimately determine future rates of carbon and GHG exchange and whether peatland remain as net coolers of the atmosphere [35]. Many studies to date highlight that feedbacks with peatland ecosystems make them somewhat resilient to climate change [36]. However, climate change can result in acceleration of other disturbances that could destabilize peatland carbon stocks. For example, thawing of permafrost in boreal and subarctic peatlands can quickly liberate large amounts of carbon from peatland soils. Warmer temperatures are also changing wildfire regimes, with droughts making peatlands more susceptible to burning. More frequent fires can convert peatlands from net sinks of carbon to net sources as GHG [37].

Human use of peatlands also alters rate of GHG exchange. Drainage for agriculture, forestry and peat extraction leads to drier conditions in the soil and this speeds of the rate of decay. These soils become a source of CO_2. At the same time CH_4 emissions usually decline, but remain high from drainage ditch areas [38]. Despite this reduction in CH_4 emissions, the large CO_2 emissions mean that these peatlands are warming the atmosphere due to GHG emissions. This is further accelerated if N_2O emissions are also enhanced by drainage and fertilization [33].

Rewetting and restoration of peatlands reduce soil carbon losses and GHG emissions and also reduce the risk of large carbon losses by lowering wildfire susceptibility [39]. Therefore, better peatland management can be an important climate change mitigation strategy [40].

1.2 Objectives

1.2.1 My objectives

In this context of CZ and peatlands, the goal of this master's thesis is to characterize the hydrology of the peat soil by the determination of hydrogeophysical properties and the monitoring of the VWC. Objective is also to study the intra site variability of peat hydraulic properties. To meet this objective, the SWRC $\theta(h)$ and VWC $\theta(t)$ were measured within the study site and related. To collect the data needed, several methods were used: an in-situ method, namely the TDR probes and a laboratory method, the pressure cell apparatus.

In the water retention curve part, the goal is to assess the SWRC of the site using the vGM model and obtain the corresponding hydraulic parameters: α, n, θ_r and θ_s. To obtain these, several samples, collected at different depths and locations, were analysed in the laboratory. These samples were subject to several stages of suction and their water content were observed. This allows to establish soil water retention curves from which the desired parameters are extracted. These, once compared, will give indications on the hydraulic capacity of the soil, depending on its depth and position in the landscape. The saturated hydraulic conductivity and the bulk density of each sample are also estimated, allowing a better understanding of water behaviour in soil, especially in peat soil.

In the TDR part, the goal is to evaluate the hydrological dynamics of the site and this was achieved by placing TDR sensors at several depths and locations. These probes measured raw water content data. These are then transformed into VWC via a calibration. There are two possible calibrations: one for peat soils and one for mineral soils. Once these data collected and calibrated, it allows to analyse the evolution of the VWC over several months and to better understand the impact of upper and lower boundary conditions.

In the direct modelling part, the goal is to cross together the TDR data and the retention curve data. To do this, a direct modelling is done on Hydrus-1D. The direct model is based on the calculated vGM parameters and the precipitation data. The objective is to see if the resulting model corresponds to the reality and to understand the limits of direct modelling. The aim is to understand and predict behaviour and perform parametric analyses.

1.2.2 LandSense project

This master's thesis takes part in a larger project: the LandSense project. This project focuses on the spatio-temporal variation in soil hydrology and its controls on carbon and nutrients fluxes, which are highly relevant in the context of global change. So, the objective is to ensure a better understanding of the CZ. Given the central role of the soil system in regulating carbon and nutrient fluxes, and the increasing environmental pressures, it is important to improve fundamental understanding of these key critical zone [41].

2 Study site

2.1 Expanded site: Belgium and the Hautes Fagnes plateau

The climate in Belgium is a temperate oceanic climate, which is found mainly on the Atlantic coasts of Europe and is influenced by the Gulf Stream. The temperate oceanic climate is influenced alternately by the polar and subtropical climate. At Belgium latitudes, cold air masses of polar origin meet warm air masses of subtropical origin [42]. The proximity of the sea has a strong influence on this climate. Because of the extent and thermal inertia of the oceans, the heat stored by them is slowly released into the atmosphere. This is why this climate mitigates climatic extremes. In addition, the country is often place in westerly atmospheric currents. Under these conditions, the air masses arrive directly from the ocean, where they are loaded with moisture, which makes the climate rainy [43]. This climate is therefore generally characterised by mild, rainy winters and relatively cool, wet summers.

Since the 19th century, the cumulative annual rainfall in Belgium has increased by about 9% [44]. The normal annual rainfall amounts in Belgium vary from simple to double over the Belgian territory: from 700 mm/year to almost 1400 mm/year for the Hautes Fagnes region. The normal rainfall amounts are generally influenced by the relief. The higher elevation sites experience on average higher amounts of precipitation than the lower areas [45].

Analysis of the average annual temperature in Belgium (Figure 4) shows that it has been rising significantly since the end of the 19th century. The average annual temperature in Belgium has risen by 1.9°C [46]. Since 1981, there has been a gradual increase in temperature, and the climate normals have continued to rise. The warming of the last decades is even more striking when one observes that the 20 warmest years between 1833 and 2019 were all recorded after 1988, and that 14 of these warmest years occurred after 2000 [44]. The annual normals of the average air temperature in Belgium vary from 7.5°C for the Hautes Fagnes to 11.5°C. The Belgian average temperature is 10.2°C. The annual normals for maximum and minimum daily temperatures vary from 11°C to 15.9°C and from 3°C to 7.7°C, respectively. These normals systematically reach their lowest values in the Hautes Fagnes. Their distribution is mainly determined by two factors: distance from the sea and altitude [45]. Figure 4 shows the evolution of the average temperature in Belgium, represented by the departure from the 1961-1990 normal, for the period 1951-2100. The lines correspond to the observed trends as well as to those of the royal meteorological institute climate model according to the various GHG emission scenarios (RCP). Different scenarios are considered: an optimistic scenario (RCP2.6) with a strong reduction of GHG emissions, a pessimistic scenario (RCP8.5) in which emissions increase strongly and an intermediate scenario (RCP4.5) [47]. The red and blue vertical bars represent the observed annual averages until 2018 [48]. Depending on the scenario, the change for Belgium is between 0.7 and 5°C by the end of the century. In general, a greater temperature increase is expected in winter than in summer.

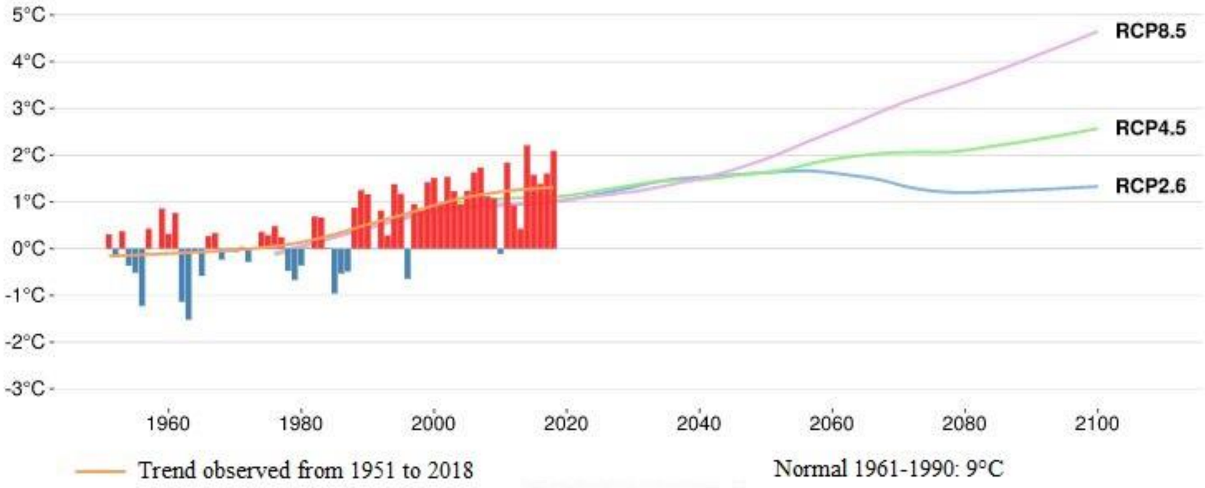

Figure 4: Evolution of the average annual temperature in Belgium and three different climatic scenarios (RCP) [48]

In terms of precipitation development compared to the current climate, the most pessimistic scenario (RCP8.5) presents two clear conclusions for the end of the century. Winters will be significantly wetter and, on average, no or only a slight decrease of precipitation is expected in summer [48].

As shown in Figure 5, average temperatures range from -1.9°C in February to 21.5°C in July. The average annual temperature in Malmedy is 8.4°C, almost 2°C below the Belgian average. The months of April and August have a greater variability in temperature. The lowest variability is in December. As for rainfall, it is abundant, with more than 1200 mm per year. In some years, it can even reach 1400 mm. This is much higher than the Belgian average of 910 mm [49].

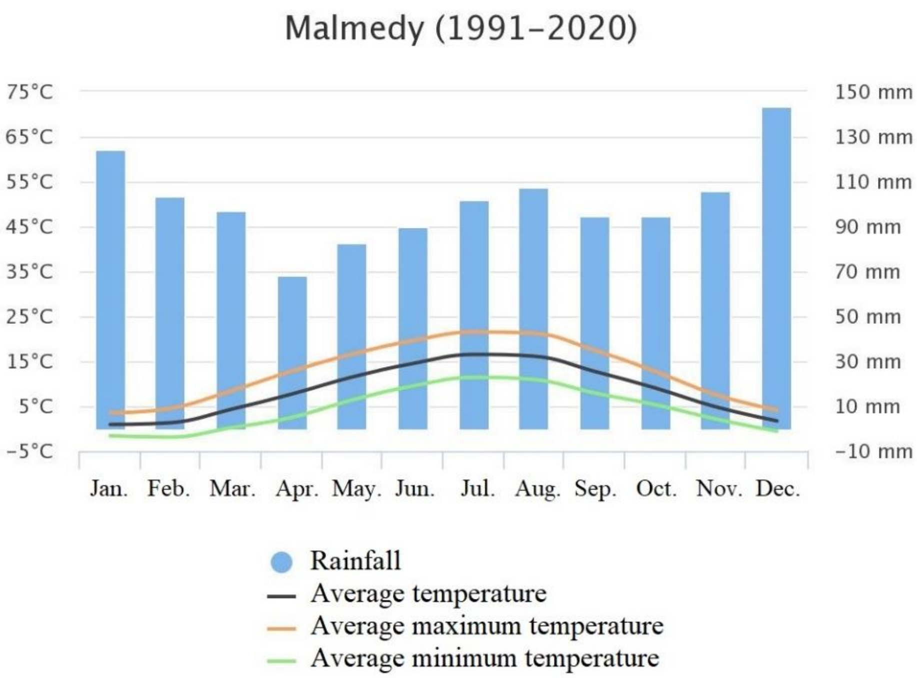

Figure 5: Average temperature and rainfall evolution in Malmedy - 1991-2020 [49]

Any climatic change in the Hautes Fagnes region could have a considerable impact on biodiversity, soils and their water content, especially in the region itself.

The Hautes Fagnes Plateau is made up of a succession of hills with an altitude of just under 700 m. The Hautes Fagnes cover more than 5000 ha. They extend over the territory of the Walloon Region and the German-speaking Community [50]. The general orientation of this chain of hills perpendicular to the prevailing westerly sea winds in Belgium explains to a large extent the particular weather conditions that can be observed there. These hills constitute the first major barrier encountered by the westerly winds, and the air masses are forced to rise abruptly. This results in internal cooling and thus in increased water condensation. The significantly higher precipitation on the western slope is due to this explanation. The vegetation cover consists of extensive, mainly coniferous forests interspersed with active bogs. In the peat bogs, the intense evaporation of the sphagnum moss mat maintains or increases the humidity of the air. This high transpiration locally lowers the ambient temperature. This phenomenon explains the relative coolness of the Fagnard microclimate in summer and the large number of foggy days. The harshness of the climate and the extreme poverty of the soil have caused it to be deserted: human communities have settled preferably on the edge of the plateau [51].

Water is a very present element in the Hautes Fagnes. Rainfall is very frequent as shown before. The subsoil is mainly made up of impermeable clays, which causes water to stagnate on the surface. On the ridges, there is often a more permeable aeolian silt that allows infiltration and the formation of groundwater at a shallow depth. However, water can infiltrate more deeply and accumulate in the folds of the rock at a depth of between 20 and 50 metres. Their stagnation loads them with iron, manganese, calcium, magnesium, sodium and lithium from the surrounding rocks. These date mainly from the primary era (shales, quartzites and sandstones; pudding in the surroundings of Malmedy). The study site is located on the northeastern part of the Cambro-Ordovician Stavelot-Venn massif. This massif lies on quartzite and slate bedrock [52]. The hydrogen sulphide that develops there allows the iron to dissolve, drives out oxygen, keeps the dissolved salts in a reducing state. The carbonic acid coming from the great depths insinuates itself and is combined with these waters, giving them the quality of mineral water essentially ferruginous and carbogeneous. The plateau is also crossed by numerous watercourses that feed various dams: the Eupen dam, which has a storage capacity of 25 million cubic metres, the Helle dam, the Getzbach dam and the Gileppe dam, the Butgenbach and Robertville dams [53] [51].

In the Fagnard High Plateau the soils are among the poorest, most acidic and least permeable. These soil qualities combined with the high rainfall and relatively harsh climate explain why we find plant species of Atlantic origin, but also of boreal origin, or even of mid-European mountain origin. The site is therefore a real migration crossroads [54].

The peat bogs, of which all types can be found, from the Atlantic to the Boreocontinental genus, have settled on the impermeable clayey silts of the slopes. They are made up of a series of turf plants in which sphagnum mosses and cottongrass are largely dominant. These are the oldest plant structures in the bogs: some peatlands are 8000 to 9000 years old [55].

The cold, wet climate and the boreo-montane vegetation influence the fauna. This is particularly the case for invertebrates [53].

In the Hautes Fagnes, intensive drainage of the peat bogs was undertaken at the end of the 19th century, with the aim of drying out the soils for the planting of spruce trees. Although these plantations failed, the network of drainage ditches remained and is incriminated in the degradation process of the peat bogs. The digging of a trench causes a lowering of the water table, and sphagnum mosses are very sensitive to a lowering of the hydrostatic level. Under these circumstances, they lose their competitive advantage over other plants [13].

In conclusion, the Hautes Fagnes plateau is important in several respects. Indeed, the plateau presents natural phenomena and a particular fauna and flora due to its geographical location. The Fagnes constitute a fragile ecosystem whose survival requires special protection and management measures. Thus, the site benefits from several legal protection measures at regional and international level.

2.2 Geographical situation

The study site is located in the Hautes Fagnes, specifically in the northern part of the municipality of Malmedy. As shown in Figure 6, there are 3 areas, different on multiple levels, which are the topography, the vegetation, the pedology, the presence of roads and deep drains (see 2.1). The area number 1 is the slope with a small river in the northern part. The number 2 is the central plateau and 3 is southern plateau, excluded by a road. The perimeter is about 900 by 350 meters.

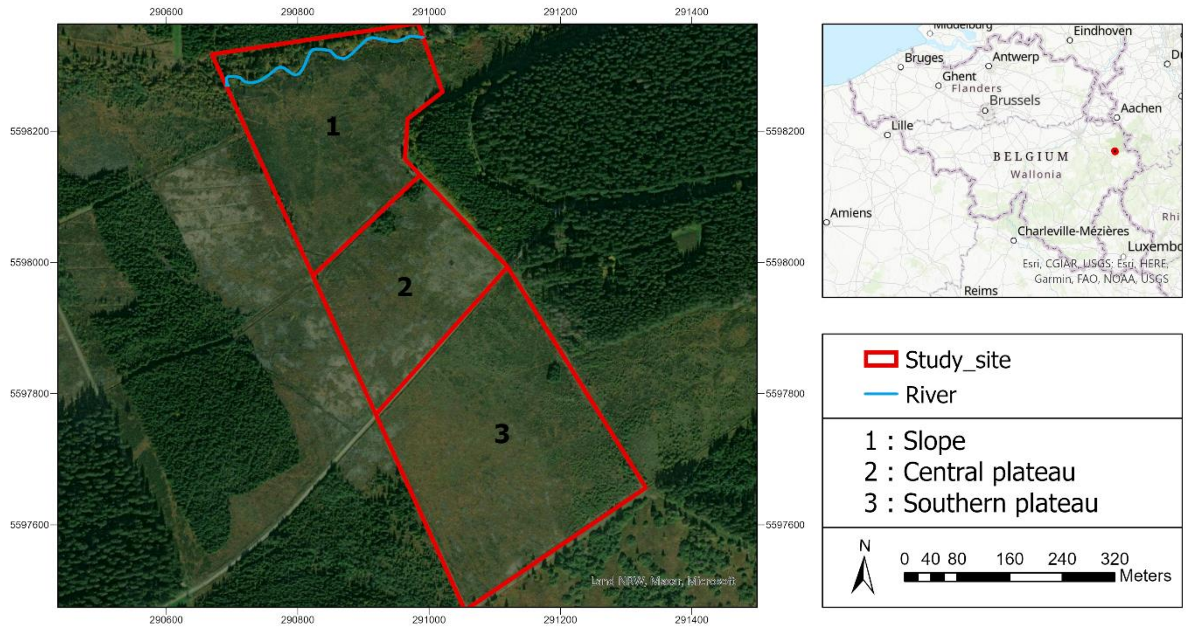

Figure 6: Study site localisation and division with river localisation.

The small river, named "Ruisseau de Polleur", located below the study area, is one of the two tributaries that give rise to the Hoëgne. The Hoëgne is a river, a tributary of the Vesdre, which is part of the Meuse watershed. The study area is located within a Natura 2000 site. This involves the protection of a number of species populations and biotopes considered important and for which a favourable conservation status must be guaranteed [56].

The choice of the site was made mainly on a hydro-pedological, not geophysical, basis. The main criteria that guided this choice were: natural site; site of societal interest; structure with a plateau, a slope and a stream; contrasting soil profiles; accessible site for measurements. This choice complicates the geophysical measurements, but it represents a source of originality, especially with peat. Indeed, peatlands are little studied and they are essential for the carbon and water cycle. Finally, they have an ecosystemic interest.

2.3 Topography

The Hautes Fagnes plateau hosts the highest point of Belgium, the "Signal de Botrange" (694 meters), which is only a couple kilometres away from the study site. As shown in Figure 7, the peak of the study site culminates at an altitude of 635 meters and is located is the south-east corner of the study perimeter. The lowest altitude point of the study site is located on the opposite corner, in the north-west, with an altitude of around 590 meters [57].

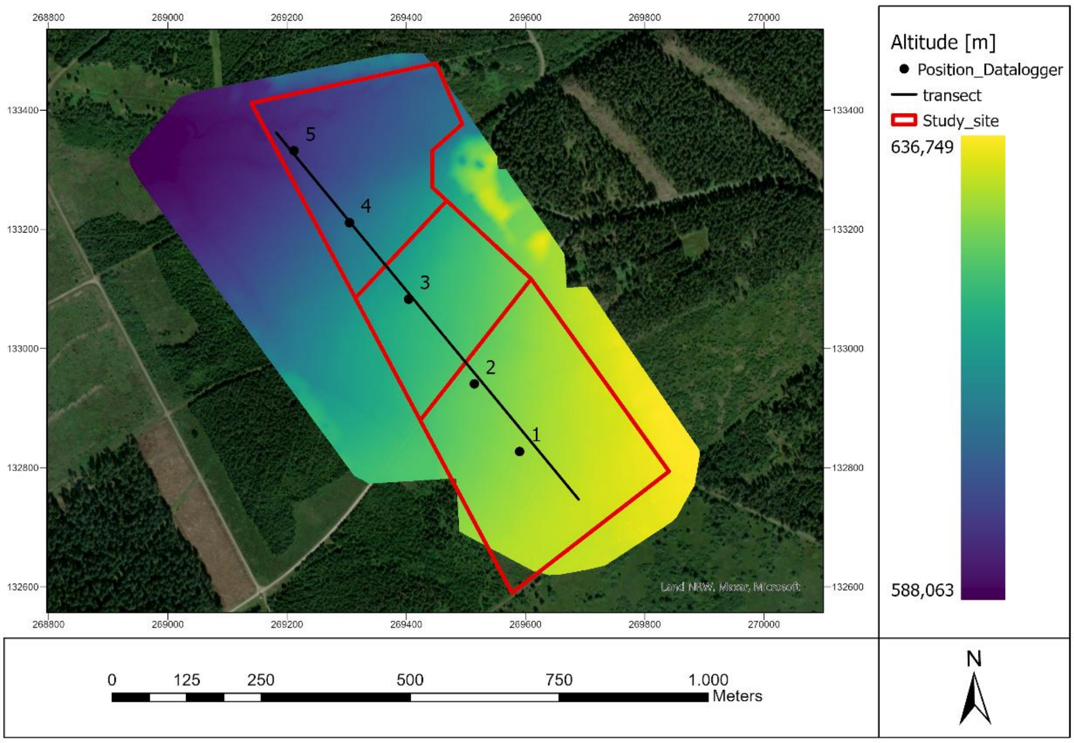

Figure 7: Topography of the study site with the study points position along the study transect.

Starting from the upper side, going south to north, there is first the fenced plateau with denser vegetation, especially towards the eastern part. This area extends to the main road, which marks the limit between the southern plateau and the central plateau. North of this road, the central plateau is populated with young trees that are surrounded by metallic fences. Between this area and the last one, there is a trail that marks the boundary. To the north of this trail, there is the slope going down towards the small river.

The evolution of the altitude along the topographic transect is presented in Figure 8. These 5 locations are study points of the transect where sensors have been placed and certain variables are monitored. Furthermore, as can be seen in Figure 7 and Figure 8, points 1 and 2 are part of the southern plateau, which has a small difference in altitude (7 meters). Point 3 is part of the central plateau, which has a gradient of 10 meters. Finally, points 4 and 5 are part of the slope, which has a gradient of 20 meters.

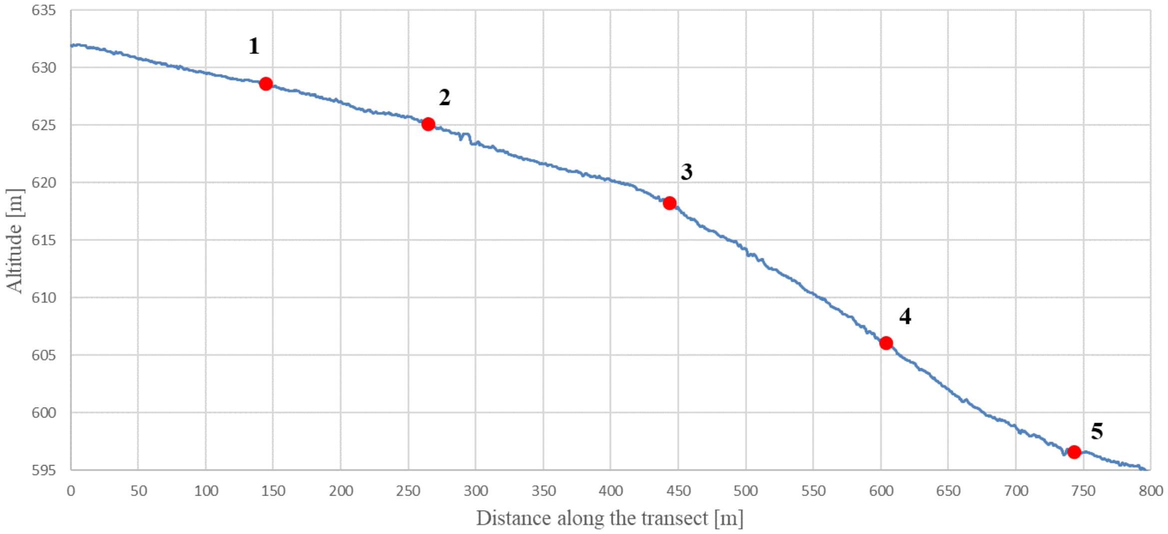

Figure 8: Altitude along the transect with the study points position [58]

This kind of system is interesting because the topography plays an important role on surface as well as subsurface water fluxes. Different results between the different areas are thus expected.

2.4 Pedology

As seen in the soil type map of "WalOnMap" [59] illustrated in Figure 9, the soil of the study site is very rich in organic matter and is mostly classified as "peatlands", represented in red. However, there are also loamy soils with moderate to poor natural drainage. After a few on site studies, it appeared that the peat layer is present throughout the study site with varying depth. The three different parts of the study site presented in Figure 6 are shown in Figure 9 to emphasize the fact that, according to the pedology map from WalOnMap, one same area may be comprised of multiple soil types.

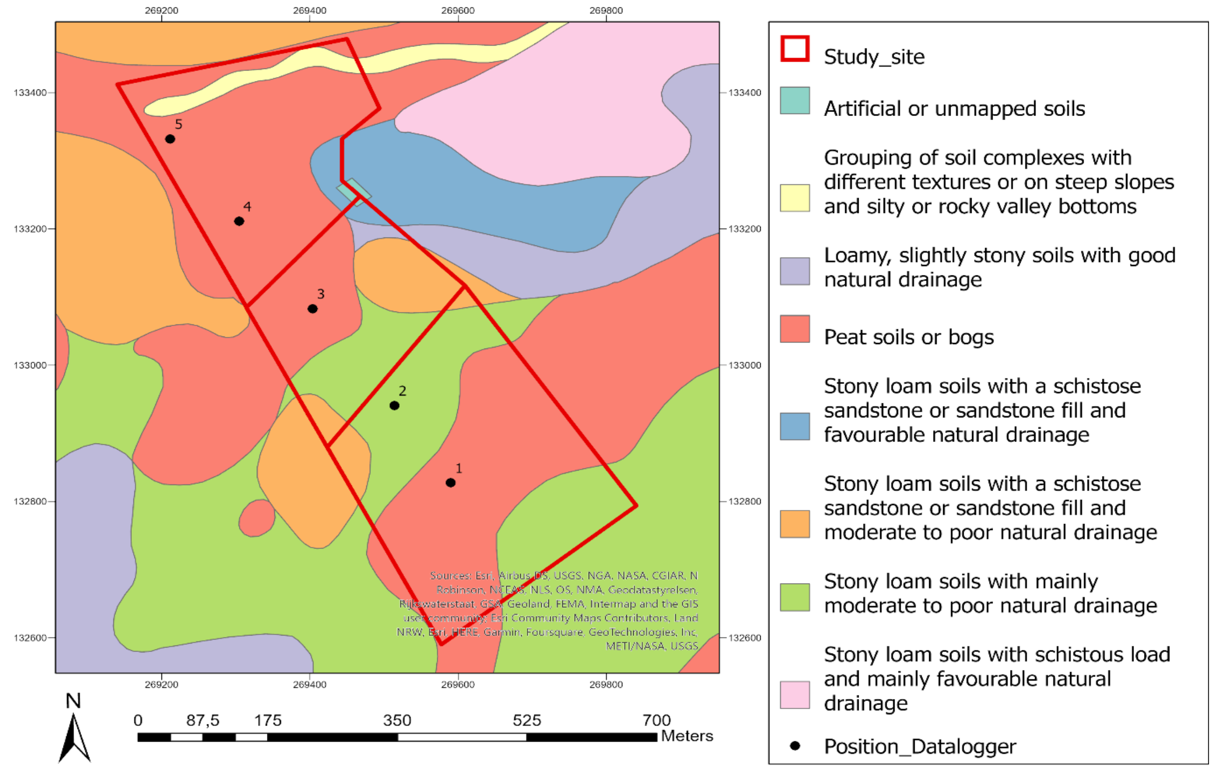

Figure 9: Main soil types covered within the study site and study points localisation [59]

Some drains are still clearly visible in the study field, as it is not uncommon in the Belgian Hautes Fagnes (see 2.1). It is thus likely that the organic matter is fairly humified as it was exposed to aerobic conditions following the drainage. The first observations on the field have shown that the peat of the study site is well humified, as it was very homogeneous with very few distinguishable and identifiable organic matter fragments. However, the soil profiling revealed that the peat was not as homogeneous as we first thought, as some fragments of vegetation, mostly wood pieces, were still distinguishable in some profiles [57].

Actually, in the field, several soil profiles, 1 to 5, were taken along the transect. The result can be seen in Figure 10. There is peat everywhere, even in point 2, but with different depths. Profile 1 and 3 are mostly composed by peat. For the first one and for pit B, after 80 cm depth, there is brown clay. In Profile 3, there is blue-grey clay in the last 20 cm of the profile. Profile 2 is composed of a minority of peat. It is composed by loamy yellow clay with stones between 20 and 70 cm depth. Profile 4-B is composed by brown clay with between 50 and 80 cm depth. Due to the presence of stones, Profiles 2 and 4-B could not be made to a depth of 1 metre. Compared to the other profiles, Profile 2 more or less coincide with the soil map, in the sense that there is little peat and there is stony loam. All other profiles are mainly composed of peat. This corresponds to the soil map. They are also composed of clay, except for profile 5, which is completely composed of peat. We can therefore say that, in general, the field study corresponds to the soil map.

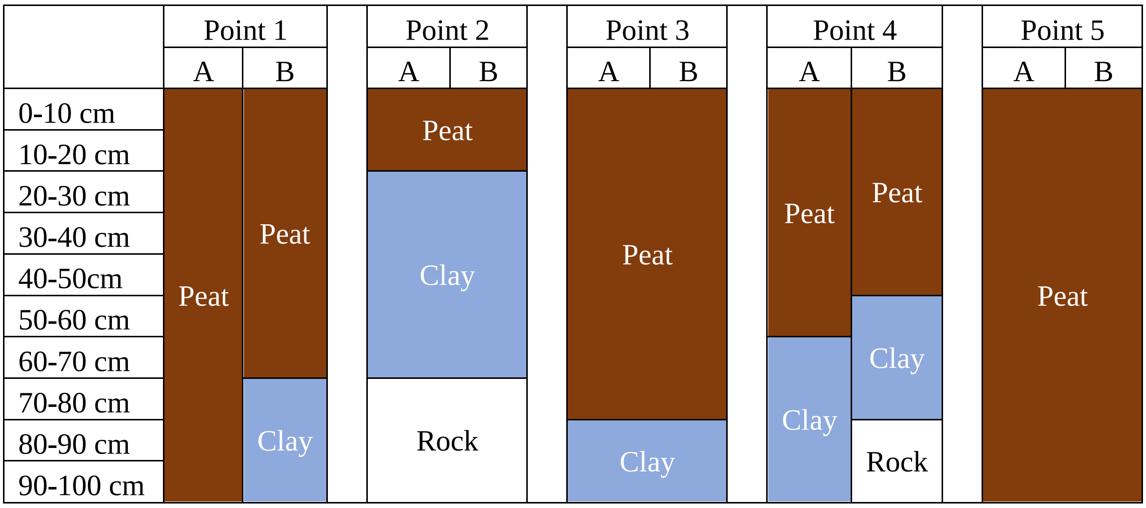

Figure 10: Scheme of different 100 cm soil profiles along the transect

3 Soil Water Retention Curves

3.1 Objectives

The goal is to determine the soil water retention curves corresponding to the evolution of the VWC as a function of suction: $\theta(h)$. This will be done according to the vGM model using these hydraulic parameters: α, n, θ_r and θ_s. Once done, it will give indications on the hydraulic capacity of the soil, depending on its depth.

3.2 Methodology

3.2.1 Sampling

Sampling was done at five locations along the study transect. For each location, there are two replicates: A and B which are separated by a few meters (appendix A). At each of these locations and for each of the replicas, three samples were collected, each at different depths. One sample near the surface, at 10 cm depth. One sample at 30 cm depth. The last sample was collected at a depth varying from 50 cm to 90 cm deep depending on the location and corresponding soil profile. A total of 30 structured samples of 100 cm^3 were collected in so-called Kopecky rings. They were analysed via sandbox and low-pressure plates. Thirty undisturbed samples were collected in plastic bags and were analysed via high-pressure plates.

Table 1: Nomenclature used to differentiate samples according to the location and depth.

LS1A-10	LS1B-10
LS1A-30	LS1B-30
LS1A-80	LS1B-80
LS2A-10	LS2B-10
LS2A-30	LS2B-30
LS2A-50	LS2B-50
LS3A-10	LS3B-10
LS3A-30	LS3B-30
LS3A-90	LS3B-90
LS4A-10	LS4B-10
LS4A-30	LS4B-30
LS4A-55	LS4B-60
LS5A-10	LS5B-10
LS5A-30	LS5B-30
LS5A-60	LS5B-60

As shown in the **Erreur ! Source du renvoi introuvable.**, the samples collected were named according to a certain nomenclature. In this one, "LS" stands for “LandSense”, the name of the global project. The number, ranging from 1 to 5, corresponds to the location of the sample along the study transect. The letter A or B indicates the location of the sample in relation to its replica located a few metres away. Finally, the number (10, 30, 50, ...) indicates the depth at which the sample was collected.

3.2.2 Bulk density

After the use of 100 cm^3 Kopecky samples for the low-pressure plates, all samples spent at least 48h in an oven at 105°c. In this way, the bulk density of each sample can be determined according to this equation:

$$\rho\ Soil = \frac{Weight\ at\ the\ exit\ of\ the\ oven}{Volume\ of\ the\ kopecky} = [\frac{g}{cm^3}] \qquad (1)$$

3.2.3 Soil water retention curves

As shown in **Erreur ! Source du renvoi introuvable.**, eight different pF were analysed. To do this, three equipments were used with adapted samples.

Table 2: Laboratory methods used to determine SWRC and metadata related.

Equipment	Sample	Duration	cm H_2O	bar	pF	Note
Sandbox	Undisturbed (100 cm^3)	10 days	10	0,01	1	
		11 days	31	0,03	1,49	
		11 days	71	0,07	1,85	Air-entry point
Low-pressure plate	Undisturbed (100 cm^3)	11 days	100	0,1	2	
		21 days	251	0,25	2,4	Field capacity
		50 days	1000	0,98	3	
High-pressure plate	Disturbed	15-20 days	3163	3,1	3,5	
		21-22 days	15849	15,54	4,2	Wilting Point

3.2.3.1 Low pF - Sandbox

Saturation is the second step after sampling. The purpose of this type of saturation tank is to saturate the samples from the bottom to minimise the "trapping" of air bubbles in the soil. The water will be able to rise into the sample by capillary action, while keeping the water level constant at the base of the sample.

The principle of the sandbox (appendix B) method is to apply negative pressure, or suction, to soil samples (100 cm^3 Kopecky rings) by means of a suspended water column. To do this, the previously saturated soil samples are placed on a substrate made of a kaolin/sand mixture that serves as a medium between the water column and the samples. The samples are subjected to successive stages of suction applied by moving a small tank connected to the sandbox, the height of which can be varied. At each stage, the samples will lose a certain amount of water until they reach equilibrium with the water column. Equilibrium is reached between 10 and 11 days depending on the pF. To check whether equilibrium has been reached, successive weightings are carried out on control samples to check whether the mass of the samples remains stable. The equilibrium is fixed when there is 0.1g of difference for three days. When the equilibrium is reached, samples are weighted and the volumetric water content is determined according to this equation:

$$\theta = \frac{(Net\ weight - Dry\ soil\ weight)}{Volume * \rho} \qquad (2)$$

where

Net weight = sample weight after concern suction without nylon, elastic and Kopecky rings weight

Dry soil weight = soil weight after spending at least 48h in an oven at 105°c

Volume = Kopecky rings volume, here 100 cm^3

ρ = density of water

Then a higher level of suction can be applied. In this case, the maximum suction that can be exerted on the sand is 71 cm, which corresponds to the air entry point of the substrate.

3.2.3.2 Middle pF – Low pressure plate

In a low-pressure plate extractor, a given air pressure is applied to soil samples placed on a porous plate (appendix C) whose downstream side is connected to atmospheric pressure. The pressure gradient is applied to the liquid phase, which passes through the porous plate and desaturates the sample until the potential equilibrium between the soil water and the applied pressure is reached. The equilibrium is fixed when there is 0.1g of difference in the tubes for three days. This equilibrium is reached between 11 and 50 days depending on the pF. When the equilibrium is reached, samples are weighted and the volumetric water content is determined according to the Equation (2). Then a higher level of pressure can be applied. In this case, the maximum pressure that can be exerted is 0.98 bar. After that, all samples were placed in an oven at 105°c for at least 48 hours. This allows to determine the density of the soil and to calculate the VWC.

3.2.3.3 High pF – High pressure plate

For high-pressure plate extractor, the method is the same as for low-pressure plate extractor except that the pressures exerted are higher. In this case, only the "textural" pores are concerned and that is why disrupted samples are used. These samples were collected in the field near the other samples and stored in plastic bags. These samples were then mixed with a solution of $CaSO_4.2H_2O$ (0,01M). This resulting "slurry" was then placed in PVC rings with 47 mm diameter (appendix D). Three replicas and therefore 3 rings per soil sample were placed on different porous plates: P1 at the top of the plate extractor, P2 at the middle and P3 at the bottom. The equilibrium is fixed when there is 0.01g of difference in the tubes for three days. This equilibrium is reached between 15 and 22 days depending on the pF. When the equilibrium is reached, samples are weighted and the volumetric water content is determined according to this equation:

$$\theta = \frac{(Weight\ of\ soil\ at\ the\ exit\ of\ the\ extractor\ - Dry\ soil\ weight) * \rho\ Soil}{Weight\ of\ soil\ at\ the\ exit\ of\ the\ oven * \rho} \qquad (3)$$

Then a higher level of pression can be applied on new samples. In this case, the maximum pressure that can be exerted is 15.54 bar, which corresponds to the wilting point. After that, all samples were placed in an oven at 105°c for at least 48 hours. This allows to determine the water content by weight of the soil and to calculate the VWC.

3.2.3.4 Outliers detection

Once the raw data were collected, it was processed with Equations (2) and (3) to determine the VWC of each sample at each suction. Once this was done and synthesized, some of the data appeared to be outliers. Indeed, for the high pF (3.5 and 4.2) the data of some plates are inconsistent. Thus, for the B series, at pF = 3.5, θ values of the first plate (P1) are always higher than the values of P2 and P3 which are similar, they are thus considered outliers. At pF = 4.2, there is a large gradient from P1 to P3. Moreover, values from P1 and P2 are higher than their corresponding values at pF = 3.5, which is a nonsense. As a result, the data from P1 and P2 were considered outliers. P3 is indeed giving the lowest water content and we consider these to be the right ones. For the A series, no problem was encountered at pF= 3.5. However, at pF = 4.2, there is also a gradient from P1 to P3 and P3 is significantly lower than the other two plates. In addition, several values of P1 and P2 are higher than their corresponding values at pF = 3.5. These two plates were considered outliers. The presence of these outliers and this heterogeneity within the plates can be due to the fact that the hydraulic conductivities of the plates are different. Therefore, some plates reach equilibrium more slowly because of a lower conductivity. The quality of the contact between the samples and the plate could be put in question but the fact that it is the whole of the data resulting from the same plate makes this hypothesis not very consistent.

3.2.3.5 Use of the RETC program

Several parameters were determined from the fitting of the collected data with the vGM model equation:

$$\theta(h) = \theta r + \frac{\theta s - \theta r}{[1 + (\alpha|h|)^n]^{1-1/n}} \qquad (4)$$

where

θ(h) = water retention curve [cm^3/cm^3]

h = the suction pressure [cm]

θ_s = saturated water content [cm^3/cm^3]

θ_r = residual water content [cm^3/cm^3]

α = form and scale empirical constant [cm^{-1}]

n = form and scale empirical constant [-]

In order to proceed in this direction, the RETC program was used [61]. The program uses the parametric models of vGM to represent the soil water retention curve, and the theoretical pore-size distribution models of Mualem to predict the unsaturated hydraulic conductivity function from observed soil water retention data. Note that the outliers have not been taken into consideration.

In the program, some parameters can be optimised and some parameters can be fixed. In this case, only α and n were optimised. Indeed, values of θ_s and values of the saturated hydraulic conductivity (*Ksat*) were determined using other laboratory methods. The value of θ_r was fixed to 0. The set of parameters used and deduced from this step can be seen in appendix E.

3.2.4 Saturated hydraulic conductivity

In this part that I did not achieve myself, the constant load permeameter method has been used. The principle is to subject the soil sample to a constant hydraulic load for a given period and measure the amount of water that flows through the sample during that time. Permeability is then calculated using Darcy's law, which relates the flow rate of water through the soil sample to the hydraulic load and soil properties such as porosity and pore size.

3.3 Results and discussions

3.3.1 Bulk density

As it can be seen in **Erreur ! Source du renvoi introuvable.**, the density of the peat samples is significantly lower than the density of the clay samples. The density of the latter varies between 0.989 and 1.385 with an average value of 1.2 [g/cm^3] which corresponds to loamy clay while for the peat it varies from 0.122 to 0.385 with an average value of 0.2 [g/cm^3]. This value is in agreement with the meta study of Liu and al., 2019 [15].

According to the literature, decomposition could increase the mass of dry material per volume of peat and therefore the bulk density of peat could increase with depth [14], [60]. But other sources have noted that this link between decomposition and bulk density is not always true [61], [62]. For the results observed here, no relationship is visible between depth and density. For clay samples, an increase of the bulk density with depth is visible. It is due to the compaction process of the soil.

This difference in bulk density between clay and peat soils is primarily due to their composition and physical structure. Clay soils have a higher bulk density due to their high compaction capacity, while peat soils have a lower bulk density due to their porous structure and high organic matter content.

Table 3: Soil type (peat or clay) and density expressed in g/cm^3 of samples.

Sample	**Density [g/cm^3]**	**Soil type**	**Sample**	**Density [g/cm^3]**	**Soil type**
LS1A-10	0,271	Peat	LS1B-10	0,152	Peat
LS1A-30	0,219	Peat	LS1B-30	0,166	Peat
LS1A-80	0,122	Peat	LS1B-80	0,989	Clay
LS2A-10	0,201	Peat	LS2B-10	0,385	Peat
LS2A-30	1,095	Clay	LS2B-30	1,169	Clay
LS2A-50	1,282	Clay	LS2B-50	1,385	Clay
LS3A-10	0,264	Peat	LS3B-10	0,227	Peat
LS3A-30	0,163	Peat	LS3B-30	0,140	Peat
LS3A-90	1,315	Clay	LS3B-90	1,218	Clay
LS4A-10	0,193	Peat	LS4B-10	0,162	Peat
LS4A-30	0,157	Peat	LS4B-30	0,159	Peat
LS4A-55	0,253	Peat	LS4B-55	1,085	Clay
LS5A-10	0,182	Peat	LS5B-10	0,214	Peat
LS5A-30	0,122	Peat	LS5B-30	0,155	Peat
LS5A-60	0,143	Peat	LS5B-60	0,133	Peat

3.3.2 Soil water retention curves

Figure 11 represents the soil water retention curves of LS1A samples and the data points used. The Y axis is the volumetric water content, θ. X axis is the suction in pF. Points are the data points from the three different samples collected. The red points are outliers which are not considered to fit the curves and calculate R^2. Curves are following the vGM model with the parameters optimised using the RETC program. θ_s values at 10 cm depth (0.81) and 30 cm depth (0.93) are consistent for a peaty soil. For LS1A-80 the value is equal to 0.99. This result seems overestimated and can be explained by the fact that θ measurement at pF = 0 was made at the outlet of the saturation tank and not after an equilibrium at h=1cm. At pF = 4.2, the wilting point, θ varies from 0.16 for LS1A-80 to 0.34 for the other two samples. As shown in the legend, R^2 being greater than 0.95, the regression model is considered a good fit to the data.

Figure 12 represents the soil water retention curves of LS1B samples and the data points used. θ_s values at 10 cm depth (0.89) and 30 cm depth (0.96) are consistent for a peaty soil. For LS1B-80 which is clay, θ_s is equal to 0.69. At pF = 4.2, θ varies from 0.19 for LS1B-10 to 0.22 for LS1B-30 and to 0.3 for LS1B-80. As shown in the legend, R^2 being greater than 0.95, the regression model is considered a good fit to the data.

As previously explained, the two pits LS1A and LS1B are located about 5 meters from each other. Therefore, it is interesting to compare the results. The first difference is that the sample at 80 cm depth is peat on one side and clay on the other side. Indeed, in pit A the clay layer began at 100 cm depth while it began at 70 cm depth in pit B. There is thus a variability in peat depth even at small scale. Therefore, its behaviour and its curve are different. LS1A-10 has a lower θ_s and a higher θ at pF = 4.2 than its counterpart. This results in a flatter curve and a less marked air entry point. LS1A-30 and LS1B-30 have a similar behaviour although the latter has a higher θ at pF = 4.2.

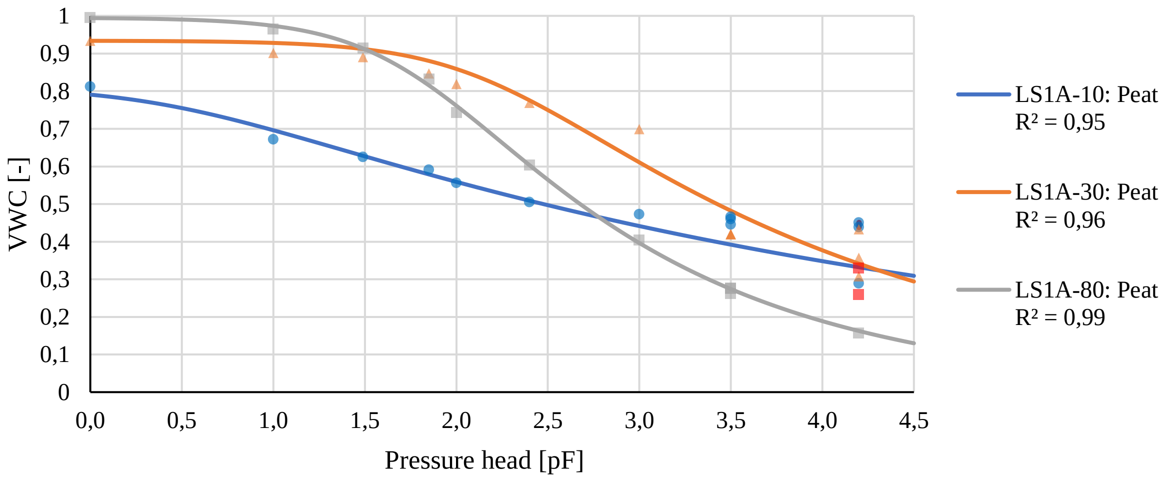

Figure 11: SWRC and data points of LS1A samples at 10, 30 and 80 cm depth

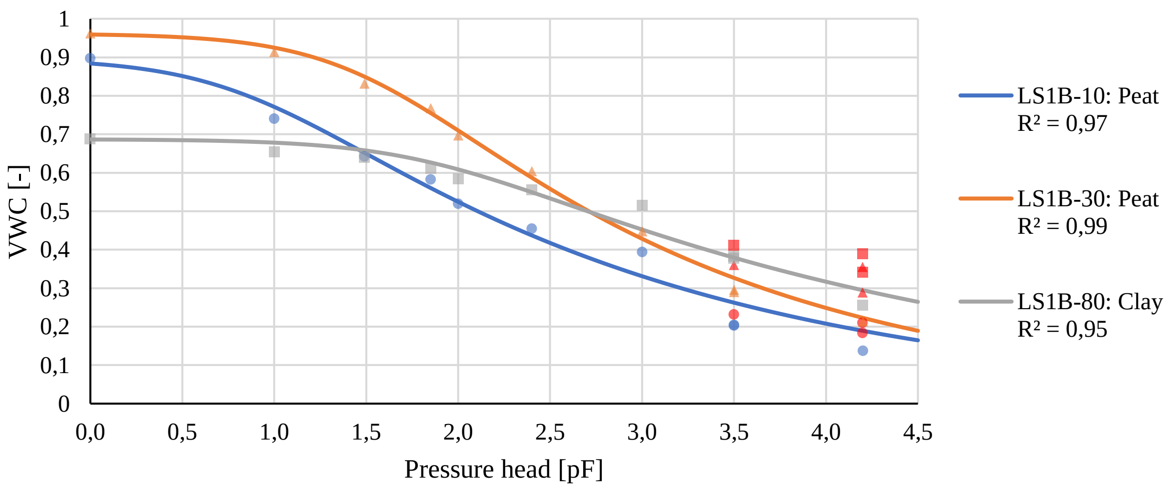

Figure 12: SWRC and data points of LS1B samples at 10, 30 and 80 cm depth

Figure 13 represents the soil water retention curves of LS2A samples and the data points used. θ_s values at 30 cm depth (0.62) and 50 cm depth (0.56) are consistent for a clay soil. For LS2A-10 which is peat, θ_s is equal to 0.93. At pF = 4.2, θ varies from 0.18 for LS2A-10 to 0.23 for LS2A-30 and LS2A-50. R^2 is equal to 0.99 for peat sample, so the regression model is considered a good fit to the data. For the other two samples, the fit of the model is less good.

Figure 14 represents the SWRC of LS2B samples and the data points used. θ_s values at 30 cm depth (0.58) and 50 cm depth (0.54) are consistent for a clay soil. For LS2A-10 which is peat, θ_s is equal to 0.84. At pF = 4.2, θ varies from 0.34 for LS2B-30 to 0.27 for LS2B-10 and to 0.3 for LS2B-50. R^2 is equal to 0.99 for peat sample, so the regression model is considered a good fit to the data. For the other two samples, the fit of the data is less good.

LS2A and LS2B being located about 5 meters from each other, it is interesting to compare the results. The two graphs are similar. The three LS2A samples have the same behaviour and very similar values as their LS2B counterparts.

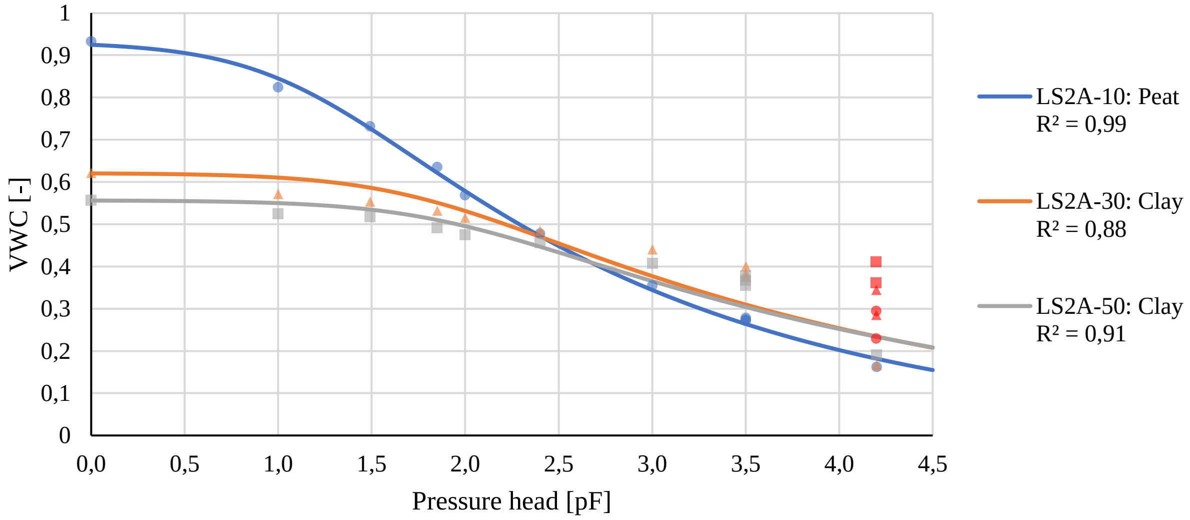

Figure 13: SWRC and data points of LS2A samples at 10, 30 and 50 cm depth

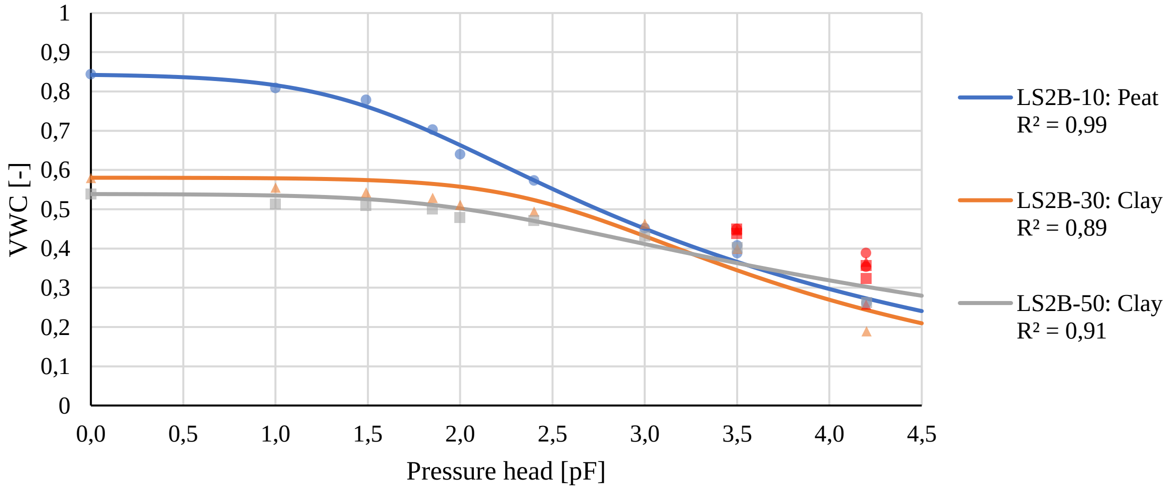

Figure 14: SWRC and data points of LS2B samples at 10, 30 and 50 cm depth

Figure 15 represents the SWRC of LS3A samples and the data points used. θ_s values at 10 cm depth (0.9) and 30 cm depth (0.95) are consistent for a peaty soil. For LS3A-90 which is clay, θ_s is equal to 0.57. At pF = 4.2, θ varies from 0.25 for LS3A-90 to 0.27 for LS3A-30 and to 0.38 for LS3A-10. R^2 being greater than 0.94, the regression model is considered a good fit to the data, especially for peat samples.

Figure 16 represents the SWRC of LS3B samples and the data points used. θ_s values at 10 cm depth (0.94) and 30 cm depth (0.95) are consistent for a peaty soil. For LS3B-90 which is clay, θ_s is equal to 0.6. At pF = 4.2, θ varies from 0.22 for LS3B-30 to 0.34 for LS3B-10 and to 0.38 for LS3B-90. R^2 being close to 1, the regression model is considered a good fit to the data.

LS3A and LS3B being located about 5 meters from each other, it is interesting to compare the results. The two LS3A peat samples have the same behaviour and very similar values as their LS3B counterparts. In both cases, the sample at 10cm depth reacts better to strong suction, it keeps more water. The LS3B-90 clay sample has a better water retention capacity at high suction, going from 0.25 for LS3A-90 to 0.38.

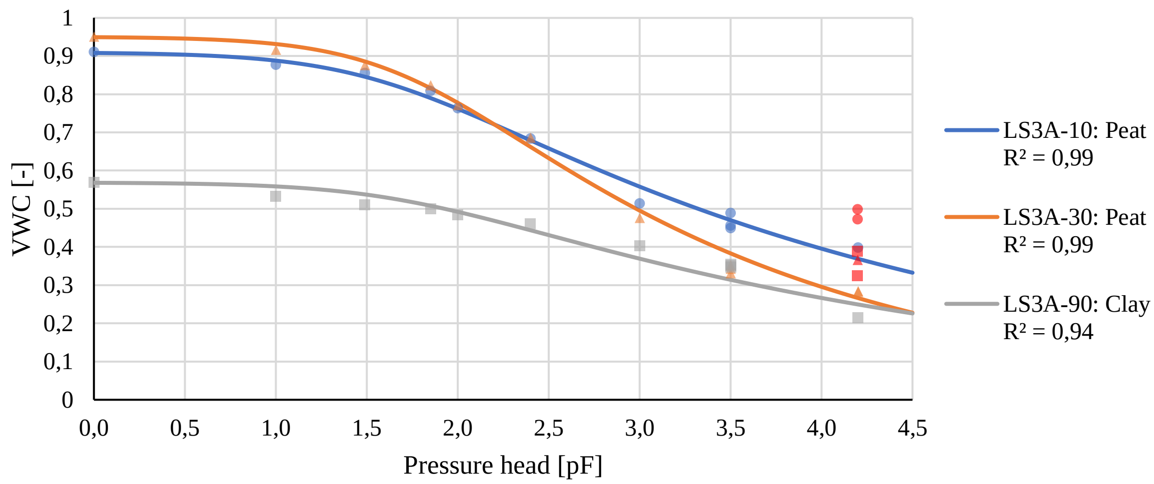

Figure 15: SWRC and data points for LS3A samples at 10, 30 and 90 cm depth

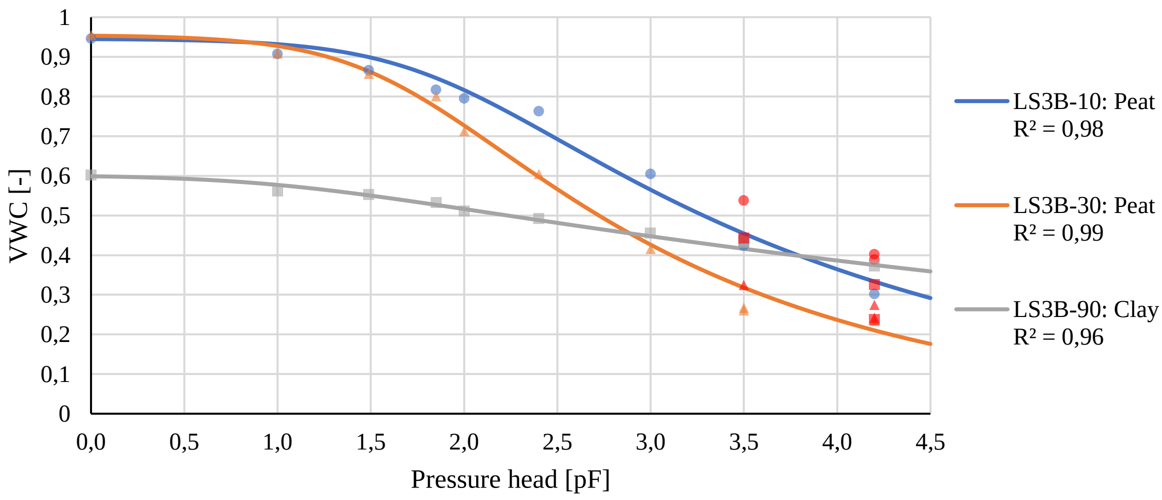

Figure 16: SWRC and data points for LS3B samples at 10, 30 and 90 cm depth

Figure 17 represents the soil water retention curves of LS4A samples and the data points used. θ_s value, 0.92, for the three samples, is consistent for a peaty soil. At pF = 4.2, θ varies from 0.18 for LS4A-30 to 0.22 for LS4A-55 and to 0.35 for LS4A-10. R^2 being greater than 0.92, the regression model is considered a good fit to the data, especially the two deepest samples.

Figure 18 represents the soil water retention curves of LS4B samples and the data points used. θ_s values at 10 cm depth (0.98) and 30 cm depth (0.95) are consistent for a peaty soil. For LS4B-55 which is clay, θ_s is equal to 0.6. At pF = 4.2, θ varies from 0.17 for LS4B-10 to 0.19 for LS4B-30 and to 0.46 for LS4B-55. R^2 being close to 1 for the peat samples, the regression model is considered a good fit to the data. For the clay sample, the fit of the data is less good. But note this curve does not look like a typical clay retention curve. Indeed, θ value at the wilting point is particularly high. This may be due to a strong clay composition, a very fine texture and therefore a very small and regular pore size.

LS4A and LS4B being located about 5 meters from each other, it is interesting to compare the results. The LS4A-10 sample having a smaller θ_s and a larger θ at pF = 4.2, its SWRC indicates a better retention capacity than its counterpart. The LS4-30 peat samples have the same behaviour and very similar values. On one side the sample at 55cm depth corresponds to peat and on the other one, to clay. Therefore, no comparison is possible. This is due to an error during the sampling campaign. The interface between the peat and the clay was located at about 60 cm depth for both pits. LS4A55 is located in the peat layer whereas LS4B55 seems to be in the clay layer and was probably taken a bit below 55 cm depth.

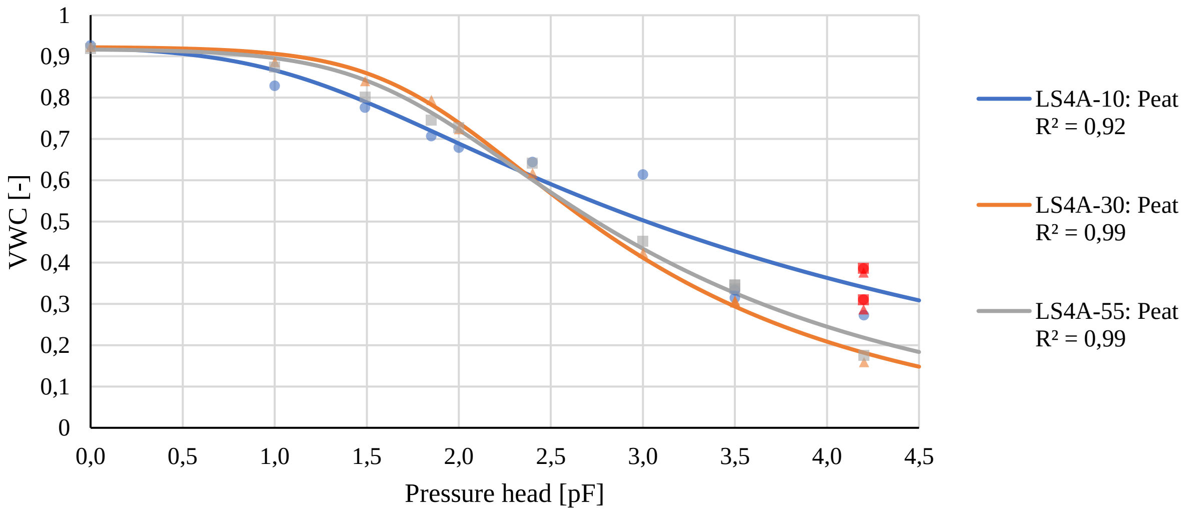

Figure 17: SWRC and data points for LS4A samples at 10, 30 and 55 cm depth

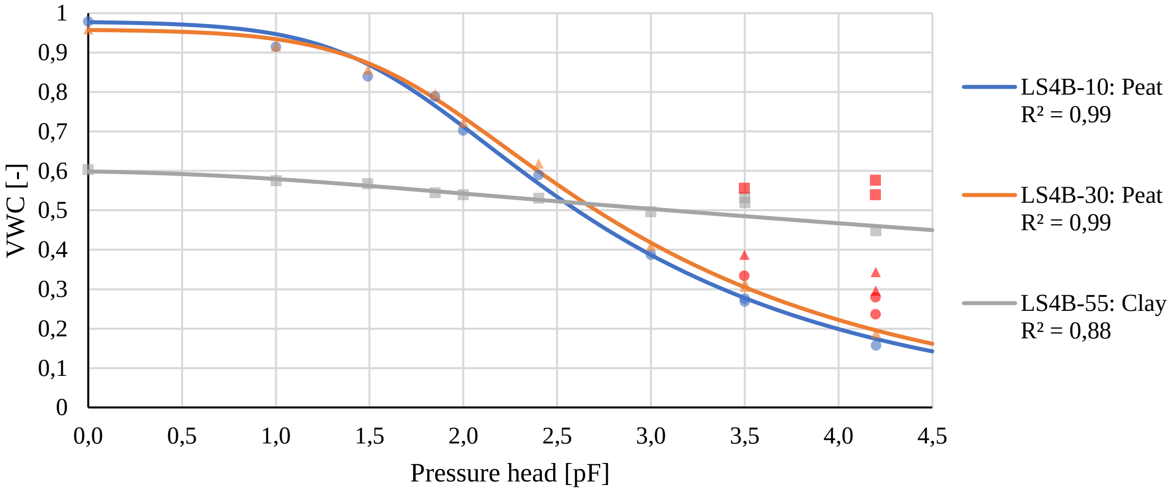

Figure 18: SWRC and data points for LS4B samples at 10, 30 and 55 cm depth

Figure 19 represents the soil water retention curves of LS5A samples and the data points used. θ_s values at 10 cm depth (0.96), 30 cm depth (0.97) and 60 cm depth (0.98) are consistent for a peaty soil but this result seems overestimated for the same reason as explain before. At pF = 4.2, θ varies from 0.13 for LS5A-30 to 0.2 for LS5A-60 and to 0.23 for LS5A-10. R^2 being greater than 0.95, the regression model is considered a good fit to the data.

Figure 20 represents the soil water retention curves of LS5B samples and the data points used. θ_s values at 10 cm depth (0.94), 30 cm depth (0.95) and 60 cm depth (0.98) are consistent for a peaty soil but this result seems also overestimated. At pF = 4.2, θ varies from 0.19 for LS5B-30 and LS5B-60 to 0.25 for LS5B-10. R^2 being greater than 0.93, the regression model is considered a good fit to the data.

LS5A and LS5B being located about 5 meters from each other, it is interesting to compare the results. The LS5A and LS5B samples have the same behaviour and very similar values. The R^2 are in the same range of values as well.

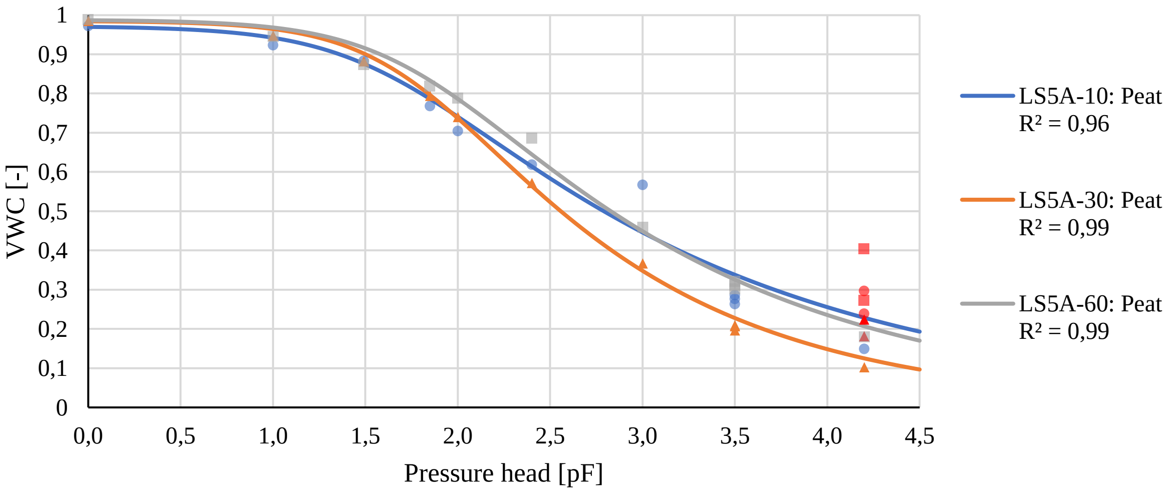

Figure 19: SWRC and data points of LS5A samples at 10, 30 and 60 cm depth

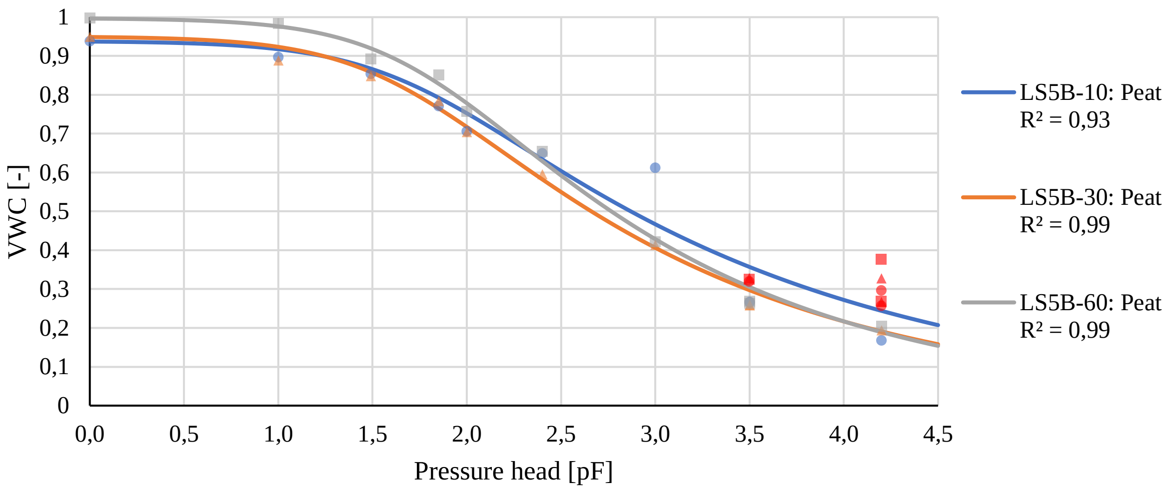

Figure 20: SWRC and data point for LS5B samples at 10, 30 and 60 cm depth

Discussion and summary

As shown in the SWRC set above, a clay soil behaves very differently from a peat soil. Note the fact that clay is based on a visual check, but it is also necessary to consider that there is a certain percentage of silt in these samples called clay. The clay samples have a θ_s ranging from 0.54 to 0.69 with an average of 0.59. According to the HYPRES database (Europe), θ_s value can vary from 0.48 for a fine-textured clay soil (between 0.35 and 0.6 of clay) located in the subsoil to 0.62 for a very fine-textured clay soil (over 60% of clay) located in the surface horizon. Thus, the resulting VWC at saturation looks like very fine-textured clay soil. In this study case, the soil is clayey with a more or less important load of silt according to the samples. While the peaty samples have a θ_s varying from 0.81 to 0.99 with an average of 0.94. Note that some values higher to 0.95 are physically inconsistent but can be explained by the fact that θ measurement at pF = 0 was made at the outlet of the saturation tank and not after an equilibrium at h = 1cm. This range of θ_s values for peat corresponds to the range of θ_s values found in the literature: from 0.75 to 0.95 [15], [61]. Also, at the wilting point, at pF = 4.2, the clay has θ ranging from 0.23 to 0.46 with an average of 0.30. At the wilting point, a clayey silt soil has a volume water content of 0.1, a silty clay soil has a θ of 0.2 and a clay soil can reach a θ of 0.4 [63], [64]. So, in this case, the soil is clayey with a more or less important load of silt according to the samples. The θ of the peat, at the wilting point, varies from 0.13 to 0.38 with an average of 0.24. This range of value corresponds to literature value [61]. Clay samples having a significantly lower θ_s and a higher volumetric water content at high suction, they have a better water retention capacity with an air entry point that requires a higher suction. This can be explained by the fact that clay soils have a layered structure and a high electrical charge, which means that clay particles have a high affinity for water and can retain water in their pores. In addition, clay particles are very small and have a large specific surface area, which allows them to hold water in large quantities. In contrast, peat soils consist of partially decomposed organic matter, which is relatively light and porous. Although the pores of peat soils can hold large amounts of water, the porous structure does not allow for as effective water retention as in a clay soil.

Regarding the co-efficient of determination (R^2), it varies between 0.92 and 0.99 for the peat samples and between 0.88 and 0.96 for the clay samples. It should be noted that on the whole of the R^2, only three are below 0.9. The three samples concerned are clayey. Overall, the values of the model fitting parameters are obtained with very high coefficients of determination for both soils. This reflects the good accuracy of the retention model parameters in describing the observed data. But it should be kept in mind that outliers have not been considered. Moreover, the results indicated that there is a trend towards better model performance, a greater R^2, for soils with higher degree of decomposition, and thus more rigid, mineral soil-like behaviour. This fact is also observed by Dettmann and al., 2014 [65].

The vGM model was originally developed to model unsaturated flow in mineral soils. This model assumes that soil properties are homogeneous and isotropic, and that there is a continuous pore size distribution in the soil. However, peat soils are organic soils that have a particular structure due to the presence of decaying organic matter. Peat soils tend to have a more heterogeneous pore structure than mineral soils, with a narrower pore size distribution and larger, more irregular pores. From a theoretical point of view, because of these structural peculiarities, it can be difficult to use the vGM model to model the relationship between water content and suction in a peat soil accurately [65]. But in fact this model is frequently used to model the hydrology of peatlands [61], [62], [66]. According to these studies, bimodal or trimodal vGM models may better describe the unsaturated hydraulic conductivity curves. However, unsaturated hydraulic parameters in a variety of peat soils have been successfully estimated using the vGM unimodal model. Moreover, bimodal or trimodal vGM models may better describe peat with little decomposition, which is not the case on this study and based on the data, a bimodal does not correspond. Therefore, in this study case, the observed water retention curve data show a quite unimodal behaviour, thereby justifying the use of the vGM model.

3.3.3 Saturated hydraulic conductivity

As shown in Table 4, the range of saturated hydraulic conductivity values varies from 10^{-7} to 10^{-3} m/s for peat samples with a mean value of 10^{-4} m/s. This range of values is consistent with several meta studies. The more decomposed a peat is, the smaller its K_{sat} will be. Conversely, the less decomposed the peat, the larger its K_{sat}. Thus, a weakly decomposed peat can have a value ranging from 10^{-3} to 10^{-5} m/s. A strongly decomposed peat can have a value ranging from 10^{-5} to 10^{-7} m/s [61], [67]. It is logical with the fact that a high saturation hydraulic conductivity indicates that the soil is permeable and water can flow through it quickly thanks to the larger pores. In contrast, a low saturated hydraulic conductivity indicates that the soil is less permeable and water flows more slowly as only small pores are present. The peat of this study site is thus moderately decomposed. The mean value of K_{sat} for peat at 10 cm depth is 3.23×10^{-4}, the mean value for peat at 30 cm depth is 1.4×10^{-4} and the mean value for deepest peat is 7.76×10^{-5}. These values agree with the above justification.

The range of saturated hydraulic conductivity values varies from 10^{-6} to 10^{-3} m/s for clay samples with a mean value of 10^{-4} m/s. However, these values are out of the ordinary. Indeed, the range of values of saturated hydraulic conductivity for clay soil is generally very low and can vary from 10^{-11} to 10^{-6} m/s. This is due to the high proportion of clay particles that make up the clay soil and that can limit the movement of water in the soil. This difference may be due to the fact that the clay here is rather clayey-silty or has a structure with larger pores which explains the higher K_{sat}. A more precise textural analysis would be necessary. For both peat and clay, no trend is observed along the transect. Moreover, even replicates generally have a difference of a factor of 10.

Table 4: Soil type (peat or clay) and Ksat expressed in m/s of samples.

Sample	K_{sat} (m/s)	Soil type	Sample	K_{sat} (m/s)	Soil type
LS1A-10	1,26E-03	Peat	LS1B-10	3,00E-04	Peat
LS1A-30	6,23E-05	Peat	LS1B-30	2,19E-04	Peat
LS1A-80	3,44E-05	Peat	LS1B-80	1,40E-03	Clay
LS2A-10	1,55E-04	Peat	LS2B-10	1,65E-04	Peat
LS2A-30	1,13E-06	Clay	LS2B-30	4,78E-06	Clay
LS2A-50	9,35E-05	Clay	LS2B-50	1,48E-06	Clay
LS3A-10	1,75E-04	Peat	LS3B-10	9,63E-06	Peat
LS3A-30	4,03E-04	Peat	LS3B-30	3,80E-05	Peat
LS3A-90	6,05E-06	Clay	LS3B-90	8,21E-05	Clay
LS4A-10	2,70E-04	Peat	LS4B-10	1,74E-05	Peat
LS4A-30	5,93E-06	Peat	LS4B-30	5,50E-07	Peat
LS4A-55	1,94E-04	Peat	LS4B-55	2,06E-04	Clay
LS5A-10	4,66E-04	Peat	LS5B-10	4,15E-04	Peat
LS5A-30	7,57E-07	Peat	LS5B-30	3,88E-04	Peat
LS5A-60	8,10E-05	Peat	LS5B-60	1,36E-06	Peat

3.4 General discussion

The following figures represent scatter plots of the saturated hydraulic conductivity and the VWC at saturation over density for peat and clay. Red lines represent trend lines. For peat, in Figure 22, there is an increase of K_{sat} with the density. This relationship is not instinctive because if the bulk density increases, the porosity decreases and there is less place for water flux. Although peat bulk density may be related to saturated hydraulic conductivity, there are several other factors (like the structure of the peat, its water content, its porosity and its chemical composition) that must be considered to fully understand the relationship between these two parameters. In Figure 21, there is a decrease of the bulk density with θ_s. This relationship makes sense because as the peat sample contains more water, θ approaches 1, indicating a lower proportion of dry soil in the sample. Thus, the bulk density is decreased.

About the clay, in Figure 24, there is a decrease of the saturated hydraulic conductivity with the bulk density. This makes sense because if the density is higher, the porosity is smaller and the water flux is smaller. In Figure 23, there is a decrease of the bulk density with θ_s which is more logical.

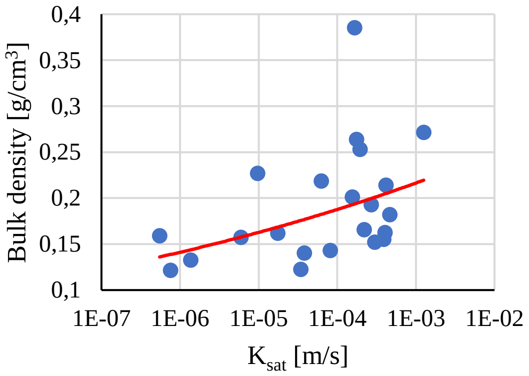

Figure 22: Scatter plot of Ksat and bulk density with related trend line for peat samples

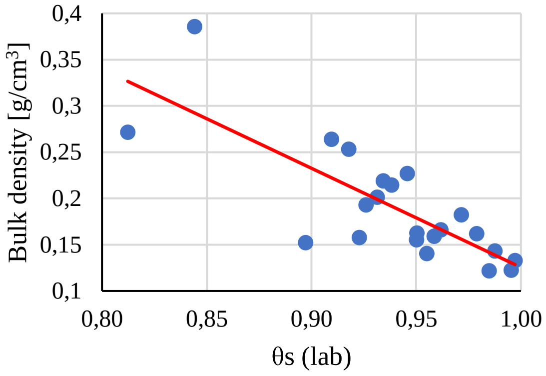

Figure 21: Scatter plot of θs and bulk density with related trend line for peat samples

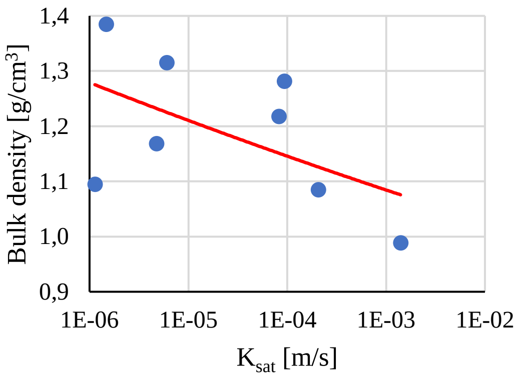

Figure 24: Scatter plot of Ksat and bulk density with related trend line for clay samples

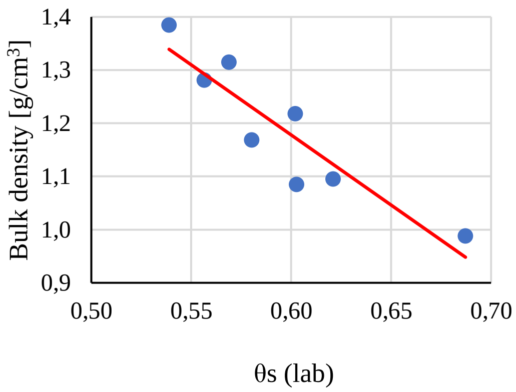

Figure 23: Scatter plot of θs and bulk density with related trend line for clay samples

3.5 Conclusion

The acquisition of samples in the field allowed a more in-depth study of the hydrological properties of the soil in the laboratory. Indeed, the density, K_{sat} and a retention curve could be determined for each sample. The two types of soil analysed, clay and peat, each have their own intrinsic characteristics and therefore have their own hydrological behaviour. Thus, a peaty soil has an average bulk density of 0.2 [g/cm^3] and a clayey soil of 1.2 [g/cm^3]. As far as the retention curves are concerned, the behaviour of clayey samples clearly indicates a better water retention. However, the peaty samples have a very high θ_s close to 1. Knowing that this type of soil is constantly saturated, it has a huge water storage capacity. Based on the values obtained for the hydraulic parameters of the "clay" samples, this soil can be characterized as sometimes clayey and sometimes clayey silt. However, it is important to note that these estimates are not definitive and that further tests, such as particle size analysis, are needed to accurately determine the soil type. SWRC and parameters related agree with the literature. Note that this conclusion was drawn for dewatering conditions. Wetting conditions and hysteresis effects were not analysed.

4 TDR – VWC time series

4.1 Objective

The objective of this part is to understand and visualize several time series of the volumetric water content at several depths and at several places within the plot. Some differences between the two substrates present, peat and clay, can be highlighted and conclusions will be drawn.

4.2 Methodology

4.2.1 Installation

The first step was to dig the pits, put in the TDR probes and backfill them. As shown in Figure 7, five positions along the study transect, spaced about 150 meters apart, were considered. Several criteria were important in the selection of these positions. The criteria are: soil type and structure, topography and soil electrical conductivity. For each location, there is a replica, so two pits dug. These are more or less 5 meters apart, perpendicular to the slope and in the same type of vegetation. In each pit, three TDR probes were placed at different depths. There is a probe at 10cm, one at 30cm and the last one is located between 50 and 90 cm depth depending on the location (Appendix F). The objective was to put the third probe in the clay layer when it was possible, thereby explaining the different depths for the deepest probes. There are therefore 30 probes in total and 5 dataloggers.

4.2.2 Sensors and dataloggers

TEROS 12 probes (Figure 25) have a nomenclature as shown in Table 1. Its measurement period is 10 minutes. It is mainly placed in peat and clay. TEROS 12 sensors use an electromagnetic field to measure the dielectric permittivity of the surrounding medium. The sensor supplies a 70-MHz oscillating wave to the sensor rods, which charge according to the dielectric of the material. The charge time is proportional to substrate dielectric and substrate VWC. The TEROS 12 microprocessor measures the charge time and outputs a raw value based on the substrate dielectric permittivity. The raw value is then converted to VWC by a calibration equation specific to the substrate [68].

Figure 25: TEROS 12 probe [66]

Figure 26: ZL6 Data logger connected to the probes.

The ZL6 (Figure 26) serve as a data collection station for six sensors and is therefore placed between the two pits in order to best wire the probes. It is designed for plug-and-play setup with TEROS 12 soil moisture sensors. The solar panel faced south to give it the maximum amount of sunlight. The ZL6 makes a measurement from each of the sensor ports in use every 60 s. When the ZL6 internal clock reaches the user-configured measurement interval, here 10 minutes, the ZL6 processes and stores the results from all the 60-s sensor readings taken since the last storage interval. So, the stored results are a simple average of the per-minute readings. It is necessary to return periodically to the site to download the stored data and to check the logger [69].

4.2.3 Calibration

4.2.3.1 Mineral soils

According to METER[1] tests, a single calibration equation will generally suffice for most mineral soil types. A linear equation is used and provided by METER for the mineral soil calibration because it provides the best predictions of VWC in the range of VWC found in mineral soils. However, METER also provides a precise protocol for self-calibration based on unstructured collected samples. In this way, a new calibration was determined in order to compare it with the one provided by METER.

The first step is to collect a relatively large sample of clay soil. Then this sample is dried for several weeks. This is logistically easier than putting all the samples in the oven (48h at 105°c). Moreover, as long as the samples are dry enough to be crushed and sieved, there is no need to put them in the oven. After that, a 2 mm sieving is necessary. Once this step completed, the calibration could take place. The sample is placed in a graduated bucket. The probe must be able to be placed in the middle of the sample. The initial water content of the dried clay is measured by taking a 100 cm^3 sample and placing it in a 105°c oven. It can be calculated by the following equation:

$$Initial\ water\ content = Volume\ of\ calibration\ sample * \frac{(Wet\ soil - Dry\ soil)}{100} \quad (5)$$

Then, a quantity of water, previously weighed, is poured into the sample. Once the sample homogenized, the TEROS probe is placed in the sample to determine the raw data. The real

[1] METER is the company that produces the TDR equipment.

VWC is known based on the initial VWC of the dried soil, the volume of soil and the volume of water added:

$$\theta = \frac{Cumulative\ water\ volume}{Volume\ of\ calibration\ sample} \qquad (6)$$

After this, the probe must be cleaned. These last three steps are repeated several times. Finally, for each raw data, a calculated VWC value can be associated. This set of data points allows the establishment of a calibration curve (Figure 27). Being close to the provided model and R^2 being close to 1, the calibration has been kept.

Knowing that, in this study case, clay is saturated, raw data ranges from 2900 to 3300, a polynomial calibration would provide VWC values close to 1. This order of magnitude is not consistent for clay soil. This consolidates the fact that a linear equation is more suitable for a clay soil. The calibration made in laboratory gives higher VWC values than the calibration provided by METER. This difference is not abnormal since the METER calibration is valid for most mineral soils and the self-calibration is specific to the study area.

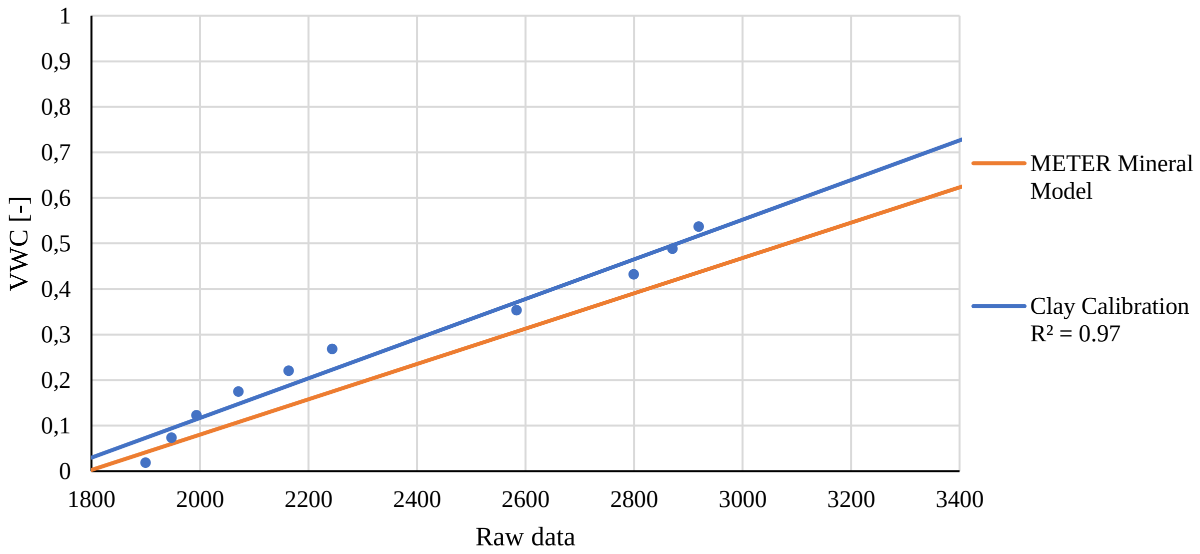

Figure 27: Calibration line in blue based on laboratory experiences and calibration model provided for mineral soils giving the VWC related to the raw data.

4.2.3.2 Soilless media

TEROS 12 sensors are calibrated in potting soil, perlite, and peat. The goal is to create a generic calibration equation that will work in many substrates with an accuracy of better than 0.05 m^3/m^3. For higher accuracy, performing a media-specific calibration should improve the accuracy to 0.01 to 0.02 m^3/m^3. The differences between mineral soil and soilless media calibrations are caused by high-air volume in the organic soils that lowers the starting dielectric of the sensor [68]. In order to increase the precision and to have a calibration specific to the samples, the same manipulations as Section 4.2.3.1 are done. So, for each raw data, a calculated VWC value can be associated and the establishment of a calibration curve can be done (Figure

28). Being close to the provided model and R^2 being close to 1, the peat calibration has been considered.

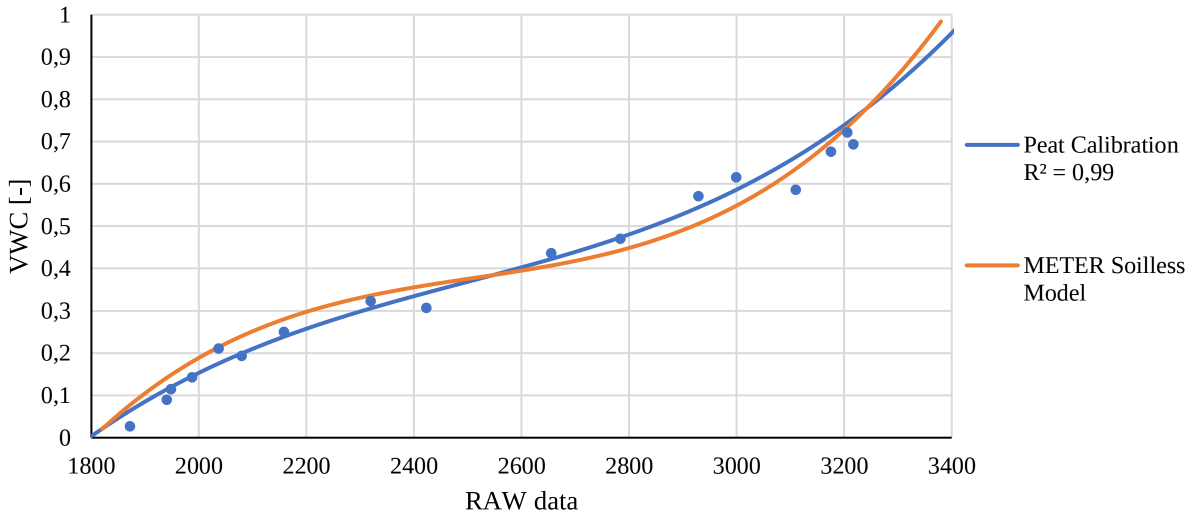

Figure 28: Calibration curve in blue based on laboratory experiences and calibration provided model for organic soils giving the VWC related to the raw data.

4.3 Results

Figure 29 shows the data precipitation from the meteorological station of Mont-Rigi. The frequency of the data is 10 minutes and the data set is from October 2022 to early May 2023. November 2022, December 2022, January 2023 and March 2023 are the wettest months. In general, there is less than 1mm of rain per 10 minutes during the observed months. Rainy events where it rains more than 1.5 mm are rather rare. There are also many days when there is no rain at all. From October 2022 to January 2023, there is an increase in cumulative rain.

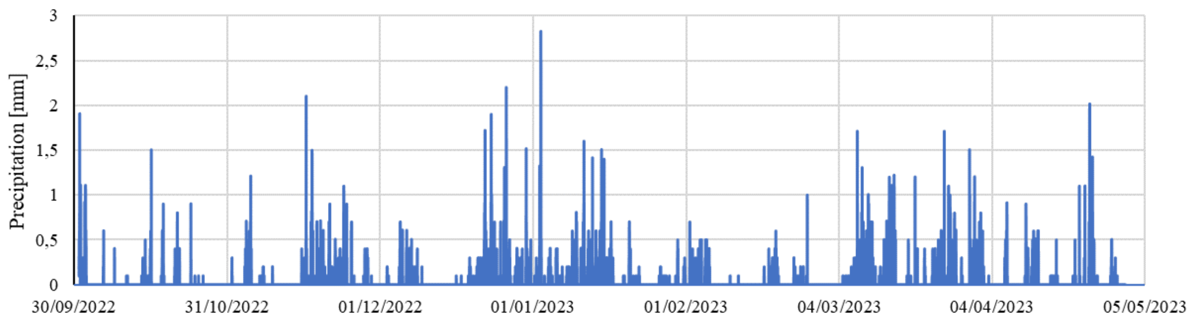

Figure 29: Precipitation level (mm) with a frequency of 10 minutes from October 2022 to May 2023

Figure 30 represents the volumetric water content time series for LS1A sensors at 10, 30 and 80 cm depth. The X axis represents the VWC. The Y axis represents the time from October 2022 to May 2023. The value of θ for LS1A-10 ranges from 0.81 to 0.86. For LS1A-30 it ranges from 0.84 to 0.87 and for LS1A-80 from 0.88 to 0.9. As shown in the graph, along the depth, there is a sensitivity gradient to the drainage and the upper boundary condition, including rain and evaporation. Indeed, θ near the surface, at 10 cm depth is more sensitive than θ at 30 cm depth and at 80 cm depth, VWC is almost constant. There is a global increase of θ from October to January then a stagnation to May but it is light and it is globally constant.

Figure 31 represents the VWC time series for LS1B sensors. The value of θ for LS1B-10 ranges from 0.78 to 0.81. For LS1B-30 it ranges from 0.83 to 0.86 and for LS1B-80 from 0.7 to 0.71. As shown in the graph, there is a sensitivity gradient along the depth. At 80 cm depth VWC is constant because of the presence of clay. There is a global increase of θ from October 2022 to January 2023 then a stagnation to May but it is light and it is globally constant.

As previously explained, the two pits LS1A and LS1B are located about 5 meters from each other. Therefore, it is interesting to compare the results. Beyond the fact that the soil type is different at 80 cm depth, the two peat time series have the same shape and are in the same range of values. Considering the behaviour of SWRC at 30 cm depth, the water table is located near this depth. The small increases observed, especially at 10 and 30 cm depth, in December and March can be explained by the high precipitation at these times as shown in Figure 29.

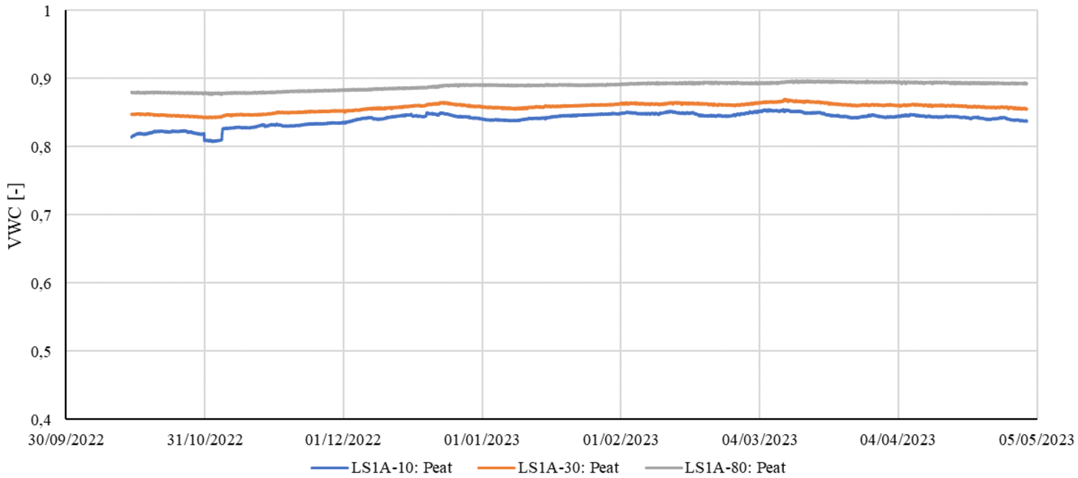

Figure 30: VWC time series for LS1A sensors at 10, 30 and 80 cm depth

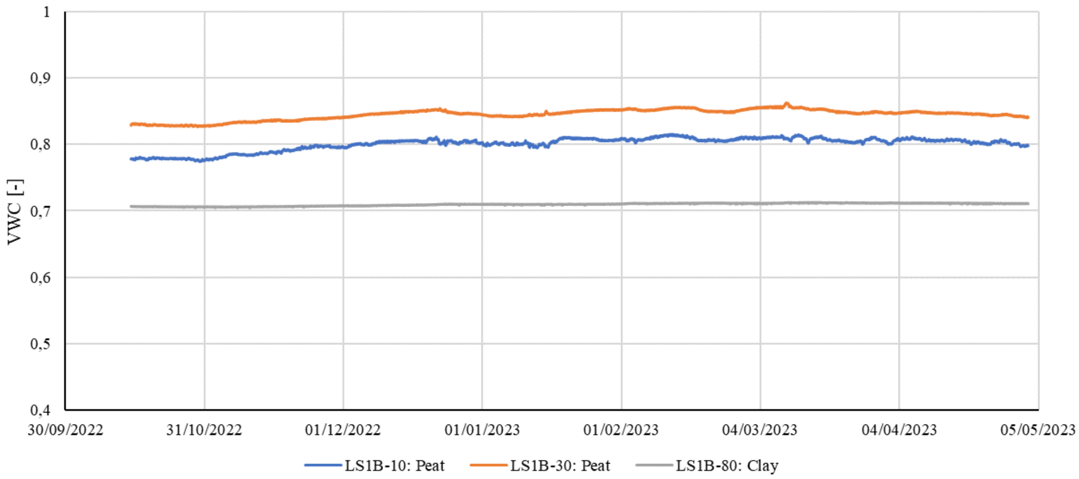

Figure 31: VWC time series for LS1B sensors at 10, 30 and 80 cm depth

Figure 32 represents the VWC time series for LS2A sensors. The value of θ for LS2A-10 ranges from 0.77 to 0.85 with greater variability in October and November. For LS2A-30 it ranges from 0.57 to 0.60 with an increase from October to January. For LS2A-50, VWC ranges from 0.56 to 0.57. There is a difference in sensitivity depending on the soil type. Indeed, θ for peat is more sensitive than clay which is almost constant.

Figure 33 represents the VWC time series for LS2B sensors. The value of θ for LS2B-10 ranges from 0.48 to 0.57 with greater variability from October to December. For LS2B-30 it ranges from 0.54 to 0.55 and for LS2B-50 from 0.51 to 0.52. There is a difference in sensitivity depending on the soil type. The VWC of clay is constant over time.

LS2A and LS2B being located about 5 meters from each other, it is interesting to compare the results. For clay, the behaviour and the range of θ (0.5 – 0.6) are the same. For peat, the VWC is much more important (~ 0.85) for LS2A-10 than for LS2B-10 (~ 0.55) and same variations occur at the same time. These variations could be due to an error of the probes. Considering the behaviour of SWRC at 30 cm depth, the water table is located at this depth or higher.

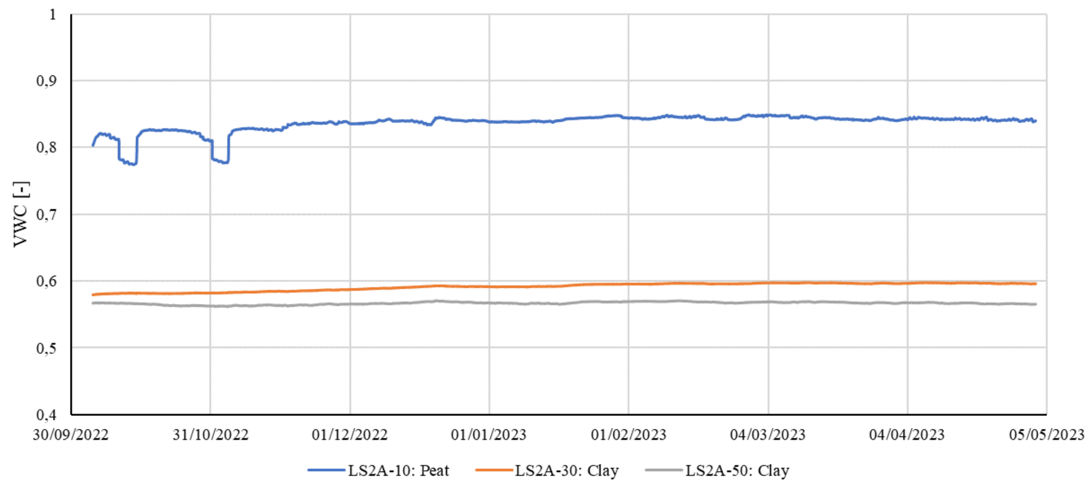

Figure 32: VWC time series for LS2A sensors at 10, 30 and 50 cm depth

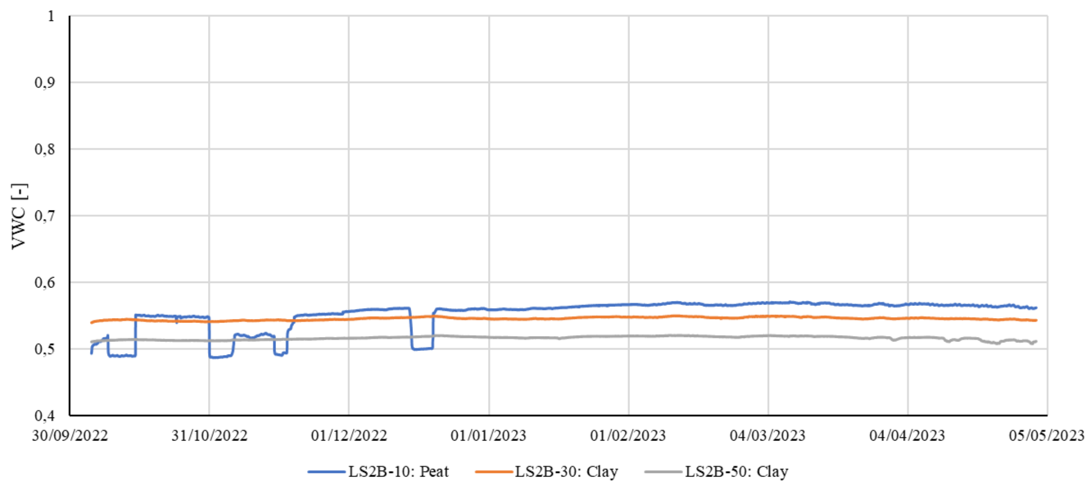

Figure 33: VWC time series for LS2B sensors at 10, 30 and 50 cm depth

Figure 34 represents the VWC time series for LS3A sensors. The value of θ for LS3A-10 ranges from 0.80 to 0.83 with a first increase from mid-November to mid-December and a second increase from mid-January to mid-February. For LS3A-30 it ranges from 0.88 to 0.92 with an increase from October to mid-December. For LS3A-90 the VWC is equal to 0.61. There is a difference in sensitivity depending on the soil type.

Figure 35 represents the VWC time series for LS3B sensors. The value of θ for LS3B-10 ranges from 0.85 to 0.88 with an increase from October to mid-December. For LS3B-30 it ranges from 0.97 to 1.0 with the same increase and for LS3B-90 θ is equal to 0.59. This value of 1 is due to the fact that the calibration is not exact for this sensor. There is a difference in sensitivity depending on the soil type.

LS3A and LS3B being located about 5 meters from each other, it is interesting to compare the results. For clay, the behaviour and the range of θ (0.6) is the same. But for peat, the VWC is much more important for B sensors than for A sensors due to θ_s value greater for B than for A. Same variations occur at the same time. Considering the behaviour of SWRC at 90 cm depth, the water table is located between 30 and 90 cm depth. The small increases observed, especially at 10 and 30 cm depth, in December and March can be explained by the high precipitation at these times as shown in Figure 29.

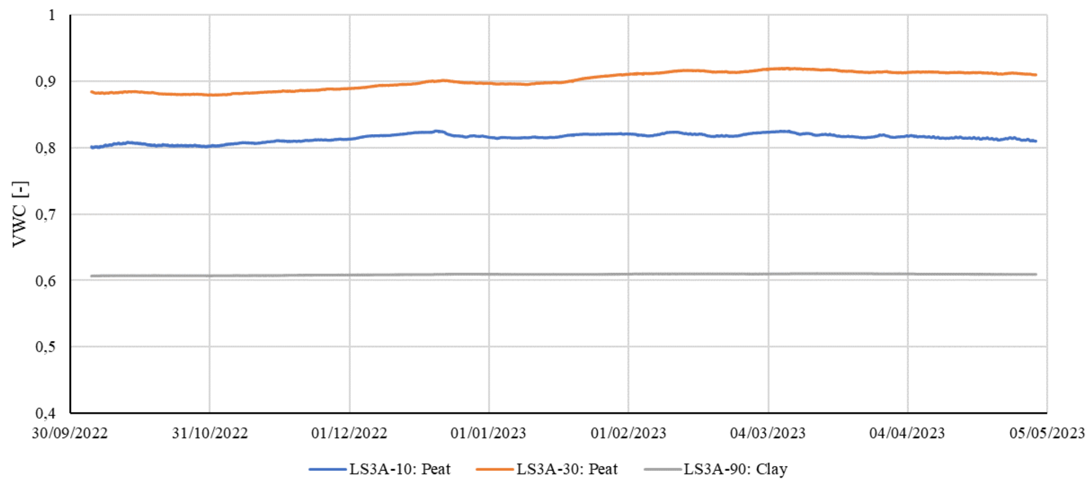

Figure 34: VWC time series for LS3A sensors at 10, 30 and 90 cm depth

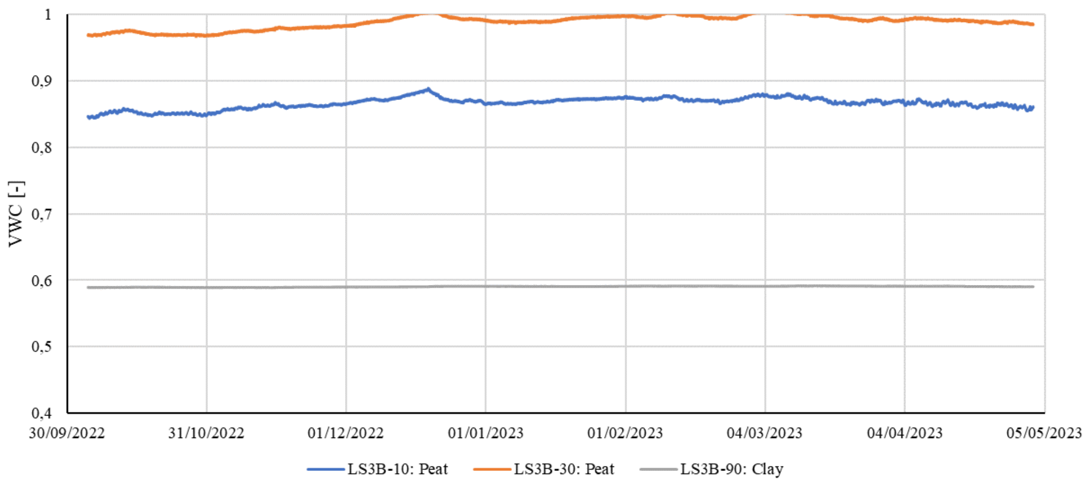

Figure 35: VWC time series for LS3B sensors at 10, 30 and 90 cm depth

Figure 36 represents the VWC time series for LS4A sensors. The value of θ for LS4A-10 ranges from 0.91 to 0.96 with an increase from October to December. For LS4A-30 it ranges from 0.88 to 0.95 with an increase from November to February. For LS4A-55 θ ranges from 0.54 to 0.87. There is a difference in sensitivity depending on soil type and on the depth. The value of VWC is more sensitive at the surface than at depth.

Figure 37 represents the VWC time series for LS4B sensors. The value of θ for LS4B-10 ranges from 0.79 to 0.99 with a big increase from November to January. For LS4B-30 it ranges from 0.87 to 0.91 with an increase from November to January. For LS4B-55 VWC ranges from 0.59 to 0.61. There is a difference in sensitivity depending on soil type and on the depth.

LS4A and LS4B being located about 5 meters from each other, it is interesting to compare the results. Beyond the fact that the soil type is different at 80 cm depth, LS4A-30 and LS4B-30 have the same shape and are in the same range of values. LS4B-55 is much more sensitive compared to LS4A-55, exhibiting a larger range of values. Considering the behaviour of SWRC at 55 cm depth, the water table is located near this depth. The increases and the sensitivity observed during November and December, especially at 10, can be explained by the high precipitation at these times as shown in Figure 29.

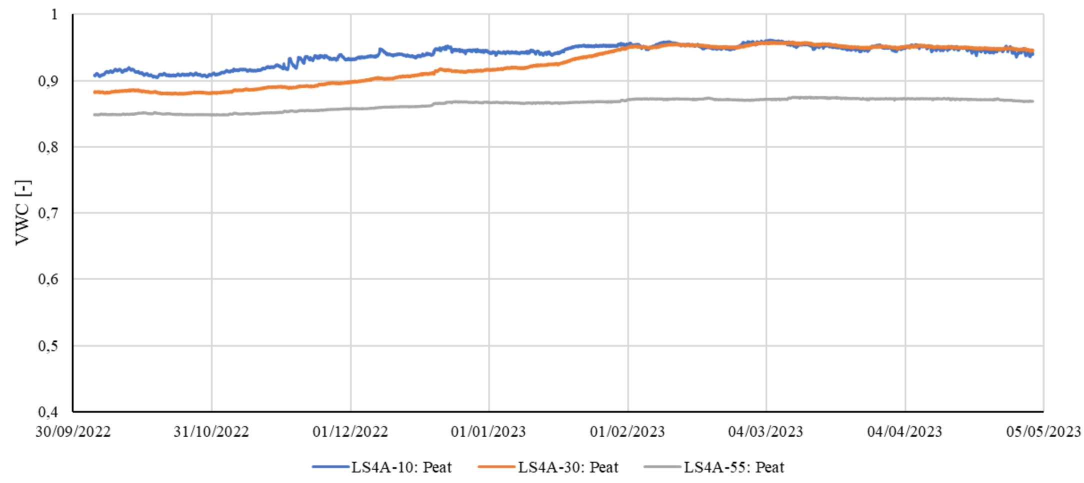

Figure 36: VWC time series for LS4A sensors at 10, 30 and 55 cm depth

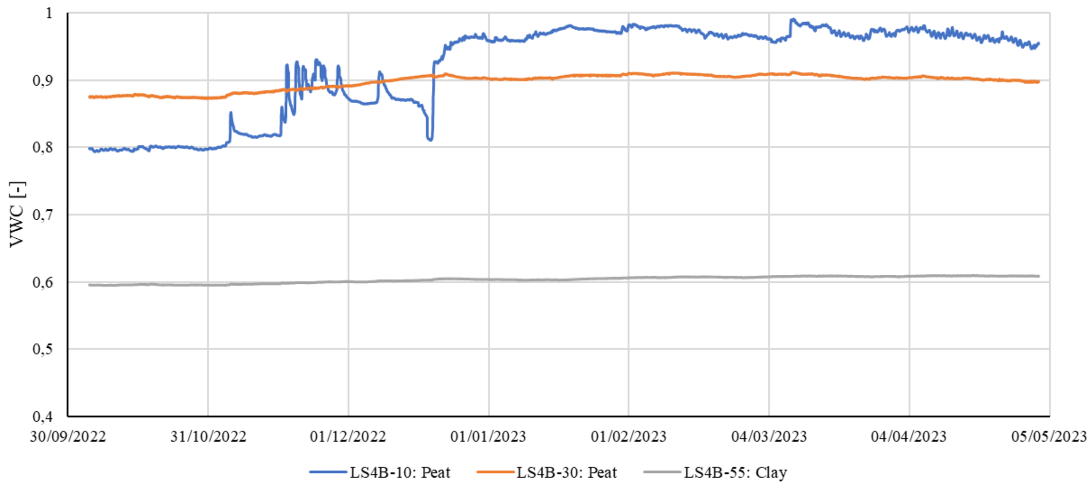

Figure 37: VWC time series for LS4B sensors at 10, 30 and 55 cm depth

Figure 38 represents the VWC time series for LS5A sensors. The value of θ for LS5A-10 ranges from 0.84 to 0.92 with an increase from October to December. For LS5A-30 it ranges from 0.93 to 0.97 with an increase from November to December. For LS5A-60 θ ranges from 0.88 to 0.90 with an increase in December. There is a difference in sensitivity depending on the depth.

Figure 39 represents the VWC time series for LS5B sensors. The value of θ for LS5B-10 ranges from 0.79 to 0.87 with a lot of variation over time. For LS5B-30 it ranges from 0.89 to 0.93 with an increase from November to December. For LS5B-60 VWC ranges from 0.82 to 0.84. There is a difference in sensitivity depending on the depth.

LS5A and LS5B being located about 5 meters from each other, it is interesting to compare the results. For 30 and 60 cm depth, the shapes are the same but with higher range of values in A series. For sensors near the surface, at 10 cm depth, there is a higher variability in B series. Considering the behaviour of SWRC at 60 cm depth, the water table is located near this depth.

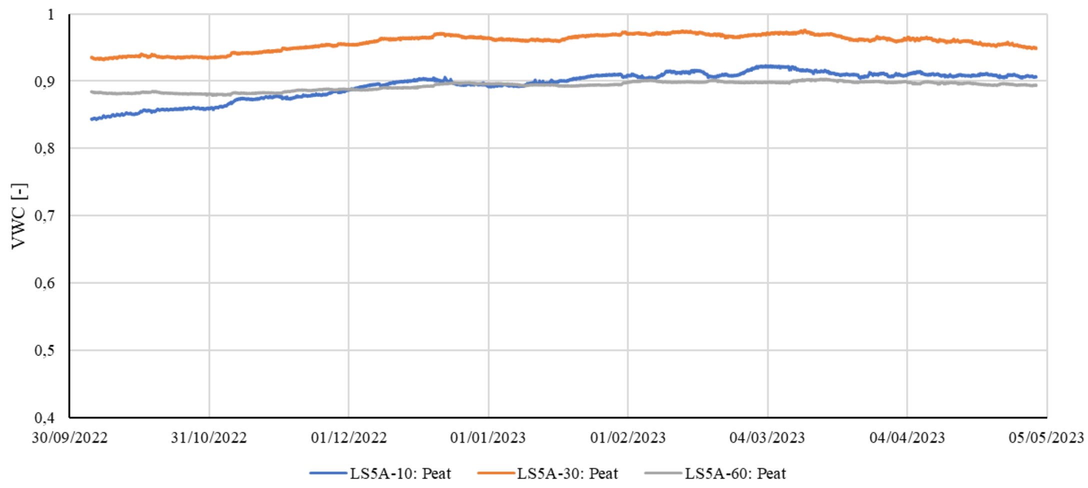

Figure 38: VWC time series for LS5A sensors at 10, 30 and 60 cm depth

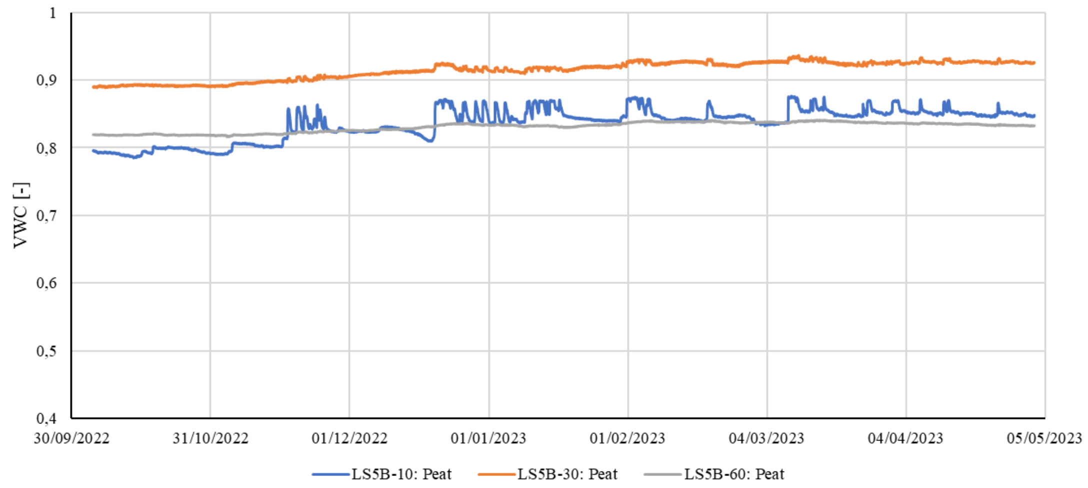

Figure 39: VWC time series for LS5B sensors at 10, 30 and 60 cm depth

4.4 Discussion

As said before, there is a sensitivity of θ that varies with depth. The VWC tends to vary less at depth than at the surface. There is also a difference in sensitivity depending on the type of soil. Indeed, a clay soil at 30 cm depth will have a different behaviour than a peat soil at the same depth. This is due to the intrinsic characteristics of each soil. Clay has a better water retention capacity and is less sensitive to suction variations. Clay therefore has a more constant and less variable VWC than peat especially the clay here is constantly saturated.

For the pits (all except 2A and 2B) where there are several peat depths, a trend is observed along the transect. Indeed, θ values observed at 30 cm depth are often (it is less clear for 4A and 4B) higher than values observed at 10 cm depth. This can be explained by the fact that the θ_s calculated for the peat samples at 30 cm depth are higher than the θ_s of the samples at 10 cm depth. In addition, the VWC at the surface is more sensitive due to soil water uptake by plants, evapotranspiration and surface runoff. Therefore, the values observed at 10 cm depth are not at saturation.

For samples 2A and 2B where there are two clay depths, higher θ values are observed at 30 cm compared to 60 cm depth. In view of the behaviour of the curves concerned, the VWC values are at saturation. The observation of the time series coincides with the laboratory measurements. Indeed, θ_s at 30 cm are higher than θ_s values at 50 cm depth.

In general, for all samples, the ranges of θ_s values calculated in the laboratory correspond to the values found on the time series. Assuming that for each TDR probe the highest observed θ value is the VWC at saturation, for 22 samples the laboratory calculated θ_s value is higher and for 8 samples the value is lower. The calculated margin of error is 0.05 (cm^3/cm^3). The value of the VWC which is higher than 1 for LS3B-30 can be explained by this margin error. Note that this margin error considers the errors incurred during handling, the calibration error and the margin of error of the probes. Moreover, for the calibration, there is no data for $\theta > 0.55$ for clay and no data for $\theta > 0.72$ while in reality it is in these ranges of values that the VWC is located. As shown in the following figures (Figure 41 and Figure 40), the scatter plots represent θ_s values from TDR sensors and from laboratory. Red lines represent the 1:1 line. For peat, in Figure 40, data determined from laboratory tend to be higher than data from TDR. The correlation is obviously positive but not very strong. An outlier, LS2B-10 sample is present in position (0.84,0.57). This may be due to a location error or it may be that the laboratory sample is peat and the TDR sample is clay. For clay, in Figure 41, both values from TDR and laboratory are close to the line and have a strong correlation. There are no outliers. From these figures, the conclusion that θ_s values for clay correspond better can be drawn.

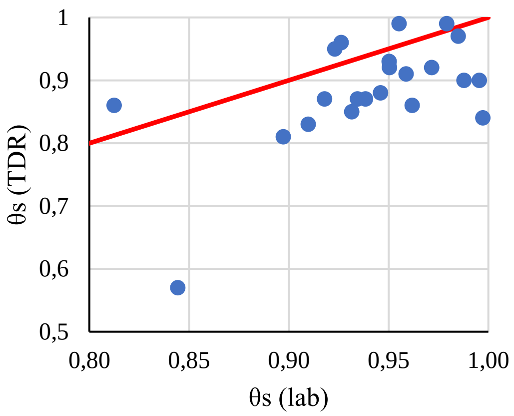

Figure 40: Scatter plot of θs determined by TDR and in laboratory for peat samples.

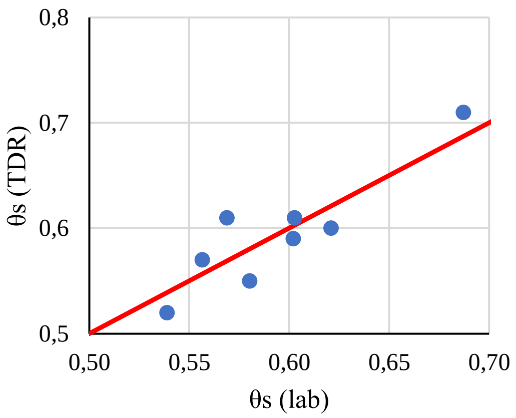

Figure 41: Scatter plot of θs determined by TDR and in laboratory for clay samples.

As shown in Figure 42, there is an increase in precipitation from October to January. This explains the global increase of the VWC on all sensors, especially for 10 and 30 cm depth, at this same period. As depicted in the VWC time series, the θ is already very high, reaching saturation in October. This can be explained by the fact that, in spite of very dry months of July and August, it rained a lot in September. This was enough to recharge the water table.

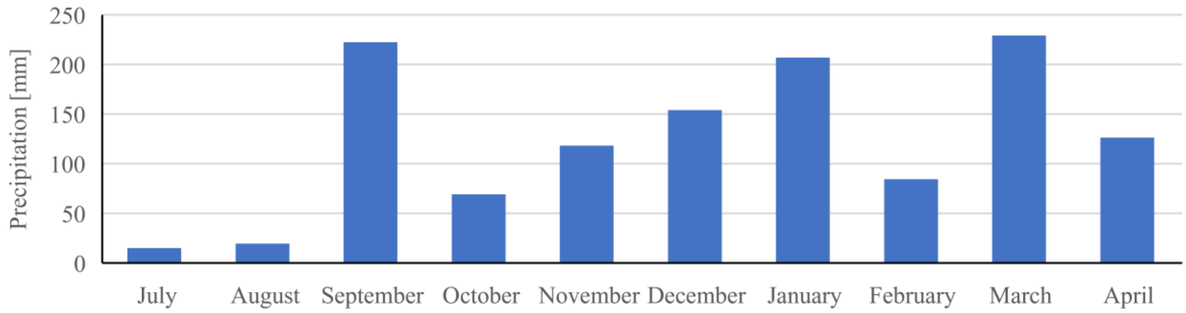

Figure 42: Mont Rigi monthly cumulative precipitation (mm) from July 2022 to April 2023 [49]

The saturated clay layer beneath the peat layer can affect the peat layer in several ways. If the saturated clay layer is thick enough and impermeable, it can prevent water from flowing through it and thus hold water below the peat layer. This causes the peat layer to become saturated and excess water to be retained. This promotes the formation of the peat bog. The saturated clay layer also affects the availability of nutrients for plants in the peat layer. If nutrients are retained in the saturated clay layer, they may not be available to plant roots in the peat layer, reducing their growth and yield. So here we have a very wet, nutrient-poor bog. These conditions limit the growth of some plants and favour the growth of plants adapted to these conditions, such as sphagnum mosses. The saturated clay layer can also affect the stability of the peat layer. If the underlying saturated clay layer is unstable, the peat layer may be subject to landslides and soil movement.

Depending on the VWC time series, the presence of the water table is assumed to be between 30 and 50 cm depth. According to Wastiaux (2008), the hydrostatic level does not deviate more than 20 cm from the surface of the bog in the Hautes Fagnes. The difference between this case and the literature, particularly the deeper water table, can be attributed to the presence of drains on the study site, as explained in Section 2.1. The hydrostatic level is mostly located at about 10 cm below the surface, while it remains in the lowest levels only for a small proportion of the year [70]. This distribution is quite characteristic of raised bogs [71]. As explained earlier, the presence of a shallow water table is a necessary condition for the functioning of the peatland ecosystem. The surface horizon experiences periodic aeration and after some burial, this horizon is below the hydrostatic level and no longer undergoes significant evolution (decomposition of organic matter). From the observations of this case study and Wastiaux (2008), the supposition that a peat bog is an almost saturated environment that will offer little absorption capacity can be done. Any excess precipitation cannot therefore infiltrate, but only run off downhill through the surface vegetation.

In view of the hydraulic behaviour along the study transect, the position of the probes along the transect has no influence on the evolution of the volumetric water content. As said, water runs down the slope but this does not influence the VWC as the slope progresses. The water goes to the outlet that is the small stream at the bottom of the study area.

This analysis demonstrates the existence of a threshold for rapid flow at very shallow depths in peatlands [72], [73]. Below this threshold, the peat is nearly impermeable and lateral/horizontal water movement is slow. This rapid flow threshold is located at the surface, confirming that the hydraulic conductivity at saturation decreases with depth and so with peat decomposition as seen in section 3.3.3. Only the surface part (living vegetation) has a high permeability, likely to generate flow when the water table is present.

4.5 Conclusion

The acquisition of TDR data allowed a study of the VWC over several months. Indeed, the data collected from October 2022 to early May 2023 provides additional information to the data of soil water retention curves. Peat, having a very high and more sensitive VWC, has a huge water storage capacity but a little absorption capacity. Whereas clay, having a lower and more constant VWC, has a higher water retention capacity.

A prior calibration was used to obtain these data. This calibration obtained via laboratory analysis is close to the calibration models provided by the manufacturer. However, it contains a margin of error that could be reduced by taking more samples and more specific samples.

The underlying saturated clay layer can affect the peat layer in several ways, including limiting drainage, affecting nutrient availability, and influencing peat layer stability. This layer of clay being saturated and impermeable, peat layer above being also saturated and impermeable, the hydrostatic level is located near the surface. So, the main water flux is on the surface and goes to the outlet at the bottom of the slope.

5 Hydraulic modelling

5.1 Objectives

The objective here is to integrate the data from the vGM model and the precipitation data in Hydrus-1D to obtain a model of the evolution of the volumetric water content over time. The last step is to compare this model with the TDR data which represent the reality. The aim is to understand and predict behaviour and perform parametric analyses.

5.2 Methodology

5.2.1 Choice of time series

Several criteria were considered when selecting the time series to be modelled. The first is the composition of the soil profile. Thus, 3 types of profile were studied:

- surface peat - clay 30 cm deep - clay at bottom.
- surface peat - peat 30 cm deep - clay at bottom.
- surface peat - peat 30 cm deep - peat at bottom.

In order to be representative, these three profile types were modelled. The second criteria is the depth of the water table and the number of soil materials (with related parameters) considered. There are two scenarios: the water table is 35 cm deep and two materials are considered or the water table is 60 cm deep and three materials are considered. Thirdly, TDR time series selected have clearly visible variations with varying amplitudes. Finally, a TDR time series, with its large variations over the entire study period, was modelled over the entire period, unlike the other time series, which were modelled over shorter periods. These shorter periods were chosen because it includes the most amplitude variations.

5.2.2 LS2A

The first step is to determine the type of simulation wanted in Hydrus. In this case, it is a water flow simulation in direct modelling. The unit of length used is the centimetre. In view of Figure 32: VWC time series for LS2A sensors at 10, 30 and 50 cm dep, the depth of the water table has been estimated at 35 cm. Indeed, for this period, the soil is not yet saturated at 30 cm depth but it is close to saturation. Therefore, the position of the water table is assumed to be a few centimetres below this level. Therefore, the depth of the soil profile in Hydrus is 35 cm and only two soil materials have been considered. The time unit used is the minute. The simulation is done over a period of 69 days from October 5 to December 12. Three print times are encoded to know the state of the simulation at different time. The iteration criteria are left by default. The hydraulic model chosen is the van Genuchten - Mualem model and the hysteresis phenomenon is not considered. The hydraulic parameters of the vGM model are encoded for the two soil materials. “Mat 1” corresponds to LS2A-10 (peat layer) and “Mat 2” corresponds to LS2A-30 (clay layer) (Figure 43).

Mat	Qr [-]	Qs [-]	Alpha [1/cm]	n [-]	Ks [cm/min]	l [-]
1	0	0,932	0,0731	1,23	0,9289	0,5
2	0	0,621	0,017	1,17	0,0068	0,5

Figure 43: vGM parameters for LS2A-10 and LS2A-30

As a reminder, the parameters α and n, were determined with the help of the RETC program based on laboratory analysis (see section 3.3.2). While K_{sat} was determined using the constant load permeameter method (see section 3.3.3). Lambda, L or l, accounts for pore continuity and tortuosity. The assumption that the L value is equal to 0.5 is made and is discussed after. Precipitation data comes from the IRM station located 3 km from the study site. Knowing the precipitation with a time step of 10 minutes, 9936 precipitation fluxes (cm/min) are integrated in the simulation. Therefore, the upper boundary condition is defined as variable pressure head/flux and the relevant data are introduced into the simulation. As the water table is located just below the studied soil profile, the lower boundary condition is defined as constant pressure head.

The first material "Mat 1", corresponding to LS2A-10 goes from 0 to 20 cm depth. The second material, corresponding to "Mat 2" goes from 20 cm to 35 cm depth. This distribution was made by trial and error and according to the soil profile established in Figure 10: Scheme of different 100 cm soil profiles along the transect. The initial conditions of the water content of the studied soil profile are h = -100 cm at the surface and h = 0 cm at 35 cm depth since the hydrostatic level is located at this depth. There is a linear interpolation between the two. Note that these initial conditions are not very important because after a certain simulation time, the simulation becomes independent of the initial conditions. Two observation points are placed at 10 cm and 30 cm depth to visualize the evolution of the VWC at the same depth as the TDR probes.

5.2.3 LS4B

In view of Figure 37: VWC time series for LS4B sensors at 10, 30 and 55 cm depth, the depth of the water table has been estimated at 35 cm. Indeed, for this period, the soil is not yet saturated at 30 cm depth but it is close to saturation. Therefore, the position of the water table is assumed to be a few centimetres below this level. Therefore, the depth of the soil profile in Hydrus is 35 cm and only two soil materials have been considered. Units, simulation and model used are the same as before. The simulation is done over a period of 68 days from October 25 to December 31. The hydraulic parameters of the vGM model are encoded for the two soil materials. “Mat 1” corresponds to LS4B-10 (peat layer) and “Mat 2” corresponds to LS4B-30 (peat layer) (Figure 44).

Mat	Qr [-]	Qs [-]	Alpha [1/cm]	n [-]	Ks [cm/min]	l [-]
1	0	0,979	0,024	1,291	0,1044	0,5
2	0	0,9587	0,02	1,276	0,0033	0,5

Figure 44: vGM parameters for LS4B-10 and LS4B-30

The first material, "Mat 1" corresponding to LS4B-10 goes from 0 to 20 cm depth. The second material, "Mat 2" corresponding to LS4B-30 goes from 20 cm to 35 cm depth. This distribution was made by trial and error because being two peaty materials, the delimitation between the two is not known. Two observation points are placed at 10 cm and 30 cm depth to visualize the evolution of the VWC at the same depth as the TDR sensors.

5.2.4 LS5A

In view of Figure 38: VWC time series for LS5A sensors at 10, 30 and 60 cm depth, the depth of the water table has been estimated at 35 cm. Indeed, for this period, the soil is not yet saturated at 30 cm depth but it is saturated at 60 cm depth and this choice allowed better results. Therefore, the depth of the soil profile in Hydrus is 35 cm and two soil materials have been considered. Units, simulation and model used are the same as before. The simulation is done over a period of 69 days from February 1 to April 10. The hydraulic parameters of the vGM model are encoded for the two soil materials. “Mat 1” corresponds to LS5A-10 (peat layer) and “Mat 2” corresponds to LS5A-30 (peat layer) (Figure 45).

Mat	Qr [-]	Qs [-]	Alpha [1/cm]	n [-]	Ks [cm/min]	l [-]
1	0	0,9716	0,024	1,243	2,7938	0,5
2	0	0,9849	0,016	1,373	0,0045	0,5

Figure 45: vGM parameters for LS5A-10 and LS5A-30

The first material, "Mat 1" goes from 0 to 25 cm depth. The second material and "Mat 2" goes from 25 cm to 35 cm depth. This distribution was made by trial and error because being two peaty materials, the delimitation between the three is not known. Two observation points are placed at 10 cm and 30 cm depth to visualize the evolution of the VWC at the same depth as the TDR probes.

5.2.5 LS5B

In view of Figure 39: VWC time series for LS5B sensors at 10, 30 and 60 cm depth, the depth of the water table has been estimated at 60 cm. Indeed, for this period, the soil is not yet saturated at 60 cm depth but it is close to saturation and this choice allowed better results. Therefore, the depth of the soil profile in Hydrus is 60 cm and three soil materials have been considered. Units, simulation and model used are the same as before. The simulation is done over a period of 194 days from October 5 to April 17. The hydraulic parameters of the vGM model are encoded for the three soil materials. “Mat 1” corresponds to LS5B-10 (peat layer), “Mat 2” corresponds to LS5B-30 (peat layer) and “Mat 3” corresponds to LS5B-60 (peat layer) (Figure 46).

Mat	Qr [-]	Qs [-]	Alpha [1/cm]	n [-]	Ks [cm/min]	l [-]
1	0	0,9383	0,0187	1,24	2,489	0,5
2	0	0,9502	0,0217	1,27	2,33	0,5
3	0	0,9972	0,0167	1,3	0,0082	0,5

Figure 46: vGM parameters for LS5B-10, LS5B-30 and LS5B-60

The first material, "Mat 1" goes from 0 to 20 cm depth. The second material, "Mat 2" goes from 20 cm to 40 cm depth and “Mat 3” goes from 40 cm to 60 cm depth. This distribution was made by trial and error because being three peaty materials, the delimitation between the three is not known. Two observation points are placed at 10 cm and 30 cm depth to visualize the evolution of the VWC at the same depth as the TDR probes.

5.3 Results

5.3.1 LS2A

Figure 47 and Figure 48 represent the evolution of the VWC as a function of time. This evolution is determined either by TDR method or by direct modelling. Lines t-10, which is valid at 10 cm depth, and t-30, which is valid at 30 cm depth, represent the time after which the simulation is independent of the initial conditions. Here, the simulation becomes independent after more than 5 days for simulation at 10 cm depth and less than one day for simulation at 30 cm depth. The Hydrus results here are the result of several trial-and-error attempts. Indeed, not knowing precisely the location of the water table, several depths were simulated and it is the last one (at 35 cm depth) that provided the best fit with the TDR data. At 10 cm depth, the simulation does not match. The simulation is more sensitive to the upper conditions, has more variability and is less "smoothed". The spikes of increase present in the simulation correspond to higher precipitation at the same times, as shown in Figure 29: Precipitation level (mm) with a frequency of 10 minutes from October 2022 to May 2023. The fact that these increases are not visible on the TDR data suggests that, in reality, the water table is located upper in the profile. At 30 cm depth, the simulation corresponds to the TDR data. The evolution at the third depth, at 50 cm, does not appear because the soil being saturated under 35 cm of depth, the value of the VWC is the saturation value determined in laboratory.

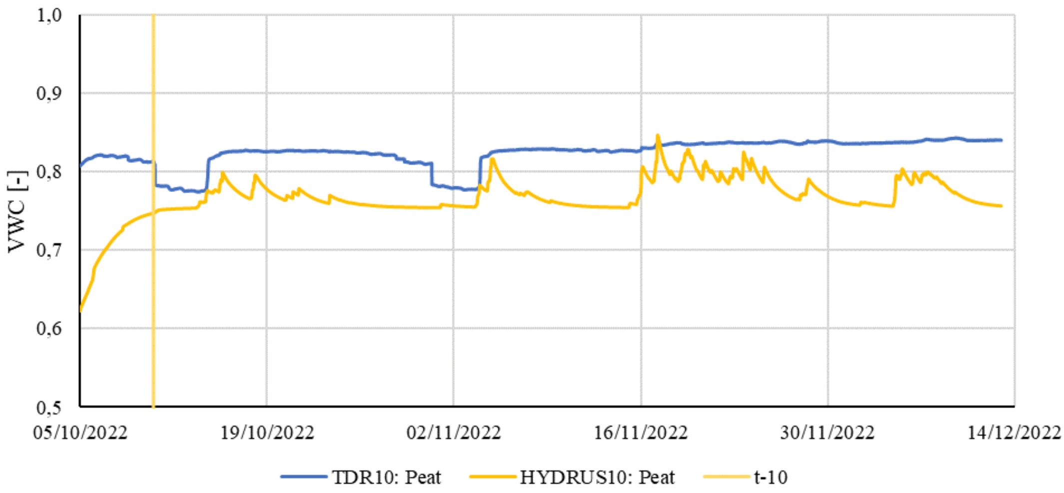

Figure 47: VWC evolution over time for LS2A-10 determined by sensors and by direct modelling.

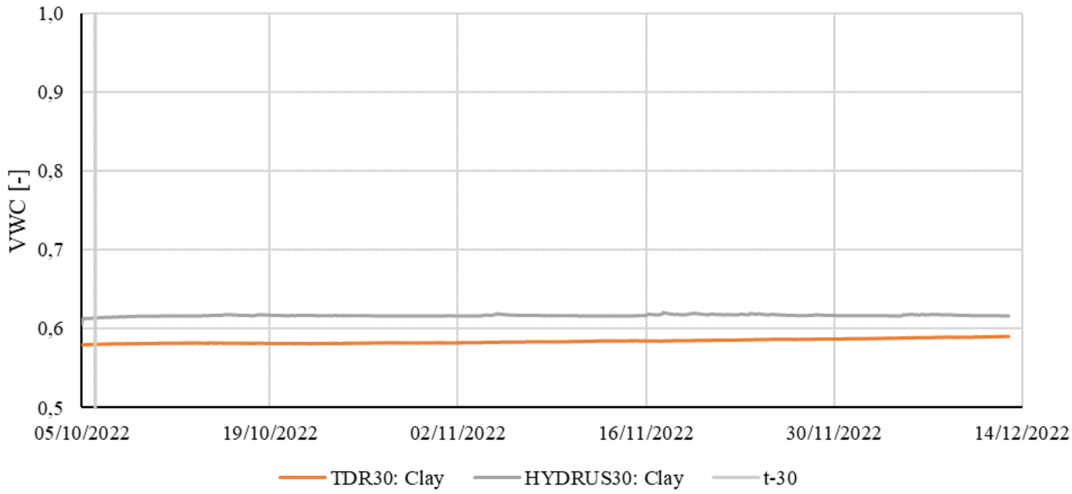

Figure 48: VWC evolution over time for LS2A-30 determined by sensors and by direct modelling.

Figure 49 represents the evolution of the pressure head along the soil profile at four different times. T0 represents the initial conditions which are h = -100 cm at the surface and h = 0 cm at 35 cm depth with a linear interpolation between the two values. T1 represents the conditions on 19/10/2022 clearly visible on the graphs above. T2 represents the conditions on 16/11/2022, T3 and T4 is the final state of the simulation. The highest pressure observed at the surface is h = -35 cm for T3 corresponding to the lowest VWC in view of Figure 47. At T1 and T2, the pressure head is less important corresponding to a higher VWC as shown in Figure 47. The change in the appearance of the lines at 20 cm depth is due to the change from LS2A-10 to LS2A-30 material.

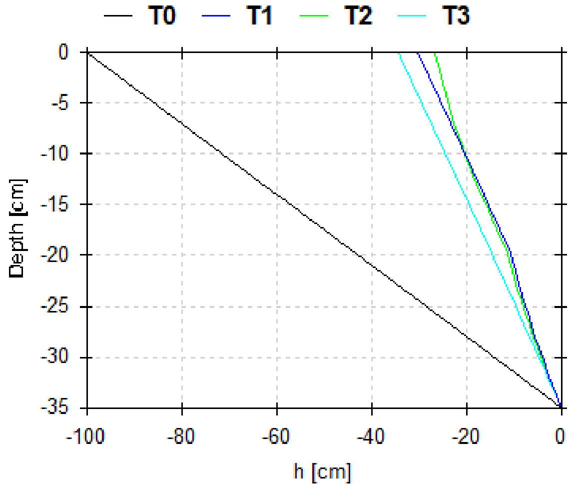

Figure 49: LS2A - Evolution of the pressure head with the depth for T0 = initial conditions, T1 = condition on 19/10/2022, T2 = conditions on 16/11/2022 and T3 = final state

5.3.2 LS4B

Figure 50 and Figure 51 represent the evolution of the VWC as a function of time at 10 cm depth and 30 cm depth respectively. This evolution is determined either by TDR method or by direct modelling. The simulation becomes independent after 7 days for simulation at 10 cm depth (t-10) and less than one day for simulation at 30 cm depth (t-30). At 10 cm depth, the simulation match with the TDR evolution. Indeed, there are the same variations at the same time with a similar amplitude. The spikes of increase present in the simulation correspond to higher precipitation at the same times, as shown in Figure 29. At 30 cm depth, the simulation also corresponds to the TDR data. The variations are slightly more pronounced for the simulation than for the TDR data but they occur at the same time. The evolution at the third depth, at 55 cm, does not appear because the soil being saturated under 35 cm of depth, the value of the VWC is the saturation value determined in laboratory.

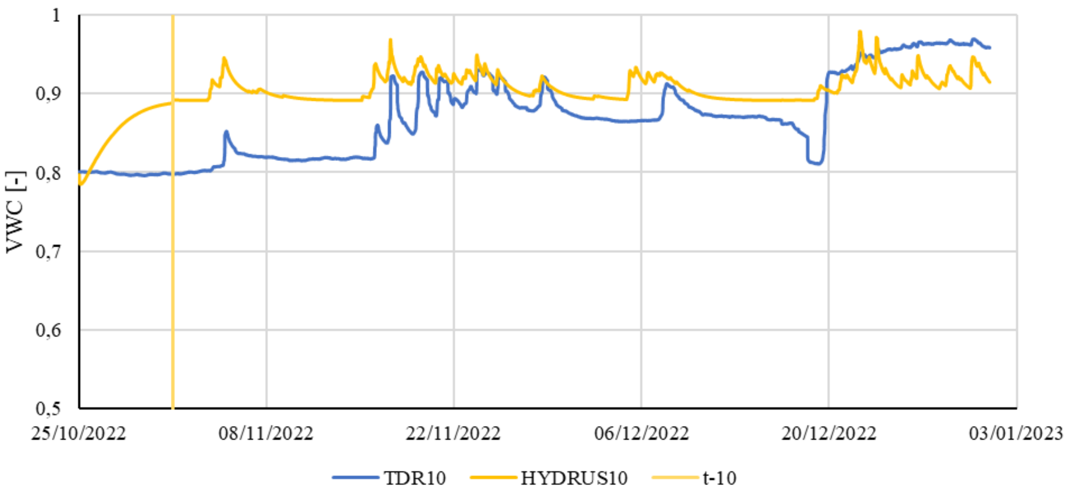

Figure 50: VWC evolution over time for LS4B-10 determined by sensor and by direct modelling.

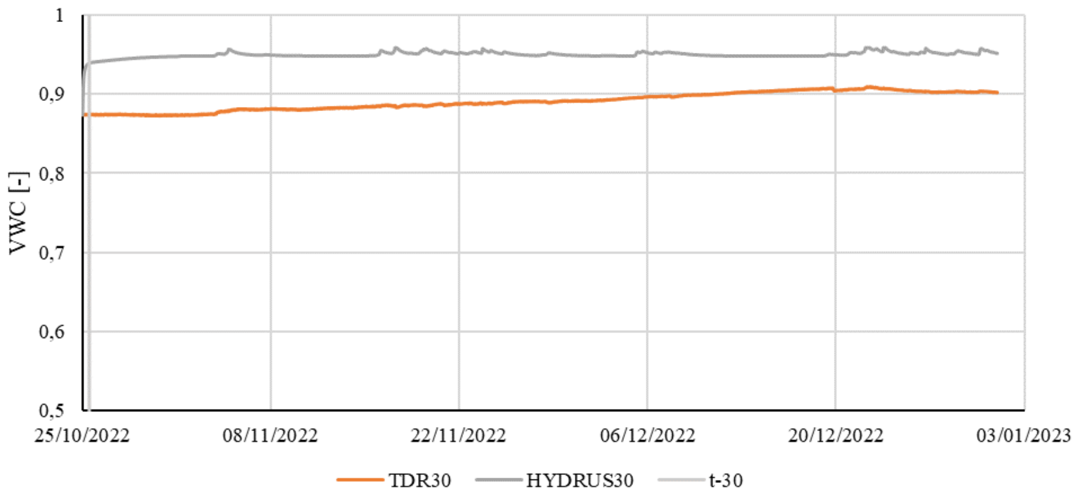

Figure 51: VWC evolution over time for LS4B-30 determined by sensor and by direct modelling.

Figure 52 represents the evolution of the pressure head along the soil profile at five different times. T0 represents the initial conditions. T1 represents the conditions on 22/11/2022. T2 represents the conditions on 20/12/2022 and T3 is the final state of the simulation. The highest pressure is observed at the surface with about h = -30 cm for T2. T1 and T3 have a lower pressure head and so a higher VWC than T2. The change in the appearance of the lines at 20 cm depth is due to the change from LS4B-10 to LS4B-30 material.

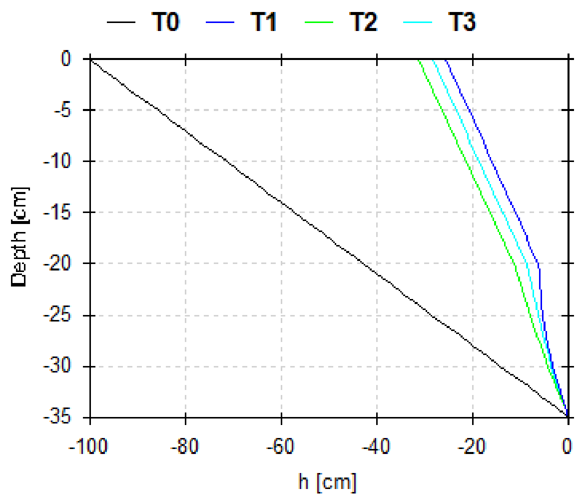

Figure 52: LS4B - Evolution of the pressure head with the depth for T0 = initial conditions, T1 = conditions on 22/11/2022, T2 = conditions on 20/12/2022 and T3 = final state

5.3.3 LS5A

Figure 53 and Figure 54 represent the evolution of the VWC as a function of time at 10 cm depth and 30 cm depth respectively. This evolution is determined either by TDR method or by direct modelling. The simulation becomes independent after one day for both simulations. At 10 cm depth, the simulation does not match with the TDR evolution. Indeed, the simulation is more sensitive to the upper conditions, has more variability and is less "smoothed. The spikes of increase present in the simulation correspond to higher precipitation at the same times, as shown in Figure 29. The fact that these increases are not visible on the TDR data suggests that, in reality, the water table is located upper in the profile. At 30 cm depth, the simulation corresponds roughly to the TDR data. The variations are more pronounced for the simulation than for the TDR data and they do not occur at the same time. The evolution at the third depth, at 60 cm, does not appear because the soil being saturated at this depth, the value of the VWC is the saturation value determined in laboratory.

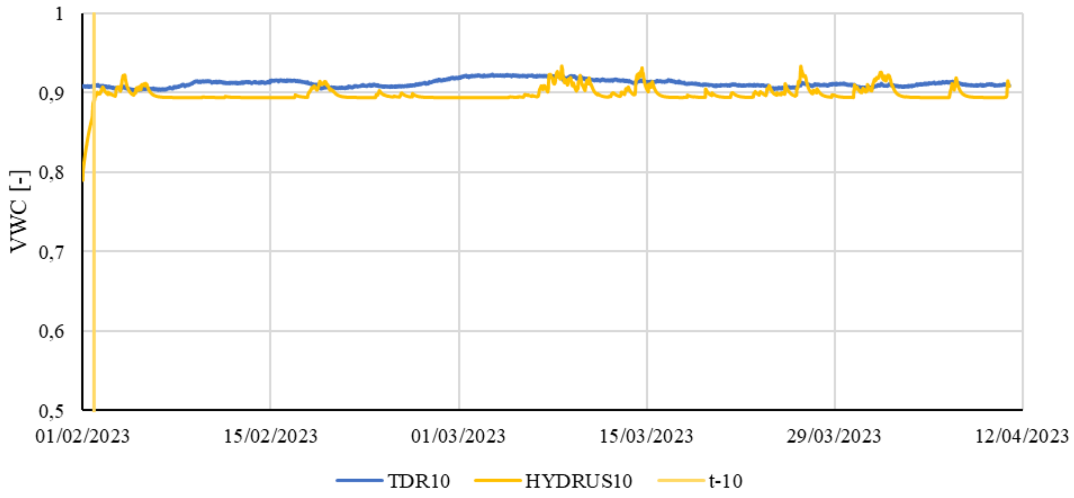

Figure 53: VWC evolution over time for LS5A-10 determined by sensor and by direct modelling.

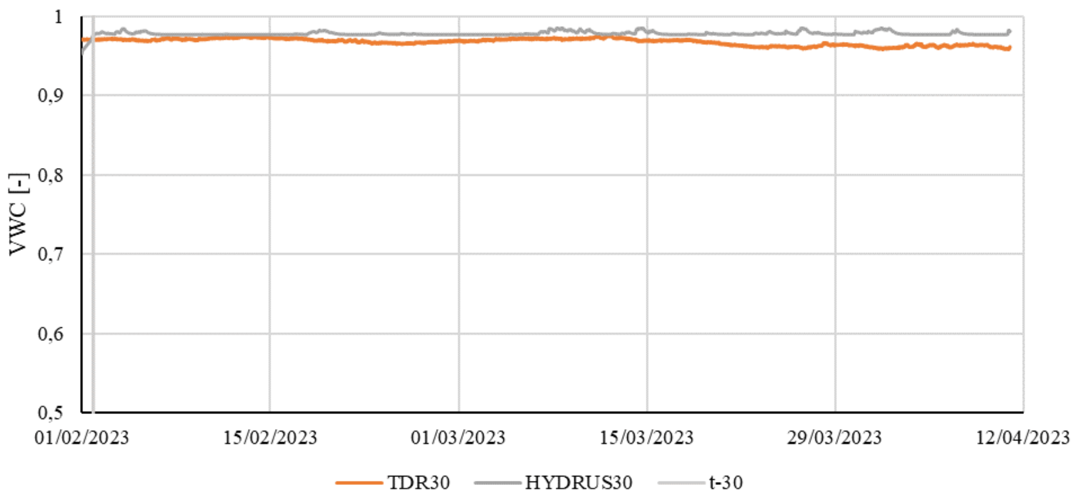

Figure 54: VWC evolution over time for LS5A-30 determined by sensor and by direct modelling.

Figure 55 represents the evolution of the pressure head along the soil profile at four different times. T0 represents the initial conditions. T1 represents the conditions on 15/02/2023, T2 on 15/03/2023 and T3 is the final state of the simulation. The highest pressure is observed at the surface with about h = -35 cm for T1. T2 and T3 have a lower pressure head and so a higher VWC. The change in the appearance of the lines at 25 cm depth is due to the change from LS5A-10 to LS5A-30 material.

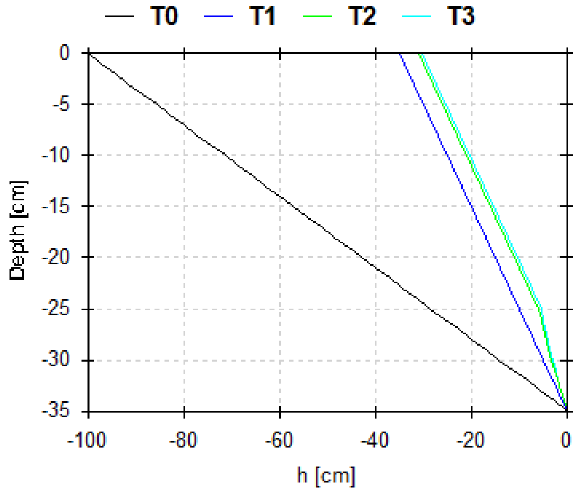

Figure 55: LS5A - Evolution of the pressure head with the depth for T0 = initial conditions, T1 = conditions on 15/02/2023, T2 = conditions on 15/03/2023 and T4 = final state

5.3.4 LS5B

Figure 56 and Figure 57 represent the evolution of the VWC as a function of time at 10 cm and 30 cm depth respectively. This evolution is determined either by TDR method or by direct modelling. The simulation becomes independent after less than one day for both simulations. This information is not shown on the graphs because it is not visible. At 10 cm depth, the simulation match with the TDR evolution. Indeed, there are the same variations at the same time with a similar amplitude. At 30 cm depth, the simulation also corresponds. The variations are more pronounced for the simulation than for the TDR data but it occurs at the same time. The spikes of increase present in the simulation correspond to higher precipitation at the same times, as shown in Figure 29. The evolution at 60 cm does not appear because the soil being saturated at this depth, the value of the VWC is the saturation value determined in lab.

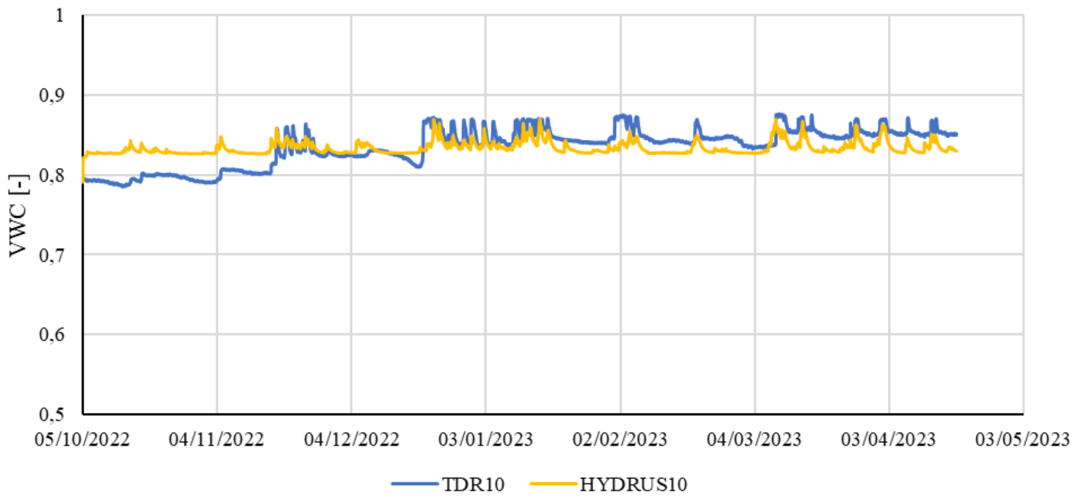

Figure 56: VWC evolution over time for LS5B-10 determined by sensor and by direct modelling.

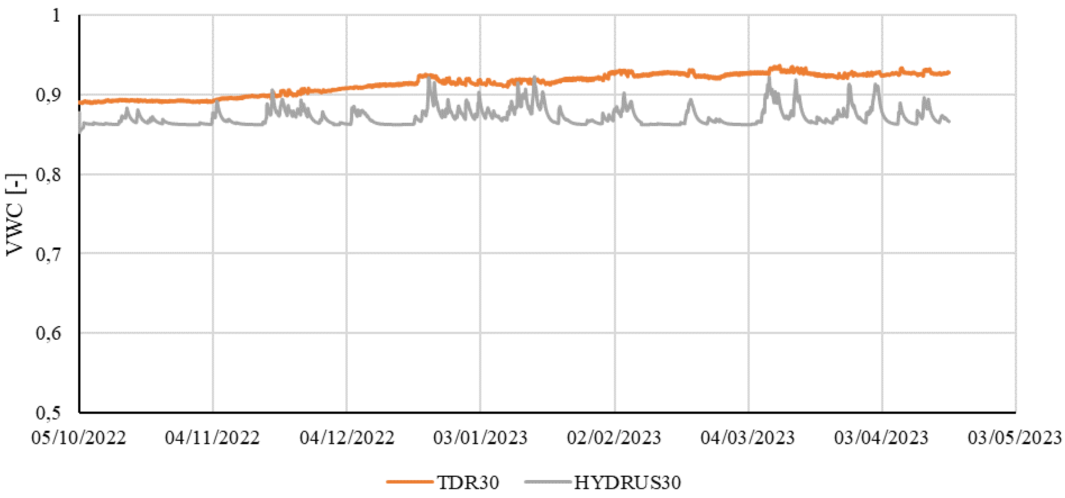

Figure 57: VWC evolution over time for LS5B-30 determined by sensor and by direct modelling.

Figure 58 represents the evolution of the pressure head along the soil profile at four different times. T0 represents the initial conditions. T1 represents the conditions on 02/02/2023, T2 after on 04/03/2023 and T3 is the final state on the simulation. The highest pressure is observed at the surface with about h = -60 cm for T2. T1 has a higher pressure head and so a lower VWC than T2 as shown in Figure 57.

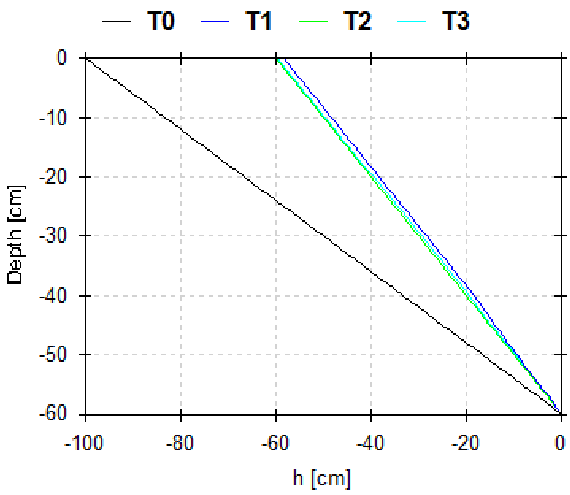

Figure 58: LS5B - Evolution of the pressure head with the depth for T0 = initial conditions, T1 = conditions on 02/02/2023, T2 = conditions on 04/03/2023 and T3 = final state.

5.4 Discussion

5.4.1 Simulation conditions

The depth of the water table has been approximated and is considered fixed. As a result, simulation results are levelled down with the VWC. This means that the VWC value does not fall below a certain level. So, every local minimum is equal to the global minimum. This is not the case for TDR probe results. To obtain better results, it would have been necessary to know the precise evolution of the hydrostatic level for the periods concerned. The lower boundary conditions would have been changed from "constant pressure head" to "variable pressure head". For upper boundary conditions, only precipitation was considered. In fact, evapotranspiration was neglected due to lack of site-specific data. Better results could have been obtained by integrating the latter. Indeed, if evapotranspiration had been considered, it would have outweighed precipitation and thus buffered the increase spikes.

Different soil materials influence simulation behaviour. Firstly, the delimitation between each soil material was made by trial and error to find the simulation that most closely matched TDR data. However, this does not reflect reality, so this is a source of error. It would have been better to know the different hydraulic parameters with a smaller depth interval, to have a better resolution of the profile. Ideally and utopianly, the hydraulic parameters should have been studied over an infinite number of depths along the profile. Secondly, the parameter of saturated hydraulic conductivity also has a major influence. Indeed, between one soil material and another, there is sometimes an order of magnitude 10^2 difference. A very low K_{sat}, 0.0082 cm/min, as shown in “Mat 3” in Figure 46, characterizes the soil layer as being impermeable, and so the upper layers have more rapid increases in VWC and are more quickly saturated. On the contrary, a very high K_{sat}, 2.489 cm/min, as shown in Figure 46, characterizes the soil layer as being very permeable and so the upper layers experience the opposite effect. Thus, this parameter has a big effect on drainage.

The L parameter values in the herbaceous peat soils are generally greater than 0 whereas in the moss peat samples they are ranging from − 5 to 5. A negative value of the parameter L can be understood as a correction factor that causes more gradual drop in hydraulic conductivity than a positive value of L [74]. Given that the peatland studied is partly mossy and partly herbaceous, it was decided to set the lambda value at 0.5. Determining the value of this parameter for each soil is therefore a key for improvement. The parameter L can be determined by conductivity measurements at different water contents [65].

5.4.2 Results

Since the water table is shallow, the deepest TDR probe is always located in saturated soil. As a result, no simulations were carried out at these depths, the only possible result being a straight line at the saturation VWC value recorded in Hydrus. At 30 cm depth, the simulations roughly match the data, but tend to be more sensitive to boundary conditions and to have larger amplitudes. This is due to the fact that, in reality, the soil buffers internal fluxes, which is not the case in the simulation. At a depth of 10 cm, the best results are observed, although in some cases the simulation and TDR data do not match. This may be explained by the fact that the surface of some pits has subsided, creating a puddle and therefore more or less stable conditions. These puddles may also explain the differences at 30 cm depth.

There are several reasons for the difference in value range between TDR data and models. Direct modelling has certain limitations that can affect its accuracy and relevance. Direct modelling requires simplifications and approximations to make the problem more manageable. This is what is done for vGM profile parameters, water table depth and precipitation. The quality of the data used as input to the direct model therefore has a significant impact on the reliability of the results. The phenomenon of water flow in the soil is complex and cannot be reduced to the single variables used here. Other variables such as tortuosity, pore size distribution, CEC, granulometry, etc. could be considered to refine the models. Calculations are based on vGM parameters on the one hand, and on TDR data on the other hand. As explained in Section 4.4, there is a margin of error between the two.

5.5 Conclusion

Modelling involves selecting the time series to be modelled. This selection is based on several criteria, such as soil profile, water table depth and variability of TDR results. The simulations become independent of the initial pressure head conditions after a certain time, which is specific to each simulation. Modelling is based on precipitation and vGM parameters as inputs. Three observation points are placed at the same depth as the relative TDR probes. Some models match the TDR data, while others do not. The value of K_{sat} plays an important role in determining soil permeability. A greater sensitivity to boundary conditions is observed in the models. Although direct modelling has certain limitations that can affect its accuracy and relevance, it can be improved by integrating evapotranspiration and a variable hydrostatic level.

6 Conclusion and perspectives

6.1 Conclusion

Critical zone is a reactive zone for the planet and plays a key role in its global regulation. This concept of critical zone questions the hydrological sciences because of its interactions on spatial scales, its interactions on temporal scales, and the interactions between biogeochemical processes. The hydrological sciences are based on soils and water. Soils play an important role in the water cycle because it filters, absorbs and retains water. Soil also buffers the surface water regime and groundwater recharge. Water in the soil plays a major role in many environmental processes. Having high porosity and so high-water storage capacity, peatlands are a very specific type of soil. Peatlands have a regulatory function and regulates the climate at global, regional and local scale. It also has a role in water regulation. But peatlands are also sensitive to climate change. Indeed, climate change may affect the ability of peatlands to take up and store carbon and GHG. Because of the peatlands climatic challenges and because this type of soil are currently not enough studied, especially in Belgium, this thesis focused on the study of the hydraulic properties of a peatland in the Hautes Fagnes region. Here are the main outcomes of the results of each chapter:

Outcomes from Soil Water Retention Curves chapter:

- The average clay density value of 1.2 [g/cm^3] which corresponds to loamy clay and an increase of the bulk density with depth is visible. The standard deviation related is equal to 0.124. For the peat, the bulk density average value is 0.2 [g/cm^3] with no relationship visible between depth and density and the standard deviation is equal to 0.061.
- The average clay θ_s value is equal to 0.59 which looks like very fine-textured clay soil. The standard deviation related is equal to 0.043. Peaty samples have a θ_s average value of 0.94 with a standard deviation of 0.045.
- At the wilting point, at pF = 4.2, the clay has θ average value of 0.31, so the soil is clayey with a more or less important load of silt according to the samples. The standard deviation related is 0.073. The average peat θ value at the wilting point is equal to 0.23, which is consistent with literature and the standard deviation is equal to 0.066.
- Clay samples having a significantly lower θ_s and a higher volumetric water content at high suction, they have a better water retention capacity with an air entry point that requires a higher suction. Having high VWC at saturation (so high porosity) and a low density, peat has a huge water storage capacity.
- The range of saturated hydraulic conductivity values varies from 10^{-7} to 10^{-3} m/s for peat samples with a mean value of 10^{-4} m/s which is consistent with literature. A decrease of K_{sat} with depth is observed for peat.
- K_{sat} varies from 10^{-6} to 10^{-3} m/s for clay samples with a mean value of 10^{-4} m/s.
- For peat, there is an increase of K_{sat} with the increase of the bulk density and there is a decrease of the bulk density with the increase of θ_s.

- For clay, there is a decrease of K_{sat} with the increase of the bulk density and there is a decrease of the bulk density with the increase of θ_s.
- Values of the model fitting parameters are obtained with very high coefficients of determination for both soils and unsaturated hydraulic parameters in peat soils have been successfully estimated using the vGM unimodal model. Parameters correspond to those expected for clay and peat.

Outcomes from TDR – VWC time series chapter:

- There is a sensitivity of θ to boundary conditions that varies with depth. The VWC tends to vary less at depth than at the surface. In other words, the VWC at the surface is more sensitive due to soil water uptake by plants, evapotranspiration and surface runoff. There is also a difference in sensitivity depending on the type of soil.
- Volumetric water content at saturation values from TDR correspond better to laboratory values for clay than for peat.
- An increase in precipitation from October 2022 to January 2023 explains the global increase of the VWC on all sensors at this same time.
- Depending on the VWC time series, the presence of the water table is assumed to be between 30 and 50 cm depth.
- Peat bog is an almost saturated environment that offers little absorption capacity. Any excess precipitation cannot therefore infiltrate, but only run off downhill through the surface vegetation.
- Existence of a threshold for rapid flow at very shallow depths in peatlands. Below this threshold, the peat is nearly impermeable and lateral/horizontal water movement is slow.
- Along the study transect, the position of the probes has no influence on the evolution of the volumetric water content.

Outcomes from direct hydraulic modelling chapter:

- As the depth of the water table is shallow, the deepest TDR probe is always located in saturated soil. As a result, no simulations were carried out at these depths.
- At 30 cm depth, the simulations roughly match the data, but tend to be more sensitive to boundary conditions and to have larger amplitudes.
- At a depth of 10 cm, the best results are observed, although in some cases the simulation and TDR data do not match.

The results of this thesis could be improved and supplemented in several ways. For the SWRC part, the data from the cell apparatus method would be better with extraction plates of the same characteristics. This would prevent heterogeneous results and outliers. For the TDR part, calibration on several samples specific to the locations studied could bring greater precision to the results. In the modelling section, taking evapotranspiration into account and knowing the evolution of the hydrostatic level would provide better results.

6.2 Perspectives

The LandSense project will continue over the next three years, offering opportunities to integrate the technologies and results presented in this document with new technologies to better understand peatlands. Figure 59 illustrates the integration of different techniques in the critical zone study. The next steps will be to carry out GPR measurements by drone. Surface temperature will also be estimated using infrared thermal sensors. In situ measurements should also be carried out in the form of a series of geochemical measurements. This will provide useful information on soil parameters to be used in subsequent simulations.

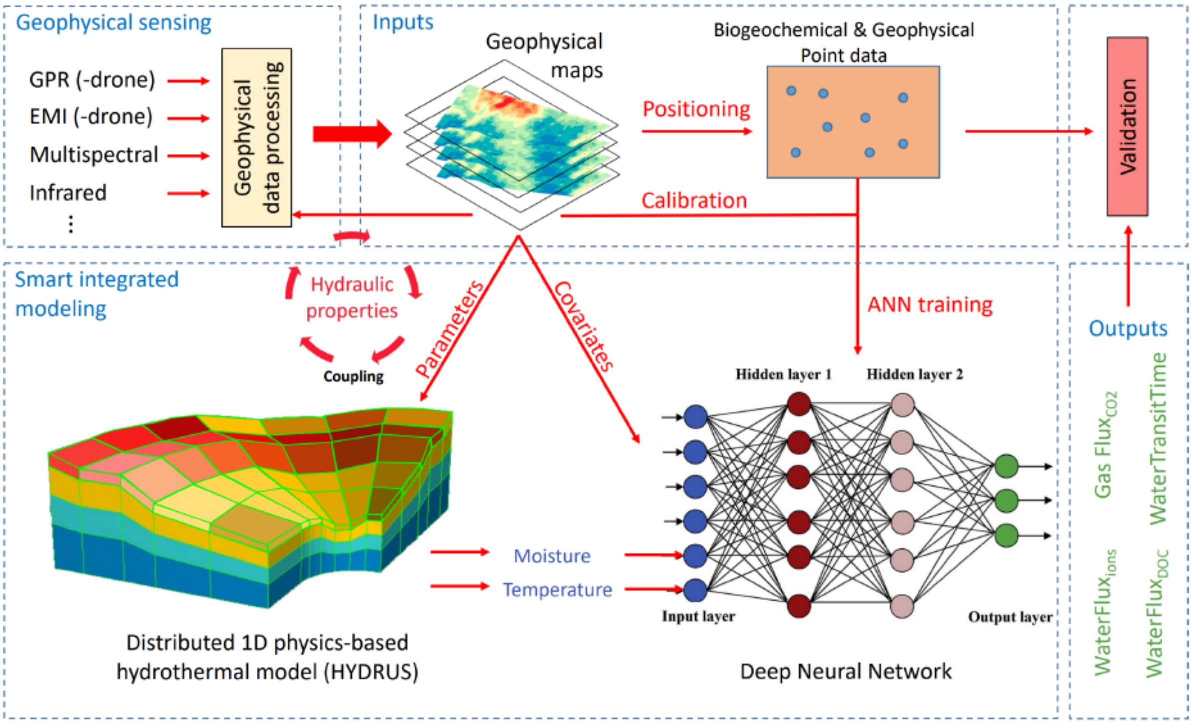

Figure 59: Conceptual diagram of the integrated critical zone model [41]

The results of this thesis will form the basis for the calibration of the intelligent CZ integration. The final goal is to develop a new critical zone metamodeling framework based on an intelligent combination of a distributed physics-based model and a series of deep neural networks fed by massive geophysical data and geochemical analyses of point samples. This will be achieved by training an artificial neural network with data, thanks to a Hydrus model [41].

References

[1] H. Cubizolle, J. Porteret, B. Etlicher, and C. Sacca, ‘Fonctionnement et conservation des tourbières’, in *Actes du colloque de Goutelas,* Saint-Etienne, 2007, pp. 365–381.
[2] E. Lappalainen, ‘General review on world peatland and peat resources’, UNESCO, Finland, 1996.
[3] J. Chorover, R. Kretzschmar, F. Garcia-Pichel, and D. L. Sparks, *Soil biogeochemical processes in the critical zone*, Elements 3. 2007.
[4] *Basic Research Opportunities in Earth Science*. Washington, D.C.: National Academies Press, 2001, p. 9981. doi: 10.17226/9981.
[5] ‘La zone critique ?’, *Institut des Géosciences de l’Environnement - UMR 5001*. https://www.ige-grenoble.fr/La-zone-critique (accessed Oct. 13, 2022).
[6] ‘Qu’est-ce que la zone critique ? – Ozcar-ri’. https://www.ozcar-ri.org/fr/la-zone-critique/quest-zone-critique/ (accessed Oct. 13, 2022).
[7] L. Susan, B. Lebedeva, and M. Lebedeva, *Understanding the Critical Zone*, vol. Annual Review of Earth and Planetary Sciences. 2011.
[8] T. White *et al.*, ‘Chapter 2 - The Role of Critical Zone Observatories in Critical Zone Science’, in *Developments in Earth Surface Processes*, J. R. Giardino and C. Houser, Eds., Elsevier, 2015, pp. 15–78. doi: 10.1016/B978-0-444-63369-9.00002-1.
[9] ‘L’eau et le sol’. https://www.u-picardie.fr/beauchamp/mst/eau-sol.htm (accessed Oct. 18, 2022).
[10] S. Zaaboubi, ‘Effets comparatifs de deux outils aratoires et de différents précédents culturaux sur les propriétés physiques d’un sol cultivé en céréales dans la région de Timgad.’, Université El-Hadj Lakhdar - Batna, 2007.
[11] Groupe d’intérêt scientifique Sol, ‘L’eau dans les sols’, France. [Online]. Available: https://www.gissol.fr/thematiques/leau-dans-les-sols-319
[12] C. Cosandey and M. Robinson, ‘Chapitre 4 - L’eau du sol. Les réserves hydriques’, in *Hydrologie continentale*, in Collection U. Paris: Armand Colin, 2012, pp. 153–196. doi: 10.3917/arco.cosan.2012.01.0153.
[13] C. Wastiaux, ‘Les tourbières sont-elles des éponges régularisant l’écoulement ?’ 2008.
[14] F. Rezanezhad, J. S. Price, W. L. Quinton, B. Lennartz, T. Milojevic, and P. Van Cappellen, ‘Structure of peat soils and implications for water storage, flow and solute transport: A review update for geochemists’, *Chem. Geol.*, vol. 429, pp. 75–84, Jul. 2016, doi: 10.1016/j.chemgeo.2016.03.010.
[15] H. Liu and B. Lennartz, ‘Hydraulic properties of peat soils along a bulk density gradient—A meta study’, *Hydrol. Process.*, vol. 33, no. 1, pp. 101–114, 2019, doi: 10.1002/hyp.13314.
[16] ‘Peat’, *International Peatland Society*. https://peatlands.org/peat/ (accessed Oct. 19, 2022).
[17] D. J. Charman, *Peatlands and environmental change*. Chichester, West Sussex, England ; New York: J. Wiley, 2002.
[18] P. Informer (Beckie), ‘Fen Vs Bog - What’s the Difference? (The Facts)’, *Pond Informer*, Jan. 11, 2022. https://pondinformer.com/fen-vs-bog/ (accessed Jan. 31, 2023).
[19] J. S. Price and S. M. Chlotzhauer, ‘Importance of shrinkage and compression in determining water storage changes in peat: the case of a mined peatland’. 1999.
[20] L. Nys, ‘Note sur un nivellement dans une tourbière bombée.’, *Annales de la Société géologique de Belgique*, pp. 19–22, 1954.
[21] R. Eggelsmann, ‘Moor und Wasser, in : K. Göttlich’, pp. 288–320, 1990.

[22] G. Grausse-Brauckmann, ‘Ablagerungen der Moore, in : K. Göttlich’, pp. 175–236, 1990.
[23] K. E. Ivanov, ‘Water movement in mirelands’, *A. Thompson and H.A.P. Ingram (translators).*, vol. London : Academic Press, p. 277, 1981.
[24] C. Wastiaux, ‘Végétation et régime hydrologique d‘une tourbière haute drainée: dégradation et régénération (Deux-Séries, Hautes-Fagnes, Belgique).’, ULg, Liège, 1990.
[25] C. Cosandey and M. Robinson, ‘Hydrologie continentale’, *Paris Colin*, p. 360, 2000.
[26] H. A. P. Ingram, ‘Soil layers in mires : function and terminology’, *J. Soil Sci.*, pp. 224–227, 1978.
[27] A.-L. Jacquemart, ‘Qu’est-ce qu’une tourbière ?’ https://sites.uclouvain.be/tourbiere/tourbiere/1._Une_tourbiere.html (accessed Oct. 19, 2022).
[28] J. Xu, P. Morris, J. Liu, and J. Holden, ‘PEATMAP: Refining estimates of global peatland distribution based on a meta-analysis’, *Catena*, vol. 160, pp. 134–140, Jan. 2018, doi: 10.1016/j.catena.2017.09.010.
[29] A.-L. Jacquemart, ‘Quelle est la répartition des tourbières en Europe et en Belgique ?’ https://sites.uclouvain.be/tourbiere/tourbiere/4._Repartition.html (accessed Oct. 19, 2022).
[30] B. Minasny *et al.*, ‘Digital mapping of peatlands – A critical review’, *Earth-Sci. Rev.*, vol. 196, p. 102870, Sep. 2019, doi: 10.1016/j.earscirev.2019.05.014.
[31] J. Limpens *et al.*, ‘Peatlands and the carbon cycle: from local processes to global implications – a synthesis’, *Biogeosciences*, vol. 5, no. 5, pp. 1475–1491, Oct. 2008, doi: 10.5194/bg-5-1475-2008.
[32] G. Whiting and J. Chanton, ‘Greenhouse Carbon Balance of Wetlands: Methane Emission versus Carbon Sequestration’, *Tellus B*, vol. 53, pp. 521–528, Apr. 2003, doi: 10.1034/j.1600-0889.2001.530501.x.
[33] J. Pärn *et al.*, ‘Nitrogen-rich organic soils under warm well-drained conditions are global nitrous oxide emission hotspots’, *Nat. Commun.*, vol. 9, no. 1, Art. no. 1, Mar. 2018, doi: 10.1038/s41467-018-03540-1.
[34] S. Page *et al.*, ‘Tropical peatland fires in Southeast Asia’, in *Tropical Fire Ecology: Climate Change, Land Use, and Ecosystem Dynamics*, M. A. Cochrane, Ed., in Springer Praxis Books. Berlin, Heidelberg: Springer, 2009, pp. 263–287. doi: 10.1007/978-3-540-77381-8_9.
[35] M. Strack, J. M. Waddington, L. Rochefort, and E.-S. Tuittila, ‘Response of vegetation and net ecosystem carbon dioxide exchange at different peatland microforms following water table drawdown’, *J. Geophys. Res. Biogeosciences*, vol. 111, no. G2, 2006, doi: 10.1029/2005JG000145.
[36] J. M. Waddington, P. J. Morris, N. Kettridge, G. Granath, D. K. Thompson, and P. A. Moore, ‘Hydrological feedbacks in northern peatlands’, *Ecohydrology*, vol. 8, no. 1, pp. 113–127, 2015, doi: 10.1002/eco.1493.
[37] M. R. Turetsky *et al.*, ‘A synthesis of methane emissions from 71 northern, temperate, and subtropical wetlands’, *Glob. Change Biol.*, vol. 20, no. 7, pp. 2183–2197, 2014, doi: 10.1111/gcb.12580.
[38] IPPC, ‘AR5 Climate Change’, 2014.
[39] G. Granath, P. A. Moore, M. C. Lukenbach, and J. M. Waddington, ‘Mitigating wildfire carbon loss in managed northern peatlands through restoration’, *Sci. Rep.*, vol. 6, no. 1, Art. no. 1, Jun. 2016, doi: 10.1038/srep28498.
[40] J. Leifeld and L. Menichetti, ‘The underappreciated potential of peatlands in global climate change mitigation strategies’, *Nat. Commun.*, vol. 9, Mar. 2018, doi: 10.1038/s41467-018-03406-6.
[41] ‘LandSense’. https://sites.uclouvain.be/landsense/ (accessed Dec. 22, 2022).

[42] ‘IRM - Contexte général’, *KMI*. https://www.meteo.be/fr/climat/climat-de-la-belgique/mois-apres-mois/contexte-general (accessed Jan. 03, 2023).
[43] ‘Le climat’. https://climat.be/en-belgique/climat-et-emissions/climat (accessed Jan. 03, 2023).
[44] D. Sandrine, ‘2. Evolution passée du climat en Région bruxelloise - Température et précipitations’.
[45] ‘Atlas climatique’, *KMI*. https://www.meteo.be/fr/climat/climat-de-la-belgique/atlas-climatique/cartes-climatiques/precipitations/quantites-de-precipitations/annuel (accessed Jan. 05, 2023).
[46] ‘Changements observés’, *Klimaat | Climat*. https://climat.be/en-belgique/climat-et-emissions/changements-observes (accessed Jan. 05, 2023).
[47] ‘IPCC — Intergovernmental Panel on Climate Change’. https://www.ipcc.ch/ (accessed Jan. 05, 2023).
[48] ‘IRM - Le climat à l’horizon 2100’, *KMI*. https://www.meteo.be/fr/climat/changement-climatique-en-belgique/le-climat-a-lhorizon-2100 (accessed Jan. 05, 2023).
[49] ‘IRM - Climat dans votre commune’, *KMI*. https://www.meteo.be/fr/climat/climat-de-la-belgique/climat-dans-votre-commune (accessed Jan. 06, 2023).
[50] SPW, ‘6006 - Hautes-Fagnes | Rechercher un site intéressant ou protégé | Sites | La biodiversité en Wallonie’. http://biodiversite.wallonie.be/fr/6006-hautes-fagnes.html?IDD=335545073&IDC=2831 (accessed Jan. 07, 2023).
[51] UNESCO, ‘Le plateau des Hautes-Fagnes’, *UNESCO Centre du patrimoine mondial*, 2008. https://whc.unesco.org/fr/listesindicatives/5358/ (accessed Jan. 06, 2023).
[52] E. Goemaere, S. Demarque, R. Dreesen, and P.-Y. Declercq, ‘The Geological and Cultural Heritage of the Caledonian Stavelot-Venn Massif, Belgium’, *Geoheritage*, vol. 8, no. 3, pp. 211–233, Sep. 2016, doi: 10.1007/s12371-015-0155-y.
[53] Ostbelgien, ‘Tout savoir sur le Parc naturel des Hautes Fagnes - Cantons de l‘Est’. https://www.ostbelgien.eu/fr/que-faire/ou-aller/hautes-fagnes/tout-savoir-sur-les-hautes-fagnes (accessed Jan. 06, 2023).
[54] ULg, ‘SSHF - Les Hautes-Fagnes’. https://www.sshf.uliege.be/cms/c_4346416/fr/sshf-les-hautes-fagnes (accessed Jan. 06, 2023).
[55] Commission de gestion du Parc, ‘Plan de gestion du Parc naturel Hautes Fagnes - Eiffel’. [Online]. Available: http://www.parcsnaturelsdewallonie.be/wp-content/uploads/2017/03/Plan_de_gestion_Parc_naturel_Hautes_Fagnes_Eifel_2016-2026_web.pdf
[56] SPW, ‘Les sites Natura 2000 | Sites | La biodiversité en Wallonie’. http://biodiversite.wallonie.be/fr/sites-natura2000.html?IDC=838 (accessed Jan. 07, 2023).
[57] S. Henrotte, ‘Hydrogeophysical characterization of the soil along a floodplain-hillslope system in the High Fens.’, Université Catholique de Louvain. Faculté des bioingénieurs, Louvain-la-Neuve, 2022. [Online]. Available: http://hdl.handle.net/2078.1/thesis:38219
[58] Y. Li, ‘Topography study site Landsense’, 2022.
[59] SPW, ‘WalOnMap’. http://geoportail.wallonie.be/walonmap (accessed Jan. 15, 2023).
[60] W. L. Quinton, D. M. Gray, and P. Marsh, ‘Subsurface drainage from hummock-covered hillslopes in the Arctic tundra’, *J. Hydrol.*, vol. 237, no. 1, pp. 113–125, Oct. 2000, doi: 10.1016/S0022-1694(00)00304-8.
[61] M. W. Menberu, H. Marttila, A.-K. Ronkanen, A. T. Haghighi, and B. Kløve, ‘Hydraulic and Physical Properties of Managed and Intact Peatlands: Application of the

Van Genuchten-Mualem Models to Peat Soils', *Water Resour. Res.*, vol. 57, no. 7, p. e2020WR028624, 2021, doi: 10.1029/2020WR028624.
[62] E. Rosa and M. Larocque, 'Investigating peat hydrological properties using field and laboratory methods: application to the Lanoraie peatland complex (southern Quebec, Canada)', *Hydrol. Process.*, vol. 22, no. 12, pp. 1866–1875, 2008, doi: 10.1002/hyp.6771.
[63] S. Hénin, 'Cours de physique du sol, II: L'eau et le sol – les propriétés mécaniques – la chaleur et le sol', *Initiat.-Doc. Tech.*, vol. 29, p. 222, 1977.
[64] D. L. Rowell, *Soil Science: Methods and Applications*. in Longman Scientific & Technical. 1994.
[65] U. Dettmann, M. Bechtold, E. Frahm, and B. Tiemeyer, 'On the applicability of unimodal and bimodal van Genuchten–Mualem based models to peat and other organic soils under evaporation conditions', *J. Hydrol.*, vol. 515, pp. 103–115, Jul. 2014, doi: 10.1016/j.jhydrol.2014.04.047.
[66] C. W. Beckwith, A. J. Baird, and A. L. Heathwaite, 'Anisotropy and depth-related heterogeneity of hydraulic conductivity in a bog peat. I: laboratory measurements', *Hydrol. Process.*, vol. 17, no. 1, pp. 89–101, 2003, doi: 10.1002/hyp.1116.
[67] P. J. Morris *et al.*, 'Saturated Hydraulic Conductivity in Northern Peats Inferred From Other Measurements', *Water Resour. Res.*, vol. 58, no. 11, p. e2022WR033181, 2022, doi: 10.1029/2022WR033181.
[68] Meter Group, 'Manual of TEROS 12 sensors'. 2018.
[69] Meter Group, 'Manual of ZL6 Dataloggers'. 2018.
[70] C. Wastiaux, 'Facteurs hydrologiques de la dégradation des tourbières hautes à sphaignes (Hautes-Fagnes, Belgique).', Université de Liège, 2000.
[71] H. A. P. Ingram, 'Hydrology. Mires: swamp, bog, fen and moor-General studies', 1983.
[72] R. Tomlinson, 'Water levels in peatlands and some implications for runoff and erosional processes', *Environ. Sci.*, 1979.
[73] S. van der Schaaf, *Analysis of the hydrology of raised bogs in the Irish Midlands: a case study of Raheenmore Bog and Clara Bog*. Wageningen, 1999.
[74] T. Gnatowski, J. Szatyłowicz, T. Brandyk, and C. Kechavarzi, 'Hydraulic properties of fen peat soils in Poland', *Geoderma*, vol. 154, no. 3, pp. 188–195, Jan. 2010, doi: 10.1016/j.geoderma.2009.02.021.

Appendix

Appendix A: Relative position of LSA and LSB.

Appendix B: Sandbox including all samples.

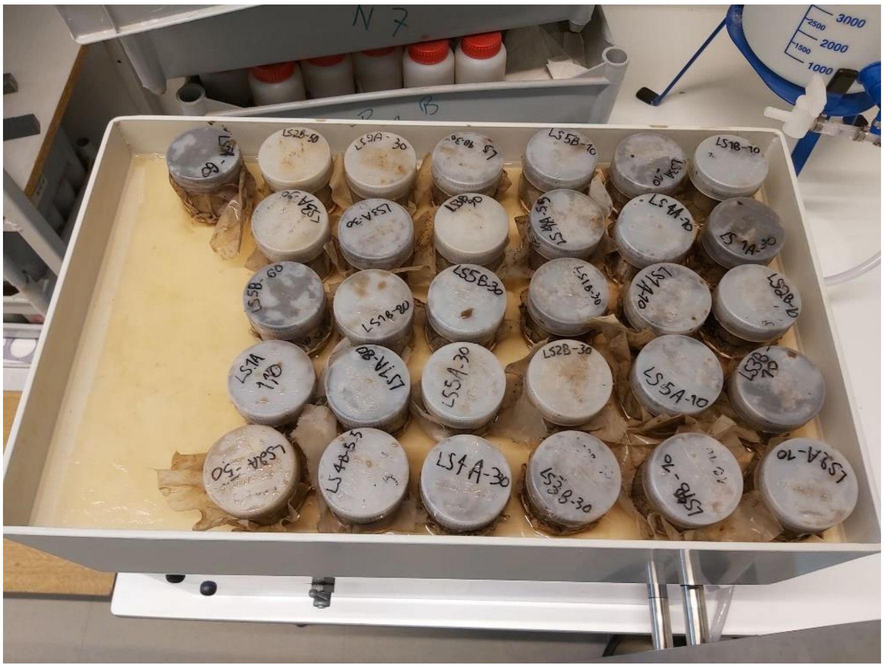

Appendix C: Kopecky samples inside the low pressure plate extractor

Appendix D: PVC samples on high pressure plate

Appendix E: Parameters used and deduced for the vGM modelling.

Sample	Type of soil	K_{sat} (m/s) (fixed)	θs (fixed)	θr (fitted)	Alpha (cm^{-1}) (fitted)	n (fitted)	R^2
LS1A-10	Peat	1,26E-03	0,812	0	0,3674	1,10	0,952
LS1A-30	Peat	6,23E-05	0,934	0	0,0066	1,22	0,958
LS1A-80	Peat	3,44E-05	0,995	0	0,0168	1,32	0,999
LS1B-10	Peat	3,00E-04	0,897	0	0,1365	1,20	0,974
LS1B-30	Peat	2,19E-04	0,962	0	0,0298	1,24	0,995
LS1B-80	Clay	1,40E-03	0,687	0	0,0137	1,16	0,954
LS2A-10	Peat	1,55E-04	0,932	0	0,0731	1,23	0,997
LS2A-30	Clay	1,13E-06	0,621	0	0,0170	1,17	0,877
LS2A-50	Clay	9,35E-05	0,557	0	0,0124	1,16	0,906
LS2B-10	Peat	1,65E-04	0,844	0	0,0308	1,18	0,993
LS2B-30	Clay	4,78E-06	0,580	0	0,0032	1,22	0,887
LS2B-50	Clay	1,48E-06	0,539	0	0,0101	1,11	0,911
LS3A-10	Peat	1,75E-04	0,910	0	0,0251	1,15	0,987
LS3A-30	Peat	4,03E-04	0,950	0	0,0174	1,23	0,993
LS3A-90	Clay	6,05E-06	0,569	0	0,0198	1,14	0,943
LS3B-10	Peat	9,63E-06	0,946	0	0,0139	1,19	0,979
LS3B-30	Peat	3,80E-05	0,955	0	0,0226	1,26	0,991
LS3B-90	Clay	8,21E-05	0,602	0	0,1020	1,06	0,960
LS4A-10	Peat	2,70E-04	0,926	0	0,0744	1,14	0,920
LS4A-30	Peat	5,93E-06	0,923	0	0,0146	1,30	0,996
LS4A-55	Peat	1,94E-04	0,918	0	0,0196	1,25	0,987
LS4B-10	Peat	1,74E-05	0,979	0	0,0241	1,29	0,995
LS4B-30	Peat	5,50E-07	0,959	0	0,0199	1,28	0,998
LS4B-55	Clay	2,06E-04	0,603	0	0,2390	1,03	0,878
LS5A-10	Peat	4,66E-04	0,972	0	0,0242	1,24	0,958
LS5A-30	Peat	7,57E-07	0,985	0	0,0160	1,37	0,997
LS5A-60	Peat	8,10E-05	0,988	0	0,0159	1,28	0,992
LS5B-10	Peat	4,15E-04	0,938	0	0,0187	1,24	0,934
LS5B-30	Peat	3,88E-04	0,950	0	0,0217	1,27	0,994
LS5B-60	Peat	1,36E-06	0,997	0	0,0167	1,30	0,994

Appendix F: Example of LS5B pit before and after installation of probes.

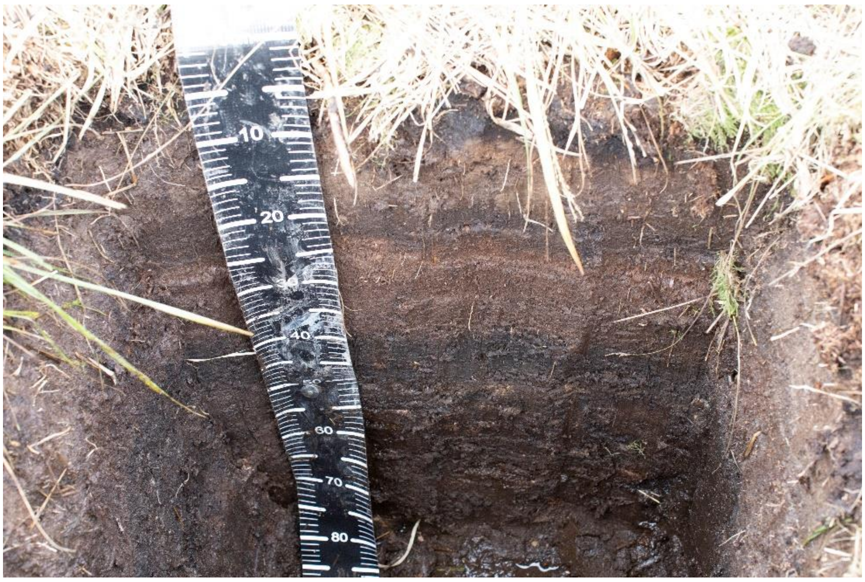

Hydrogeophysical characterization and monitoring of a peatland in the Hautes Fagnes.

BULLIARD Florentin

Although they represent only 3% of the land surface, peatlands contain almost 30% of the world's soil carbon stock. Because of their high organic content, peatlands are important carbon stores. Peatlands have high-water storage capacity, which allows them to function as water reservoirs. The hydraulic properties of peatlands therefore play a key role in maintaining conditions favourable to carbon accumulation. Peatlands have a regulatory function and a water regulation function. It has also an essential role in biodiversity.

In critical zone research, the integrated study of peatland remains a key knowledge gap, especially in Belgium. This master's thesis aims at addressing this problem by studying hydraulic parameters in a hillslope peatland in the Hautes Fagnes. To collect the data needed, several methods were used: an in-situ method, namely the TDR (Time Domain Reflectometry) probes and a laboratory method, the pressure cell apparatus. Direct modelling allows to integrate these parameters into a Hydrus model.

Soil water retention curves have been established and values of the model fitting parameters are obtained with very high coefficients of determination for both soils. Unsaturated hydraulic parameters in peat soils have been successfully estimated using the van Genuchten-Mualem unimodal model via the RETC program.

Clay bulk density, with an average value of 1.2 [g/cm^3], corresponds to loamy clay and an increase of the bulk density with depth is visible. The average value of bulk density of peat is equal to 0.2 [g/cm^3] with no relationship between depth and density. The clay samples have an average value of the volumetric water content (VWC) at saturation (θ_s) of 0.59 which looks like very fine-textured clay soil. For peat samples, this value is 0.94. The values of these hydraulic parameters for peat confirm the great water storage capacity of the studied peatland.

Several TDR probes were placed along the slope at 5 locations and 3 depths each. This enabled a long-term study of the VWC. The variations observed are closely linked to precipitation. Along the study transect, the position of the probes has no influence on the evolution of the VWC. The presence of the water table is assumed to be between 30 and 50 cm depth. Therefore, peatland is an almost saturated environment that offers little absorption capacity. Any excess precipitation can not infiltrate, but only run off downhill through the surface vegetation. There is a threshold for rapid flow at very shallow depths in peatlands. Below this threshold, the peat is nearly impermeable and lateral/horizontal water movement is slow.

In direct modelling part, the simulations roughly match the data, but tend to be more sensitive to boundary conditions and to have larger amplitudes at 30 cm depth. At a depth of 10 cm, the best results are observed, although in some cases the simulation and TDR data do not match.

UNIVERSITÉ CATHOLIQUE DE LOUVAIN
Faculté des bioingénieurs
Croix du Sud, 2 bte L7.05.01, 1348 Louvain-la-Neuve, Belgique | **www.uclouvain.be/agro**